CHALMERS

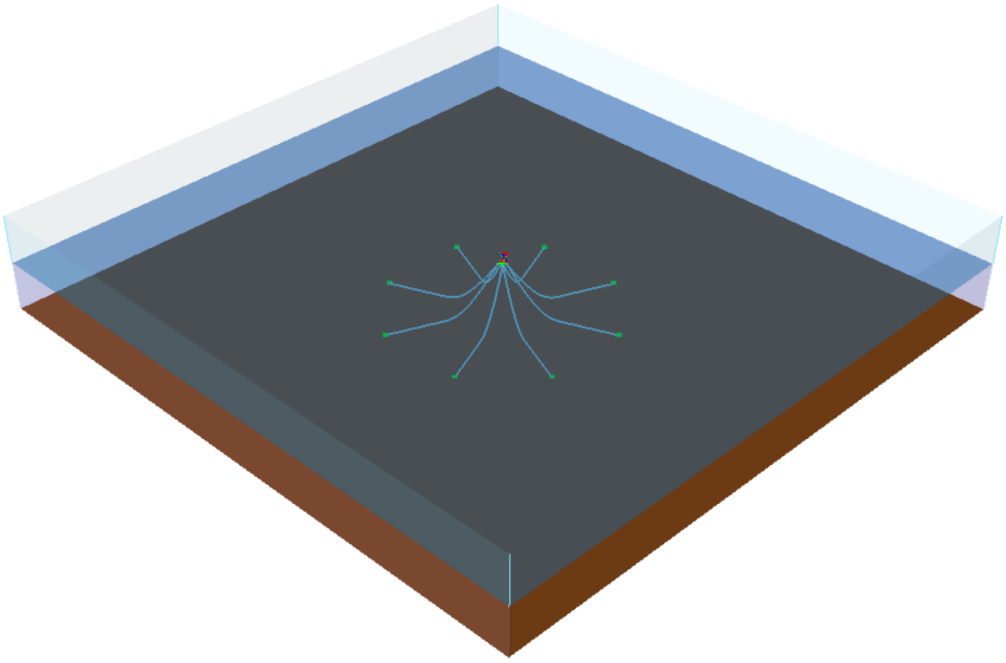

Viscous damping levels in mooring computations and the effect of increasing water depth

Master's Thesis in the International Master's Programme Naval Architecture and Ocean Engineering

MIKAEL CARLSSON AND ROBERT ERIKSSON

Department of Shipping and Marine Technology
Division of Marine Design, Research Group Marine Structures
CHALMERS UNIVERSITY OF TECHNOLOGY
Göteborg, Sweden 2013
Master's thesis: X-13/292

MASTER'S THESIS IN THE INTERNATIONAL MASTER'S PROGRAMME IN NAVAL ARCHITECTURE AND OCEAN ENGINEERING

Viscous damping levels in mooring computations and the effect of increasing water depth

MIKAEL CARLSSON AND ROBERT ERIKSSON

Department of Shipping and Marine Technology
Division of Marine Design
Research Group Marine Structures
CHALMERS UNIVERSITY OF TECHNOLOGY
Göteborg, Sweden 2013

Viscous damping levels in mooring computations and the effect of increasing water depth
MIKAEL CARLSSON AND ROBERT ERIKSSON

Master's Thesis: X-13/292
ISSN 1652-8557
Department of Shipping and Marine Technology
Division of Marine Design
Research Group Marine Structures
Chalmers University of Technology
SE-412 96 Göteborg
Sweden
Telephone: + 46 (0)31-772 1000

Cover:
Calculation domain in the DNV software DeepC.

Chalmers Reproservice
Göteborg, Sweden 2013

Viscous damping levels in mooring computations and the effect of increasing water depth

Master's Thesis in the International Master's Programme in Naval Architecture and Ocean Engineering

MIKAEL CARLSSON AND ROBERT ERIKSSON
Department of Shipping and Marine Technology
Division of Marine Design
Research Group Marine Structures
Chalmers University of Technology

ABSTRACT

With an increased demand for operations in deeper water, the requirements of vessels to withstand the environmental loads and stay in position become more important. The increased water depth puts higher requirements of the mooring system; the weight of the lines is an important factor since it affects the amount of payload. The mooring system can be made less heavy if the line damping contribution is included in the mooring calculations and so reduces the motions as well as the line tensions. In the classification rules there is limited information regarding the damping contributions from the mooring lines and the guidance note in DNV-OS-E301 gives conservative and rather low damping levels for mooring systems.

The aim with this thesis is to achieve a better understanding of when and how the viscous damping of mooring lines and risers should be accounted for. In addition to this, the aim is to establish realistic levels for viscous damping contribution from mooring lines and to compare the time-domain and frequency-domain methods with regard to the mooring-line damping. The study has been performed on a generic semi-submersible drilling platform at 5 water depths ranging from 100 to 1,250m.

The study shows that the performed simulations in time-domain compared to frequency-domain methods give a greater contribution of mooring line damping to the system. The damping levels in surge from mooring lines are between 8 and 28 per cent of the critical damping and in sway 10 and 36 percent, depending on water depth and heading. The damping in absolute numbers decreases with increasing water depth, although the relative percentage of critical damping remains at the same order of magnitude.

For further investigation a different system is recommended with a higher pre-tension in order to achieve a stiffer system and to not allow such large static displacements, and, in addition, also to include risers to study the influence on the damping. Moreover, the damping is dependent on sea state and it is of interest to perform the study in another sea state than the extreme sea state used.

Keywords: DeepC, frequency-domain analysis, MIMOSA, mooring lines, time-domain analysis, viscous damping.

Viskösa dämpningsnivåer i förankringsberäkningar och dess inverkan vid ökande vattendjup

Examensarbete inom Naval Architecture and Ocean Engineering

MIKAEL CARLSSON OCH ROBERT ERIKSSON

Institutionen för sjöfart och marin teknik

Avdelningen för Marine Design

Forskargruppen Marina Strukturer

Chalmers tekniska högskola

SAMMANFATTNING

Med ökad efterfrågan av operationer på större djup ökar kraven på fartyg och plattformar att stå emot väderkrafter och behålla positionen. Med ökande vattendjup ställs allt högre krav på förankringssystemet och linornas vikt blir en viktigare faktor för att kunna ha så hög lastkapacitet som möjligt. Förankringssystemet kan göras lättare om dämpningsbidragen från linorna tas med i förankringsanalysen, vilket reducerar plattformens rörelse och spänningarna i förankringslinorna. Det finns begränsad information i klassningsregler om dämpningsbidraget från förankringslinorna och de givna riktlinjerna i DNV-OS-E301 är konservativa och ger relativt låga dämpningsbidrag.

Målet med detta examensarbete är att skapa en bättre förståelse om hur och när den viskösa dämpningen från förankringslinor och stigrör bör tas hänsyn till. Fastställa realistiska nivåer för linornas dämpningsbidrag samt att jämföra lindämpningen i tids- och frekvensdomänberäkningar. Studien har utförts med en fiktiv semi-submersible borrplattform på 5 vattendjup från 100 till 1250 m.

Studien visar att beräkningar i tidsdomän jämfört med frekvensdomän ger ett större bidrag från lindämpningen till systemet. Dämpningsnivåerna från förankringslinorna i surge är mellan 8 och 28 procent, sway 10 och 36 procent utav den kritiska dämpningen, beroende på vattendjup och väderriktning. I absoluta tal minskar lindämpningen med ökande vattendjup, men som del av den kritiska dämpningen är den i samma storleksordning.

Rekommendationen för vidare undersökning är att använda ett styvare förankringssystem med en högre förspänning som på så sätt inte tillåter alltför stora statiska förflyttningar, i tillägg bör även inverkan av stigrör på dämpningen studeras. Ytterligare är dämpningen beroende av väderförhållanden och det är av intresse att utföra en liknande studie för ett annat förhållande än det extremväder som använts.

Nyckelord: DeepC, frekvensdomänanalys, förankringslinor, MIMOSA, tidsdomänanalys, viskös dämpning.

Contents

Preface

This thesis is a part of the requirements for the master's degree in Naval Architecture and Ocean Engineering at Chalmers University of Technology, Göteborg, and has been carried out between January and June of 2013 at the Division of Marine Design, Department of Shipping and Marine Technology, Chalmers University of Technology, and in cooperation with Det Norske Veritas, Division of Marine Operations, in Høvik.

We would like to acknowledge and thank our examiner, Associate Professor Carl-Erik Janson, and our supervisor, Professor Jonas Ringsberg, at the Department of Shipping and Marine Technology for their guidance and support throughout the work with this thesis. We would also like to thank our co-supervisors Florus Korbijn at Marine Operations and Erik Falkenberg at Hydrodynamics and Moorings at Det Norske Veritas for the time and supervision they have given us. Furthermore, we would like to thank Professor Emeritus Lars Bergdahl and PhD Student Johannes Palm at the Department of Shipping and Marine Technology for their support with the thesis.

Figures with references used in this thesis are printed with the permission of the copyright owners and we would like to thank you for this permission.

Göteborg, May, 2013
Mikael Carlsson and Robert Eriksson

Abbreviations

DNV	Det Norske Veritas
DP	Dynamic positioning
FE	Finite element
HF	High frequency
ISO	International Organization for Standardization
LF	Low frequency
MBL	Minimum breaking load
MODU	Mobile offshore drilling unit
NMD	Norwegian Maritime Directorate
RAO	Response Amplitude Operator
SF	Safety Factor
ULS	Ultimate limit state
VIM	Vortex induced motions
WF	Wave Frequency

Notations

A	Cross sectional area [m^2]
C_D	Drag coefficient [-]
C_M	Added mass coefficient [-]
D	Diameter [m]
E	Energy dissipation of one mooring line per cycle [Nm]
F_D	Drag force [N]
F_M	Inertia force [N]
H_s	Significant wave height [m]
$\mathbf{R}^I$	Inertia force vector
$\mathbf{R}^D$	Damping force vector
$\mathbf{R}^S$	Internal structural reaction force vector
$\mathbf{R}^E$	External force vector
T	Period of motion [s]
T_h	Horizontal component of line tension [N]
T_t	Line tension [N]
T_p	Peak wave period [s]
T_v	Vertical component of line tension [N]
V	Displaced volume [m^3]
k	Stiffness [N/m]
m	Mass [kg]
p	Weight per unit length of line submerged in [N/m]
$\mathbf{r}$	Structural displacement vector [m]
$\dot{\mathbf{r}}$	**V**elocity vector [m/s]
$\ddot{\mathbf{r}}$	Acceleration vector [m/s^2]
s	Horizontal fairlead motion in direction of line [m]
s_0	Amplitude of horizontal fairlead motion in direction of line [m]

t	Time [s]
u	Displacement [m]
x_0	Horizontal position of the lift-off point [m]
Δz	Peak to peak vertical motion of line during one cycle in [m]
β	Jonswap form parameter [-]
γ	Jonswap peakedness parameter [-]
ε	Horizontal motion in the mooring line plane [m]
ε_0	Amplitude of the horizontal motion in the mooring line plane [m]
η	Transverse motion of mooring line [m]
η_0	Amplitude of the transverse motion of the mooring line [m]
ρ_W	Density of water in [kg/m^3]
φ	Tangential angle of the mooring line [rad]
σ_a	Jonswap spectrum width parameter [-]
σ_b	Jonswap spectrum width parameter [-]
τ	Dynamic line tension [N]
τ_0	Amplitude of the dynamic line tension [N]
ω	Circular frequency in [rad/s]

Definitions

Surge	Motion of the platform along the x-axis
Sway	Motion of the platform along the y-axis
Heave	Motion of the platform along the z-axis
Roll	Rotation of the platform about the x-axis
Pitch	Rotation of the platform about the y-axis
Yaw	Rotation of the platform about the z-axis

1 Introduction

There are different types of floating vessels such as barges, ships and offshore platforms operating in the North Sea. The choice of vessel depends on what purpose that has to be performed (semikolon); this study focuses on offshore platforms. These can be divided into two groups, permanent and mobile platforms. Mobile platforms are moved to different locations i.e. drilling platforms while permanent platforms, i.e. production units, are designed to be moored in one location for 20-30 years.

Offshore vessels and structures can also be bottom- supported. There are a variety of structures that are bottom-supported, i.e. gravitybased structures, jackets, jack-up rigs, etc. Gravitybased structures are large fixed towers standing on the seabed which are held in place by their own weight and are used in harsh weather conditions. Jackets are fixed truss member constructions built in steel and piled to the seabed, see Figure 1.1, and used for shallow water depths down to about 150 metres. A jack-up is a mobile drilling unit that consists of 3-4 legs that can be lowered down to the seabed so that the platform becomes self-elevated out of the water and is commonly used to a water depth down to 100 metres, Journèe and Massie (2001).

Floating offshore structures can be ships, barges or semi-submersibles, etc., see Figure 1.1. These types of floating units have the mobility to operate at various depths and environmental conditions. Smaller semi-submersibles are commonly used in drilling operations, while larger semi-submersibles are used as production facilities. The spar platform consists of a large cylindrical hull- shaped body standing vertically and generally tautly moored to the seabed. If the middle section is replaced by a truss structure to reduce weight, the platform is called truss spar. Another type of floating structure is the tension leg platform, TLP, which is similar to a semi-submersible but is vertically moored by taut mooring lines called tendons instead of catenarymoored, Chakrabarti and Subrata (2005).

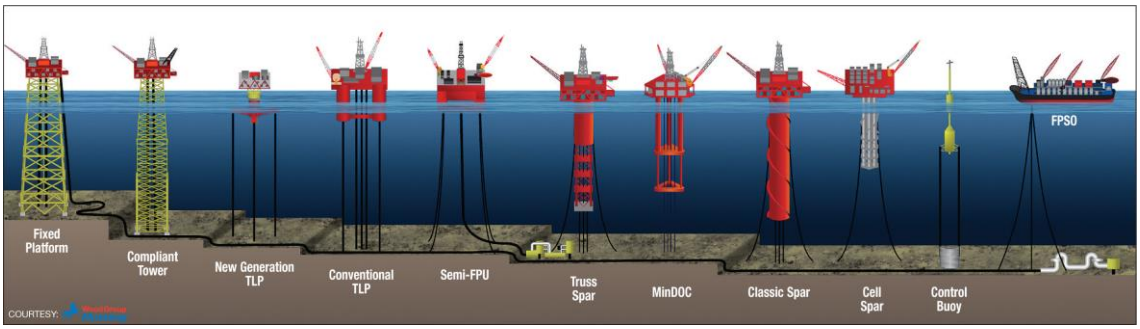

Figure 1.1 Various types of bottomsupported and floating platforms, courtesy of Wood Group Mustang.

This thesis focuses on a catenarymoored semi-submersible drilling platform. The main components of the structure are the pontoons, space frame bracers, stability columns and deck. The deck is supported by the columns which are connected to the pontoons. The pontoons are linked to each other with spaceframe bracers, see Figure 1.2. Semi-submersibles have mainly two operating modes, semi-submerged during operation and afloat for transportation between areas. The main advantage of this type of platform is the good motion characteristics in severe environments and low

vertical motions and therefore have the highest degree of workability, Chakrabarti and Subrata (2005). For a drilling semi-submersible this results in less downtime during drilling operations than, for example, for a drillship.

Figure 1.2 Semi-submersible drilling platform, courtesy of GVA Consultants.

For a floating unit operating at sea it is necessary to stay in the intended position and withstand environmental loads. This can be achieved by using a mooring system, a dynamic positioning system, DP, with thrusters or a combination of both. The largest loads on the structure will appear when the environmental forces have the same heading and coincide with the platform's resonant frequency . The mooring systems are designed so that the resonant frequencies are outside the wave- frequency range, DNV (2005). Stationkeeping systems for floating structures are commonly used in the offshore industry and how the system is designed depends on the environmental condition at the location and the characteristics of the structure. Ship or ship-shaped floating structures frequently use singlepoint mooring systems, while platforms use spread mooring systems as a particular orientation is important to maintain.

The characteristics of the mooring system is that it should be flexible in order to allow motions and avoid extreme tensions in the lines. On the other hand the system must be stiff enough to keep the vessel within position restrictions. For a drilling platform the mooring system usually consists of between 8 and 12 mooring lines with one end connected to the unit and the other anchored to the seabed, Journèe and Massie (2001). DP systems are often used for assisting and maintaining the particular

orientation and reducing line tension, ISO (2005). Mooring systems are used at water depths down to 2000m, Wilson (2003), and the length of the lines are normally considerably longer than the water depth to prevent lift forces at the anchor. The lines are made of steel chain, steel wire rope or synthetic fibre rope. For shallow water it is most common to use chains, and, for increasing depths, wire or fibre ropes are an option. The weight of the system is of interest not only for line tensions due to its own weight but will also be more sustainable if the payload can be increased with a less heavy system and thereby reduce the amount of supply transports.

1.1 Background

It has been customary to neglect the damping contribution from the mooring system and risers when predicting viscous damping and resonant motion in surge and sway of moored platforms. Drag forces on the mooring lines and friction on the seabed can give rise to significant energy dissipation, which may represent a major damping effect on the platform in a surge and sway motion, Huse (1986). The reason for neglecting drag forces on mooring lines and risers has been mainly that the area represented by the lines is rather small compared to the drag area of the platform itself, Huse (1991). Reduction of the surge and sway amplitude due to mooringline damping is shown with calculations and experimental verifications and can account for a reduction in the order of 20 per cent (=per cent) or more. The damping contribution of the mooring systems and risers should be taken into consideration when motions in surge and sway for offshore platforms are predicted, Huse (1988).

The main contributions to the surge and sway damping of the platform arise from radiation of waves due to motion, wavedrift damping, friction and drag forces on the structure including effects of appendages. Factors affecting the mooringline damping are line pre-tension and tension, water depths, line elasticity, line type, line size, catenary shape and seabed friction. The importance of drag forces on mooring systems and risers, together with friction between the seabed and mooring lines has been discussed by Huse (1986) regarding its contribution to platform damping.

Interaction between platform and waves results in motions of the platform that can be divided into three categories; mean wave drift, first-order motion and second-order motions. Mean wave drift is a steady offset of the platform. Firstorder motions, known as high frequency or wave frequency motions, are generated from the waves. Secondorder motions, known as low frequency motions, are the viscous forces acting on the platform. For motions in the vertical plane (i.e. heave, pitch and roll), the firstorder motions dominate while in the horizontal plane (i.e sway, surge and yaw) the secondorder motions are the most important and especially near the natural frequency of the platform, ISO (2005). Damping achieved from a mooring system is complex and difficult to account for and therefore often neglected even if it is stated in research as a significant damping mechanism contributing with 30 to 40 per cent of the total platform damping, Lie, Gao and Moan (2007).

The rules in ISO (2005) state that frequency- domain or time-domain simulations shall be carried out for mooring analysis . The frequency-domain analysis is sufficient for temporary moorings but not recommended for permanently moored

platforms. In the frequency-domain computations the viscous damping contribution from the platform is included, but not from the mooring lines.

1.2 Objective

The main purpose of this study is to achieve a better understanding of when and how the viscous damping of mooring lines and risers should be accounted for. The aim is to establish realistic levels for viscous damping contributions for a standard drilling platform at five water depths (100m, 200m, 400m, 750m, 1250m) in typical North Sea survival conditions with regard to the 100year wave, the 100year wind and 10year current. This study is a comparative study and will use available methods, and hence not develop new ones. The platform used in the analysis is a generic semi-submersible and is of a similar size as the drilling platforms operating in the North Sea and Norwegian Sea.

1.3 Methodology

In order to establish levels for the viscous damping it is of interest to study different calculation methods. A comparison is made between frequency-domain calculations, both with and without added viscous damping, and fully coupled time-domain calculations with regard to the effects on platform motions and line loads as well as the transition to a taut mooring system. This will be related to the guidance note given in DNV-OS-E301 Ch. 2, Section 2, B303 for the total viscous damping which can be applied for lack of available data.

For the viscous damping level of mooring lines a generic model of a semi-submersible drilling platform has been implemented in two different softwares. In the software, mooring line setups have been designed with respect to the specific water depths of the fields and to withstand North Sea survival conditions with regard to 100-year waves, 100year wind and 10year currents. Three types of calculations will be performed in the mooring analysis; a frequency-domain analysis, with and without added viscous damping, and a fully coupled time-domain analysis. The frequency-domain and time-domain calculations will be carried out using the DNV software MIMOSA and DeepC, respectively. Each of these parts will be described briefly with respect to the methods and sub-programs used. The methodology and workflow is presented in Figure 1.3.

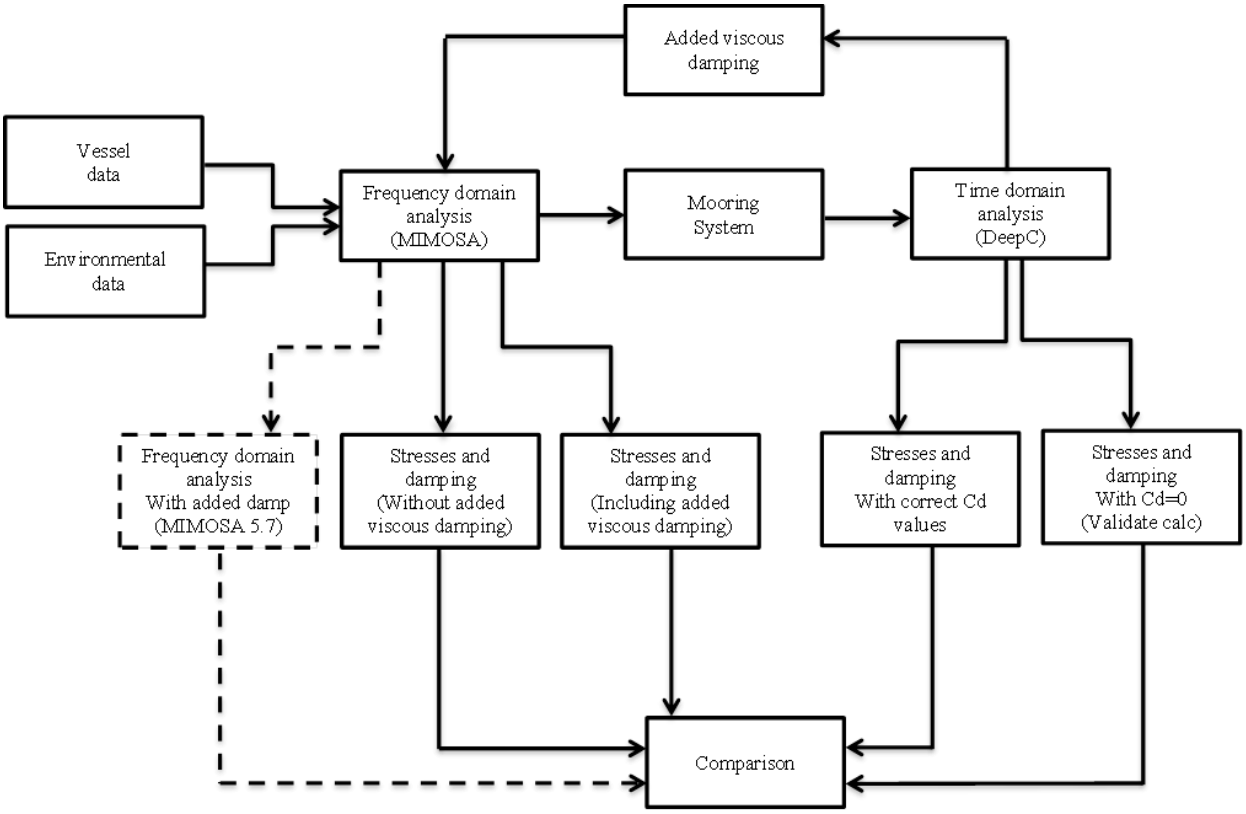

Figure 1.3 Schematic figure of the methodology and workflow.

The frequency-domain using quasi-static calculations in combination with the catenary equations provides a fast and good first estimation of the loads acting on the system compared to the more timeconsuming time-domain method, Lie et al. (2007). From this, an overview of how the system should be designed for further investigation is obtained. The disadvantage with the method is that it neglects damping effects from the mooring system and focuses only on the motion of the platform and tensions in the mooring lines. The frequency-domain solution is to be considered more conservative than the time-domain since it neglects effects that would otherwise contribute to the damping and reduce motions, Vasudevan and Westlake (2012).

For further investigation, the coupled time-domain method will be used for its ability to incorporate more effects than the frequency-domain method. It calculates the interaction of mooring lines and the platform in the time-domain. Time domain calculations give the possibility to calculate seabed interaction and fatigue of the mooring lines in a more accurate way, but the drawback is that it is more timeconsuming.

Frequencydomain calculation is carried out with the software MIMOSA. It is used in analyses of moored vessels for calculating the vessel's wave frequency, low frequency motions, and static and dynamic line tension. In the first part of the study, a frequency-domain analysis is performed, without added viscous damping, and the designed mooringline configurations are exported from MIMOSA and implemented into DeepC.

Timedomain calculations are carried out in the software DeepC. DeepC includes the software SIMO and RIFLEX to perform the non-linear time-domain finite element simulation. SIMO is used for time-domain simulations of motions and station-keeping behaviour of moored vessels. RIFLEX is a time-domain analysis tool for flexible marine structures such as mooring lines. The results from SIMO and RIFLEX can be viewed within the DeepC interface. The non-linear time-domain calculations in DeepC provides the data regarding the added viscous damping of the mooring system, which will be implemented into MIMOSA for calculations in the frequency-domain analysis with the correct mooring system configuration and system damping.

The viscous damping calculated in DeepC will be compared to the damping estimated in MIMOSA v.5.7. The viscous damping from frequency-domain and time-domain are analysed in order to achieve an understanding of how the effect from increasing water depths and a transition to a more taut mooringline system affects the viscous damping levels in the mooring lines.

The analysis methods are general and not specific for the cases investigated, and the results should not be code-dependent but differences between different codes may be due to different theory, coding errors and user input.

1.4 Limitations

In this thesis, a semi-submersible drilling platform operating in North Sea conditions is studied. The platform is in survival mode and disconnected from the well and has therefore no restrictions in horizontal displacement. The mooring system consists of 8 lines equally distributed and spread over the seabed. The riser is neglected even though it would contribute to the viscous damping of the platform.

The sea state used in the analysis is considered to be omnidirectional and an average of weather data for different fields representing the five different water depths in the North Sea, with regard to extreme weather as stated in NMD (2009) which is 100year waves, 100year wind and 10year currents. The significant wave height is 15m, the average wind speed is 34 m/s, the surface current speed is 1 m/s and a current profile with constant current speed of 1m/s down to 30m and then linear to zero speed at the seabed.

Safety factors regarding ULS for line tensions are to be evaluated. The focus of this thesis is the hydrodynamics of the mooring lines therefore the safety factors stated in ISO (2005) with the addition for Norwegian waters from NMD (2009) do not necessarily have to be fulfilled. In order to have a more practical meaning, it should to as great an extent as possible be fulfilled. The platform uses thrusters, which will decrease the line tensions and improve the safety factors, as well as decrease the platform motion. These thrusters only give a constant thrust and do not contribute to the damping of platform motions.

The attachment of the mooring lines to the seabed will be considered as fixed points and the friction of the anchors to the seabed will not be considered

The WF motion transfer function corresponds to a water depth of 300m, which will cause a minor overestimation of the RAO for water depths greater than 300m and a small underestimation for depths less than 300m. The RAO for deep water is commonly valid to water depths down to 100m.

1.5 Outline of thesis

This thesis is divided into 7 chapters. In Chapter 2, background information to the mooring systems is described followed by a more detailed description of damping contributions in Chapter 3. The software procedure is given in Chapter 4 with the results presented and further discussed in Chapter 5. Finally, the conclusions are presented in Chapter 6 and recommendations for further study of the topic are given in Chapter 7.

2 Mooring of floating offshore platforms

To keep a floating offshore platform in the intended position a mooring system with lines, thrusters or a combination can be used. Depending on the shape of the mooring lines a spread mooring system can be either catenary and/or (= and/or) taut.

A mooring system is comprised of a number of lines which are attached to the floating platform with the lower ends anchored at the seabed. The dimensions and configuration of the mooring system is determined by the design environment, line tension safety factors and positioning accuracy. It is common to use a system consisting of eight mooring lines in a standard mooringline pattern. The arrangement of the mooring lines is often equally or symmetrically distributed and can be seen in Figures 2.1a and 2.1b.

a) b)

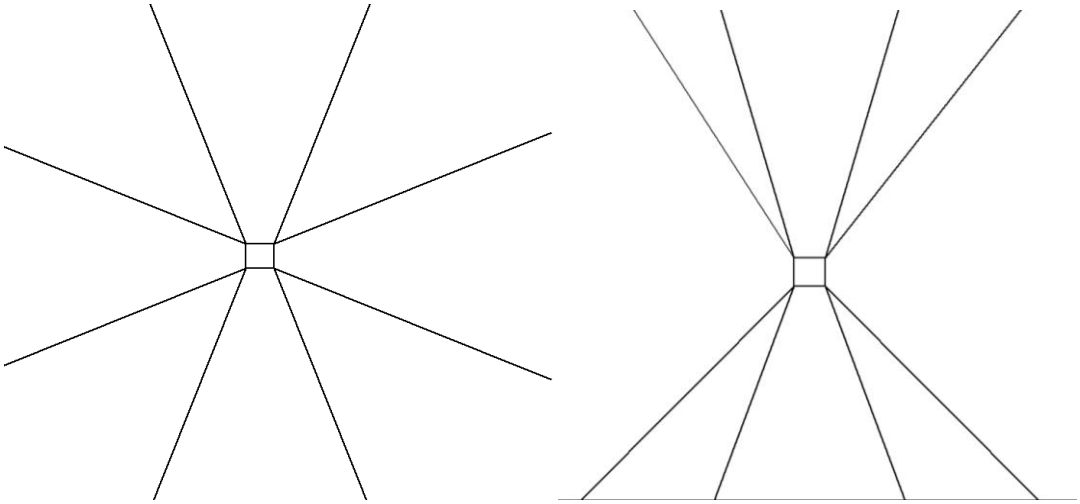

Figure 2.1 a) Equal and b) symmetric mooring- line configurations

In mooring systems the lines are pre-tensioned to keep the platform in the intended position (ej komma – tankestreck) - a larger pre-tension gives less offset for a given external force, since the mooring system's stiffness increases due to the catenary effect. In taut line systems the catenary effect is small and increased pre-tension has a smaller effect on the calculated offsets. The pre-tension in the lines is achieved by winches on the platform, Faltinsen (1993). There are mainly three types of materials used for mooring lines; steel chain, steel wire rope and synthetic fibre rope, ISO (2005). Depending on the situation and water depth the materials in the mooring lines can be different.

2.1 Mooring systems

Catenaryline mooring is the most common mooring system and can be seen in Figures 2.2 and 2.3a. The characteristics in a catenary system are determined by the length and weight of the mooring lines, Sjöberg and Bergdahl (1981). The length is longer than the depth so that a significant part of the mooring line lies on the seabed to ensure that loading on the anchor is always horizontal. The advantages of this type of system are a softer absorption of big motions and loads, and large damping effects due to energy dissipation caused by line motion in the water and on the seabed. The disadvantage is that the mooring system becomes heavy, requires a large seabed area and the horizontal displacement for the platform increases with increasing water depth. For larger depths a taut mooring system can be an option, see Figure 2.3b, Journèe and Massie (2001),

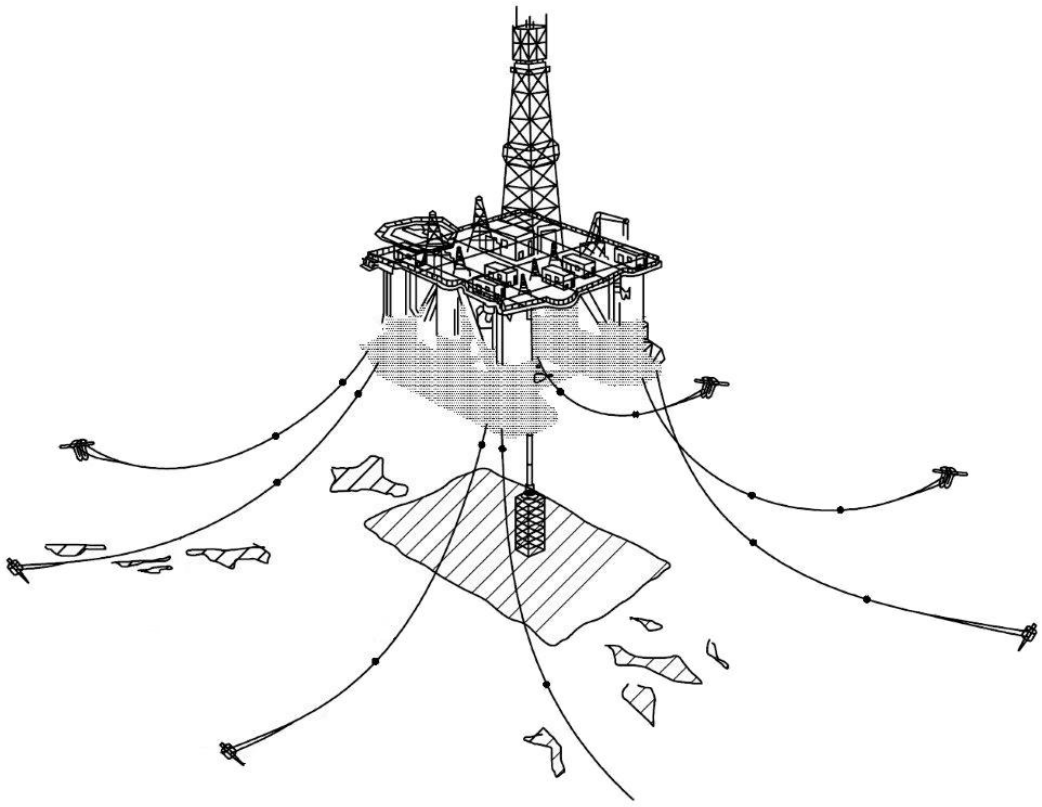

Figure 2.2 Schematic figure of a catenary mooring system, modified from ISO (2005) courtesy of SIS.

Tautline mooring systems have their lines stretched in a pattern radiating outwards from the platform. Typically, synthetic lightweight lines are used for this, which have a low net submerged weight. For a taut mooring system the catenary effect has been eliminated and the anchors have to be able to withstand vertical loading. The restoring horizontal force acting on the system originates from the elasticity in the lines (tankestreck) - the risk of an extreme tension in the lines increases with this higher pre-tension, Journèe and Massie (2001).

Another type of mooring system is used for tension-leg platforms in deep water, a so-called tension-leg mooring, see Figure 2.3c. The mooring lines are vertically tensioned, which prevents vertical motion and the vertical displacement becomes small. The horizontal displacement becomes significant since the restoring force on the platform only depends on the horizontal components in the mooring tension leg, Journèe and Massie (2001).

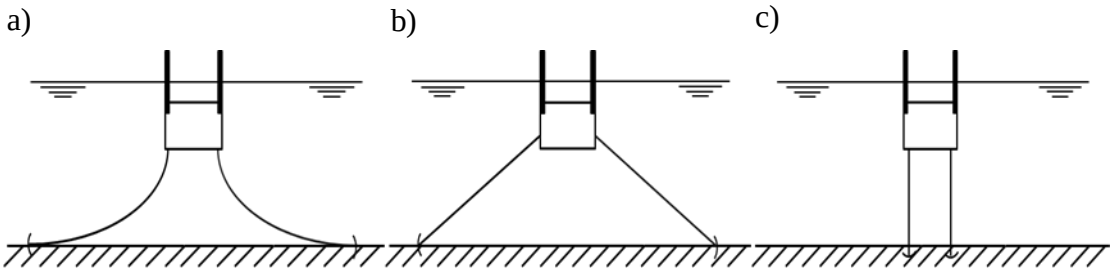

Figure 2.3 Overview of a a) catenary b) taut and c) tension-leg mooring

2.2 Mooring line materials

There are mainly three types of material used for mooring lines; steel chain, steel wire rope and synthetic fibre rope. Due to their different properties it is common to combine chain and rope to achieve the most suitable system.

For shallower water depths, steel chain is the most common choice of mooringline material. It has good resistance to bottom abrasion and hold capacity of the anchors. The disadvantage is the decrease of platform payload capacity in deeper water due to the weight of the chain. Steel wire rope is used in moderate water and deep water It is not common to only use steel wire rope in a mooring system because of the long length required to prevent anchors' uplift as well as the large space required on the seabed, ISO (2005).

Synthetic fibre ropes are increasingly being used in deep water mooring systems. The advantage is their lower weight compared to steel wire rope and longer fatigue life as well as higher elasticity, ISO (2005). A combination of chain and rope is favourable, usually with a chain at the top of the line, then a fibre rope segment and near the seabed a chain segment which is connected to the anchor. For use in deep water this combined system is compelling since it has the advantage of reducing the pre-tension requirements with higher restoring force and hence increase the payload, ISO (2005).

3 Damping contributions

The slowly varying resonant vessel motion is central for estimating the mooringline damping - the damping mechanisms from the lines are important since they reduce the platform's LF motion. Mooringline damping is affected by a number of parameters such as line pre-tension and tension, water depth, line elasticity, line type, line size, line shape and seabed friction. An estimation of the line damping from the mooring system can be obtained in both a frequency-domain and time-domain analysis, Huse (1992).

The most general analysis method for mooring- line damping calculations is a complete time-domain analysis of the mooring line, Huse (1992). In time-domain simulations all effects from the environment, mooring lines and platform are included. Timedomain simulations or model tests have to be performed in order to verify the accuracy of the more simple frequency-domain analysis. For semi-submersible platforms, viscous forces on the hull is the main source of damping, but a contribution from the mooring lines can still be up to 30-40 percent of the total damping, Lie et al. (2007). The damping contribution of the system can be divided into viscous forces on the hull, wave drift forces and forces on the mooring system, Huse (1991).

3.1 Viscous forces

The viscous damping contributions depend on the flow separation and vortices behind the pontoons and columns, which give rise to a viscous force. Morison's equation is applied and assumed to be valid for the calculations of viscous forces which give the main damping contribution of the platform, Liu (1998).

The viscous force suggested by Morison can be divided into two parts, drag force F_D and inertia force F_M, see Equations (3.1) and (3.2), respectively. The drag force is mainly due to pressure differences over the body, caused by separation of the flow creating a low pressure region behind it, Moberg (1988).

The drag force per unit length can be written as:

$$F_D = \frac{1}{2}\rho C_D A u^2 \tag{3.1}$$

The inertia force is present due to the acceleration of the flow caused by a pressure gradient acting on the displaced volume of the body, Moberg (1988).

The inertia force per unit length can be written as:

$$F_M = C_M \rho V \frac{\partial u}{\partial t} \tag{3.2}$$

3.2 Wave drift forces

Wavedrift damping is related to the wavedrift forces, also known as secondorder wave forces, consisting of a constant and an oscillating part to which the moored platform is exposed . In irregular weather conditions a platform shows an LF motion in the horizontal plane, i.e. surge, sway and yaw. These motions are caused by the various LF parts of the wavedrift forces. Analyses of the horizontal motions of moored structures show that the response from the weather includes three components, a mean displacement and an oscillating displacement due to WF and LF loads, Journèe and Massie (2001). A mean displacement of the platform is caused by the constant force components in the wind and current, and in addition to these there is a mean wavedrift force. By summing up these forces together with the restoring force from the platform and mooring system a new equilibrium position is obtained.

An oscillating displacement of the platform will occur from both the WF and LF contributions of the waves. HF correspond to the waves' rapidly varying parts and will give rise to first- order wave loads and displacement. Slow-drift forces are caused by the LF contribution of the waves, the LF wave drift forces, which can cause large motions if they coincide with the natural frequency of the platform, Journèe and Massie (2001).

The platform will be excited by the mean-drift and slowdrift forces caused by the current and waves. The waves' interaction with the platform and the velocity of the platform will cause a damping, and the current and waves will cause both damping and excitation simultaneously. The forces are reduced when the current and waves have opposite headings, MARINTEK (2010a).

3.3 Mooring system

The catenary mooringline damping of the platform motion is determined by the shape of the line, tension, and water depths, etc. For a platform operating in shallow and moderate water depths the damping will be more significant than for a platform in deep water, Huse (1992). This is due to the fact that the shape of mooring lines tends to become more taut instead of catenary with increasing depth, resulting in a platform motion that has a stronger coupling between the mooringline system and WF motions, Sjöberg and Bergdahl (1981).

3.4 Vortex effects on the mooring line

The forces due to viscous flow separation around the platform and mooring system causes vortex- induced motions, VIM. These motions are induced by vortex shedding, which gives rise to the VIM and contributes to the damping. Therefore this is to be included in the mooring analysis, ISO (2005).

Even though the time-domain method should incorporate all the effects, the oscillatory forces due to vortex shedding are not considered, MARINTEK (2008). Huse (1992) made a study of drag coefficients and came up with recommendations for both chain and wire rope including the effect of VIM. For wire rope the recommendation is to use $C_D = 1.8$ and for chain $C_D = 2.6$. The wire rope drag coefficient includes typical effects due to vibrations or vortex shedding, and it is further concluded that chains do not vibrate. These drag coefficients also correspond with the DNV recommendations in DNV-OS-E301.

3.5 Damping coefficient

The energy dissipation representing damping due to the mooring system can be determined by multiplication of the instantaneous horizontal line force in the direction of motion and the velocity and sumup over a period of time, Huse (1992). When computing energy dissipation, the mooring lines are the main contributors to the LF motion damping, but the effect of the HF motions should be considered since it can increase the damping considerably, Dercksen et al. (1992). The total energy dissipation, the sum of all the lines, can then be used for determining the linearized damping for the platform, Liu (1998).

The mechanical work done by the mooring system can be described as in Equation (3.3), with vectors in surge and sway, for the force experienced by the mooring system and the vessel velocity.

$$W = \int_0^T F(t)v(t)\,dt \tag{3.3}$$

Mean work done by the system is of more interest as in Equation (3.4), since the total work increases with time.

$$W_{mean} = \frac{1}{T}\int_0^T F(t)v(t)\,dt \tag{3.4}$$

The force term can be rewritten as a linear damper as in Equation (3.5).

$$W_{mean} = \frac{1}{T}\int_0^T F_d(t)v(t)\,dt = \frac{1}{T}\int_0^T cv(t)v(t)\,dt = \frac{1}{T}\int_0^T cv(t)^2\,dt \tag{3.5}$$

Using Equations (3.4) and (3.5) the damping coefficient c can be solved

$$\frac{1}{T}\int_0^T F(t)v(t)\,dt = \frac{1}{T}\int_0^T cv(t)^2\,dt \tag{3.6}$$

$$c = \frac{\int_0^T \frac{F(t)v(t)}{T}\,dt}{\int_0^T \frac{v(t)^2}{T}\,dt} = \frac{\frac{1}{T}\int_0^T F(t)v(t)\,dt}{\frac{1}{T}\int_0^T v(t)^2\,dt} = \frac{\int_0^T F(t)v(t)\,dt}{\int_0^T v(t)^2\,dt} \tag{3.7}$$

The mooringline damping contributions are dependent on the velocity of the platform and the force on the platform from the mooring lines. Depending on which motions that are included in the force and velocity the damping contribution will be different. In this thesis two types of calculations have been carried out, the first considering the total velocity and force as described above, while the second type uses only the LF force and the LF velocity. Due to the different damping contributions this leads to two damping coefficients; LF+HF and LF. According to Huse (1992), the LF damping coefficients are strongly influenced by the HF motion.

The damping coefficients for surge and sway, using the total force and total velocity components in each direction, can then be described as:

$$c_{surge} = \frac{\int_0^T F_x(t) v_x(t)\, dt}{\int_0^T v_x(t)^2\, dt} \tag{3.8}$$

$$c_{sway} = \frac{\int_0^T F_y(t) v_y(t)\, dt}{\int_0^T v_y(t)^2\, dt} \tag{3.9}$$

While using the second type with the total force but LF motion:

$$c_{surge} = \frac{\int_0^T F_{LF,x}(t) v_{LF,x}(t)\, dt}{\int_0^T v_{LF,x}(t)^2\, dt} \tag{3.10}$$

$$c_{sway} = \frac{\int_0^T F_{LF,y}(t) v_{LF,y}(t)\, dt}{\int_0^T v_{LF,y}(t)^2\, dt} \tag{3.11}$$

The mooringline damping can be expressed as a ratio of the critical damping, see Equation (3.12), to relate how large the mooringline damping is and its influence. With k as the restoring coefficient at the mean platform position, m is the platform mass including added mass, DVN (2010).

$$c_{critical} = 2\sqrt{km} \tag{3.12}$$

3.6 Energy dissipation

Energy dissipation from mooring systems due to drag forces can be calculated numerically according to Huse (1986). Analysing the motion of one individual line and summing up the contribution of energy dissipation from all lines, the total

approximate energy dissipation for the system is achieved. This theory was presented by Huse to predict and understand the damping contributions from mooring and riser systems. The damping effect can lead to a reduction in surge and sway amplitudes of the order of 20 per cent or more, such a reduction will have an important influence on, for instance, peak tension and safety factors in the mooring lines, Huse (1986).

Figure 3.1 shows Huse's model for a single catenary mooring line with a surge or sway motion s at the top of the line resulting in a transverse motion η of the mooring line. The energy dissipation per cycle is due to the transverse mooring line's drag force. The transverse motion of the line is the major contributor to the overall damping of the lines, Huse (1991). For this theory to be valid, the motion of the top end must be sinusoidal - drag forces must be normal to the line and motion components in the vertical plane of the line and the motion's frequency is sufficiently low so that a catenary shape of the line is obtained all the time, Huse (1986).

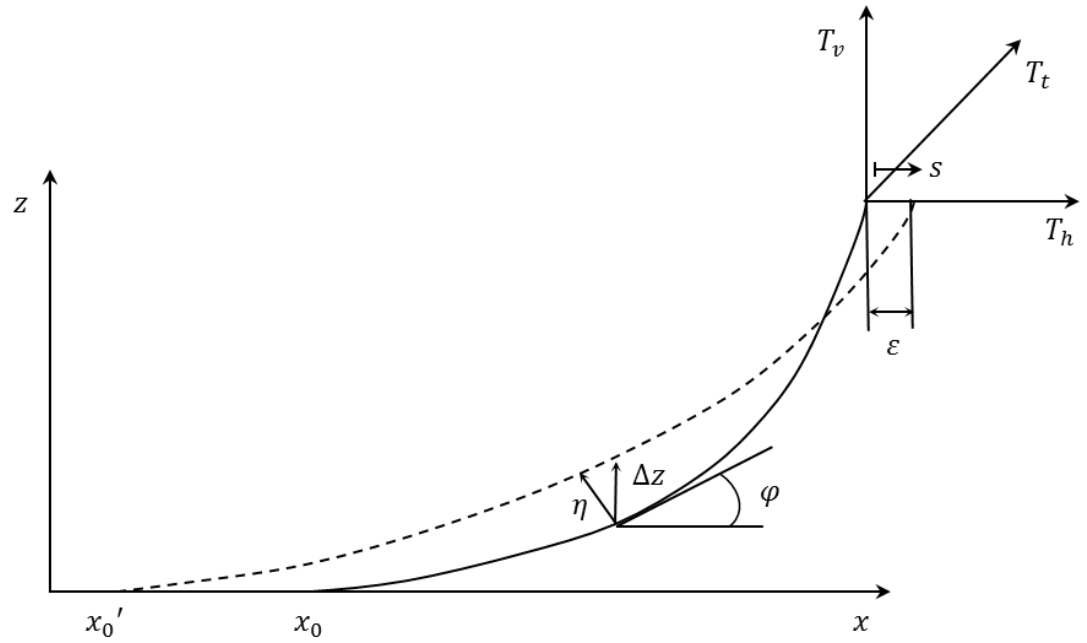

Figure 3.1 Change of single mooringline geometry due to motion at the top end of the line and the coordinate system

If a sinusoidal motion at the top of the line at the fairlead moves the mooring line a distance ε in the horizontal plane, see Figure 3.1, the displacement can be described by Equation (3.10). Assuming sufficiently low frequency motions the dynamic line tension τ given by Equation (3.11) can be added to the horizontal line tension component T_h in order to obtain the total horizontal tension. The transverse motion of the mooring line contributes to a motion of a line element with a distance η normal to the line tangent, as in Equation (3.12).

$$\varepsilon = \varepsilon_0 \sin \omega t \tag{3.10}$$

$$\tau = \tau_0 \sin \omega t \tag{3.11}$$

$$\eta = \eta_0 \sin \omega t \tag{3.12}$$

The energy dissipation ΔE per cycle of an element along the line can be calculated according to Equation (3.13) with the drag force ΔF_D in Equation (3.14).

$$\Delta E = 2\int_{-\eta_0}^{\eta_0} \Delta F_D \, d\eta \tag{3.13}$$

$$\Delta F_D = \tfrac{1}{2}\rho_W D C_D |\dot{\eta}|\dot{\eta}\Delta s \tag{3.14}$$

Inserting Equation (3.14) into (3.13) yields the energy dissipation for an element along the mooring line, as in Equation (3.15).

$$\Delta E = \tfrac{4}{3}\rho_W D C_D \omega^2 {\eta_0}^3 \Delta s \tag{3.15}$$

In order to calculate the energy dissipation by the whole line it is necessary to integrate Equation (3.15) along the line length. It is also necessary to know the amplitude of the transverse motion as a function of the surge or sway motion s or the horizontal lift-off point x. Let Δz in Equation (3.16) be the distance between the upper position z_u and lower position z_l of the mooring line during the period. Inserting Equation (3.16) into the motion amplitude equation (3.17) with the tangent angle φ in Equation (3.18) yields, according to the catenary formula, Equation (3.19).

$$\Delta z = z_u - z_l \tag{3.16}$$

$$\eta_0 = \tfrac{1}{2}\Delta z \cos\varphi \tag{3.17}$$

$$\cos\varphi = \frac{T_h}{T_t} \tag{3.18}$$

$$\cos\varphi = \frac{T_h}{\left({T_h}^2 + (T_h \sinh(\frac{p}{T_h}(x - x_0)))^2\right)^{\frac{1}{2}}} \tag{3.19}$$

Integrating Equation (3.15), together with Equations (3.17) and (3.19) the equation for energy dissipation for the whole line during one surge or sway cycle is obtained and presented in Equation (3.20), Huse (1986).

$$E = \tfrac{1}{6}\rho_W D C_D \omega^2 \int_{x_0'}^{x_{\max}} \frac{(\Delta z)^3 dx}{1 + \sinh^2(\frac{p}{T_h}(x - x_0'))} \tag{3.20}$$

4 Software procedure

The DNV software package SESAM has been used in this thesis for carrying out the analysis. The software package consists of different softwares depending on what simulations are intended to be performed. The following SESAM-softwares have been used; for the frequency-domain MIMOSA v.6.3-05, MARINTEK (2010a), and in the time-domain DeepC v.4.5-05, DNV (2010), which uses the software SIMO v.3.6, MARINTEK (2007), and RIFLEX v.3.6, MARINTEK (2010b). More information about the interaction can be found in Appendix A. All the software mentioned in the report refers to the versions and manuals stated above unless otherwise stated.

In addition to MIMOSA v.6.3, MIMOSA v.5.7-03 has been used. This is an older version but has the ability to calculate the mooringline damping, which is not possible in MIMOSA v.6.3. This option was removed in the versions following MIMOSA v.5.7 due to experiencing a non-stable behaviour.

Figures 4.1-4.3 show the graphical interface of the calculation domain generated in DeepC with the mooring system, lines and anchor points as well as the water surface and seabed.

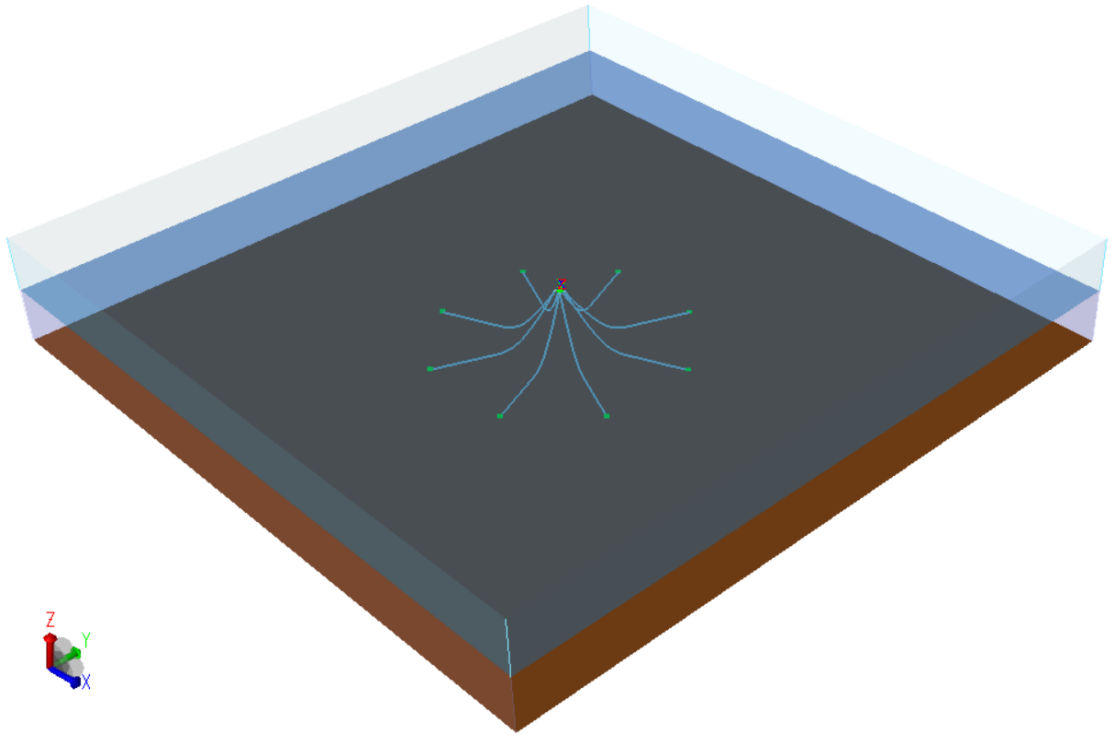

Figure 4.1 Isometric view of the domain in DeepC

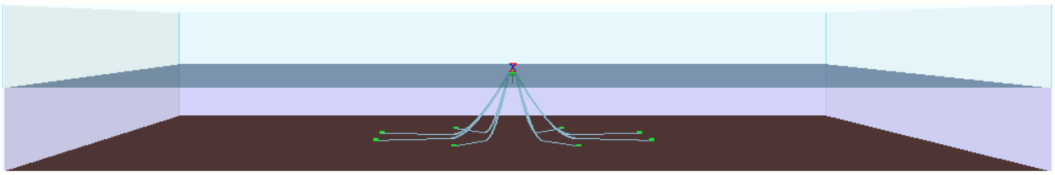

Figure 4.2 Side view of the domain in DeepC

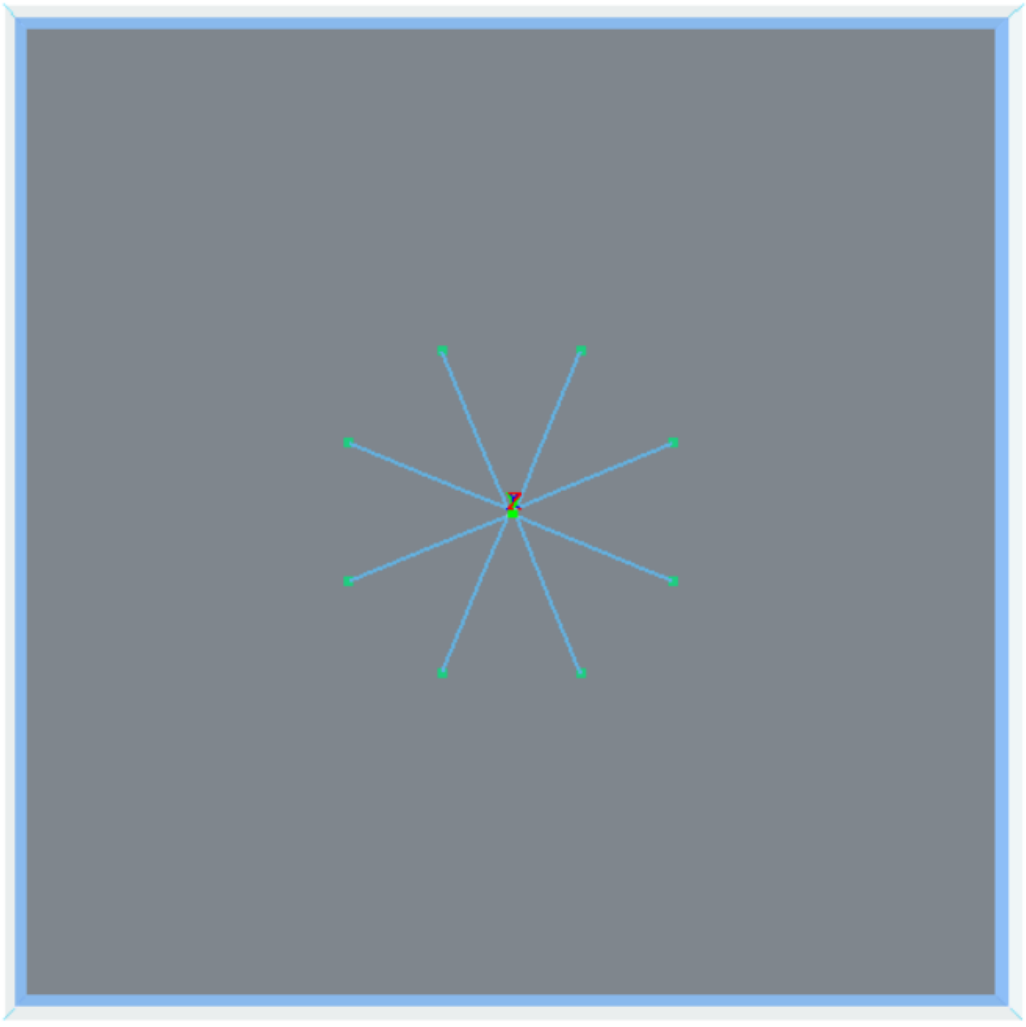

Figure 4.3 Top view of the domain in DeepC

4.1 Input data

The data used in the analysis for both MIMOSA and DeepC will be described in this section; the main particulars of the platform, environmental data and mooringsystem configuration.

The main particulars for the generic semi-submersible drilling platform can be seen in Table 4.1.

Table 4.1 Main particulars of the generic semi-submersible drilling platform

Length over all [m]	118.56
Breadth [m]	75.01
Depth [m]	45.15
Draught [m]	23.5
Gross tonnage [tonne]	35 568
Columns	6
Pontoons	2

The line characteristics and material data for the chain and steel wire rope used in both MIMOSA and DeepC are found in Table 4.2. For the different water depth either a chain or a combination of chain and steel wire rope is used.

Table 4.2 Mooring line characteristics

Characteristics	Chain	Steel wire rope
Nominal diameter [mm]	76	77
Weight in water [kN/m]	1.324	0.2845
Weight in air [kN/m]	1.5201	0.33
Axial stiffness, EA [kN]	5.235 E5	5.262 E5
Non-dimensional normal drag coefficient	2.6	1.8
Non-dimensional longitudinal drag coefficient	0.1	0.1
Minimum breaking load (MBL) [kN]	6013	6013

4.1.1 Mooring configuration

The configuration of the mooring system is governed by the safety factors in line tension stated in ISO (2005) with the additional note from NMD (2009) for Norwegian waters. To meet the requirements, the following has to be taken into account; line length, platform displacement and sea state.

The length of the mooring lines affects both the force experienced by the anchor and the line- tension safety factor. To ensure not having vertical forces on the anchor and getting anchor lift, a part of the mooring line has to lie on the seabed. The pre-tension of the lines will affect the surge and sway motion as well as the line-tension safety factor. With increasing water depth the weight of the mooring line will increase and a combination of materials such as steel wire rope and chain is suitable (kanske bättre med 'suitable') for reducing the weight, Bergdahl (1981)

The weather is omnidirectional and the safety factors in line tension have to be fulfilled for any given direction. To be able to meet the requirements, a thruster force is applied opposite to the environmental direction in order to decreases the static offset of the platform and reduce the line tensions.

The platform is in a survival condition with the riser disconnected and has no limitations in surge and sway displacement. Otherwise, the connection to the well would be a limiting factor and the pre-tensions would have been increased, a typical design criterion for the drilling riser joint angle is a maximum of 4° in drilling conditions and a maximum of 9° in non-drilling conditions, Bai and Bai (2005).

The line configurations have been designed in MIMOSA v.6.3 with respect to the various water depths and the chosen line configurations can be seen in Table 4.3. These configurations meet the linetension requirements with the aid of a thruster force. The pre-tension is chosen to not give too large a displacement and cause lift at the anchors. For more detailed data with different mooring system configurations, see Appendix B.

Table 4.3 Line configurations for the various water depths

Water depth [m]	Pre-tension [kN]	Thruster Force [kN]	Component length [m]		Total length [m]
			Chain (lower)	Steel wire rope (upper)	
100	800	3400	1800	-	1800
200	800	2700	1600	-	1600
400	800	1500	1600	-	1600
750	900	800	1300	700	2000
1250	900	800	1500	1100	2600

4.1.2 Environmental effects

The platform is considered to be in a survival condition with the environmental loads such as wave, wind and current acting on the platform. The weather is omnidirectional and the loads have both a static and a dynamic component. In the analysis, three main headings of the environmental loads have been implemented: 0°, 45° and 90° in the global coordinate system, see Figure 4.4. The northerly direction denotes the surge motion and the easterly direction denotes the sway motion.

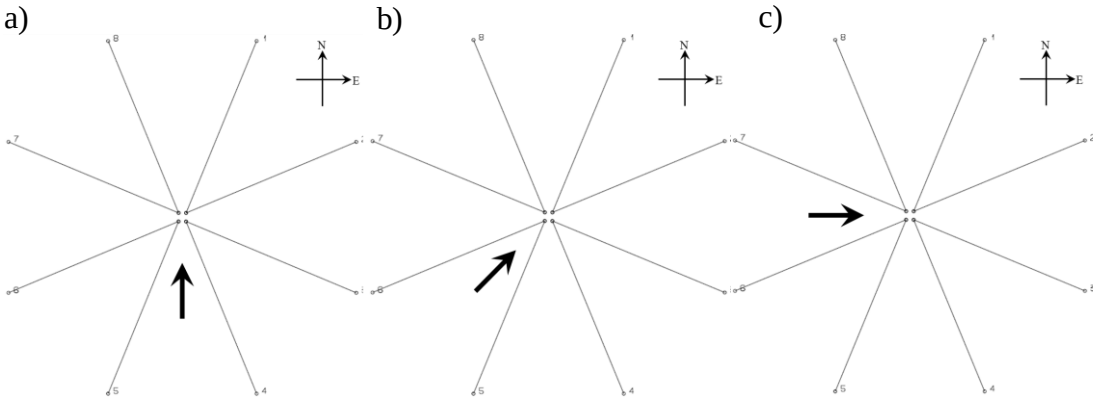

Figure 4.4 Environmental headings in a) 0° b) 45° c) 90°

The guidelines in NMD (2009) denote the extreme weather as a combination of a 100year wind and a 100year wave together with a 10year current at the location. The wind speed data refers to a design speed at an elevation of 10m above the still water level, ISO (2005). The wind spectrum is modelled as a constant speed onto which a varying speed component is added. The varying part of the wind is modelled by a gust spectrum, which gives the power density of the wind speed. In this analysis, the ISO 19901-1 spectrum has been implemented with a mean speed of 34 m/s.

The waves are represented by a JONSWAP spectrum with a significant wave height of 15m and a peak wave period of 16s with more detailed information in Table 4.4. The current acting on the platform is modelled as a constant horizontal force, and the current acting on the mooring lines is modelled as a horizontal force with a depth profile. The used weather data in the analysis is an average of fields in the North Sea for extreme weather conditions, see Table 4.4. Five different fields corresponding to water depths at 100m, 200m, 400m, 750m and 1,250m are analysed in MIMOSA and DeepC.

Table 4.4 Environmental parameters

Significant wave height (H_s) [m]	15
Peak wave period (T_p) [s]	16
Wave spectrum	JONSWAP
Form parameter (β)	1.25
Peakedness parameter (γ)	3.3
Spectrum width parameter (σ_a)	0.07
Spectrum width parameter (σ_b)	0.09
Mean wind speed [m/s]	34
Wind spectrum	ISO 19901-1
Surface current speed [m/s]	1

4.2 Analysis in the frequency-domain

The behaviour of the platform in a dynamic system is determined with respect to motion, displacement and mooringline tension. This can be achieved in a frequency-domain model or time-domain model. Dynamic analysis is carried out for both firstorder HF motions and secondorder LF motions in the frequency-domain, MARINTEK (2010a).

In frequency-domain approaches the equations of motion are described with respect to frequency rather than time. To be able to convert and linearize a given function or dynamic system into the frequency-domain a transformation operator has to be applied, either by an iterative approach or by linearization, for example a Laplace or Fourier transform. The frequency-domain method is always linear, based on the principle of linear superposition by, for example, linearization. All non-linearities should be eliminated, ISO (2005). In the transform of a dynamic system into the frequency-domain, the system is decomposed into a sum of sinusoidal waves with different amplitudes, frequencies and phase angles in order to generate a linear system representing the dynamic system.

The frequency-domain calculation for static and dynamic analysis of moored vessels is performed with the software MIMOSA. In the frequency-domain it is easy to obtain a first setup of the mooring system, the calculations include; static and dynamic environmental loads, platform motions and displacement, and line tension. The viscous damping from the platform is an input to the software from estimated values, for example model testing in a wind tunnel or wave basin. Damping analysis made in

MIMOSA has a tendency to be more conservative compared to analysis made in DeepC when calculating the damping, Lie et al. (2007).

Quasi-static and static analyses in the frequency-domain can be performed for nearly any type of mooring system, MARINTEK (2010a). A dynamic frequency-domain analysis is performed for both HF, LF motion and tension responses. The non-linear mooring and vessel response due to a secondorderinduced wave motion, i.e. LF motions, is calculated by linearizing the motions with a linear frequency-domain method in MIMOSA. The mooring and vessel response caused by the first-order waveinduced motion, i.e. HF motion, is calculated using a transfer function to linearize the motions.

In some cases for strongly non-linear systems it is not possible to assume loads to be linear. Then the frequency-domain assumption of a linear system is not valid and a time-domain analysis has to be applied, Journèe and Massie (2001). The calculations should then be verified with a time-domain analysis program that can account for non-linear systems, for example DeepC.

4.3 Analysis in the time-domain

The time-domain method can include non-linear effects such as drag and inertia forces, interaction between seabed and the lines, as well as the motion of the mooring line. At each time step the mass term, stiffness term and damping term are calculated and updated, ISO (2005).

The time-domain analysis can be either coupled or uncoupled. The uncoupled analysis computes the vessel and mooringline load effects separately. First it calculates the motions of the vessel and then applies these motions to the mooring lines. The disadvantage with this uncoupled analysis is that the dynamics of the mooring lines will not influence the WF motions of the floater. Mooring lines do not normally influence WF motion, but, for example, TLP is of importance. Mean loads are not accounted for in the mooring lines and the damping effect from the lines are not fully included. These effects affect the solution for deeper water and the analysis may not be correct, and this effect can alternatively be included in calculations of RAOs and implemented into the method. The coupled analysis solves the vessel and load effects simultaneously at each time step, which offers the advantage of including the interaction between the vessel and mooring lines, DNV (2005).

The time-domain analysis used in this thesis is non-linear, but the mass, damping and stiffness matrices are linearized. The fully non-linear dynamic analysis is rather timeconsuming due to the repeated assembly of mass, damping and stiffness matrices during the iteration at each time step, MARINTEK(2008).

The coupled equations of motion governing for the dynamic equilibrium can be seen in Equation (4.1), DNV (2005):

$$\mathbf{R}^I(\mathbf{r},\ddot{\mathbf{r}},t)+\mathbf{R}^D(\mathbf{r},\dot{\mathbf{r}},t)+\mathbf{R}^S(\mathbf{r},t)=\mathbf{R}^E(\mathbf{r},\dot{\mathbf{r}},t) \quad (4.1)$$

$$\mathbf{R}^I(\mathbf{r},\ddot{\mathbf{r}},t)=\mathbf{M}(\mathbf{r})\ddot{\mathbf{r}} \quad (4.2)$$

$$\mathbf{R}^D(\mathbf{r},\ddot{\mathbf{r}},)=\mathbf{C}(\mathbf{r})\dot{\mathbf{r}} \quad (4.3)$$

The inertia force vector $\mathbf{R}^I$ contains contributions from the mass matrix which includes structural mass and hydrodynamic mass being accounting for; added mass and structural acceleration terms in the Morison equation, and mass due to internal fluid flow in pipes.

The damping force vector $\mathbf{R}^D$ takes into account the internal damping matrix and hydrodynamic damping matrix which includes diffraction effects for partly submerged elements and specified dash pot dampers.

The internal structural reaction force vector $\mathbf{R}^S$ accounts for the energy dissipation from the structure.

The external force vector $\mathbf{R}^E$ accounts for weight and buoyancy, drag and wave acceleration terms in the Morison equation, specified discrete nodal point forces and forced displacements due to support vessel motions, MARINTEK (2008).

For more detailed information about the calculations, one may refer to the SIMO and RIFLEX theory manuals.

5 Results and discussion

This chapter presents the results of the analyses performed in the frequency-domain and time-domain. It is divided into three sections; the damping contribution from each line, followed by the total line damping, and, finally, a comparison of the platform motions and the influence of damping. In each section the results are discussed.

5.1 Mooringline damping

The mooringline damping in the time-domain has been calculated by using two methods, the first including both the low and high frequency platform motion, while the second only considers the LF platform motion. In the graphs following this section the first method will be referred to as LF+HF and the second as LF. The main focus is the LF+HF damping, but for comparison the LF will be considered, since ISO (2005) states that the LF motion is the dominant factor to the mooring- line damping and is also used in the study by Lie et al. (2007) .The results of the 400m case will be presented in this section and the other water depths are found in Appendix C, followed by a general discussion regarding all cases.

The results from the case of a 400m heading of 0° can be seen in Figure 5.1 showing the mooringline damping for LF+HF. In surge, the line damping is largest for lines no. 4 and 5 followed by lines no. 3 and 6 - these lines are opposite the environmental loads. The remaining lines go slack and do not contribute significantly to the damping since they have the same direction as the environmental loads. In sway, the damping is more evenly distributed between the lines - lines no. 4 and 5 contribute the most to the damping but are of less magnitude than in the surge direction. The remaining lines in sway show a higher degree of damping compared to the surge direction. The sway motion in 0° is not of interest because of its small motion and uncertainties.

In Figure 5.2, the comparison between the LF+HF and LF damping is shown. In surge, the LF predicts a higher damping, especially for lines no. 4 and 5. In sway, the damping is more evenly distributed and the magnitudes are similar between the methods.

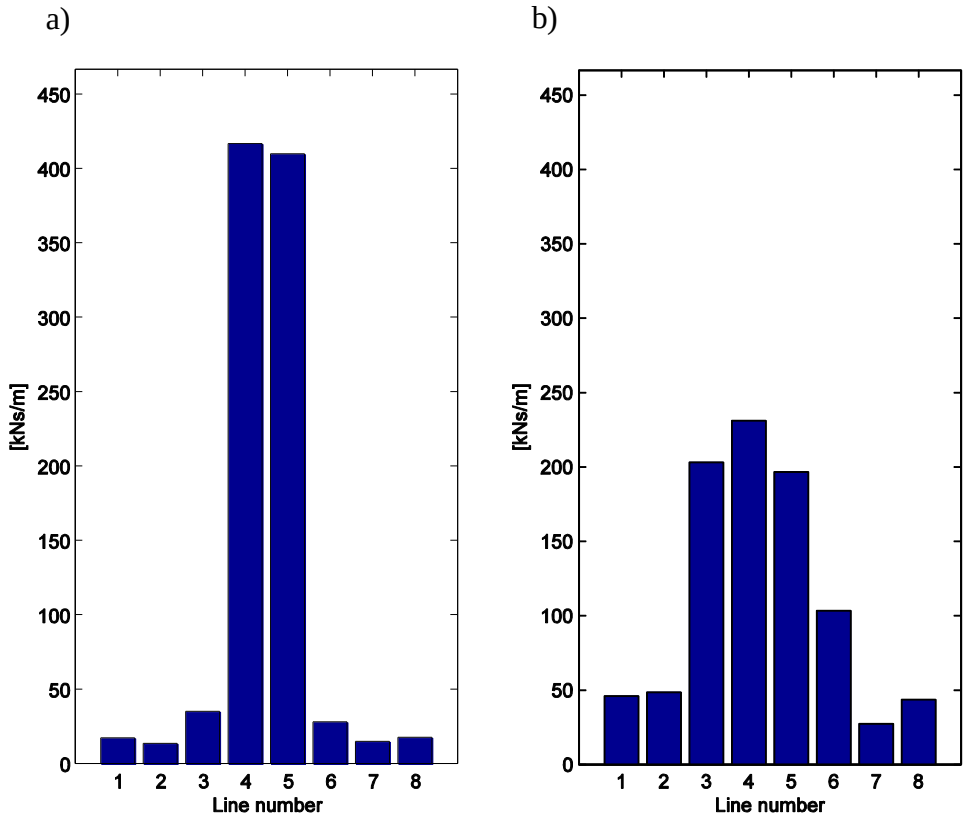

Figure 5.1 Line damping LF+HF for 400m heading 0° in a) surge and b) sway.

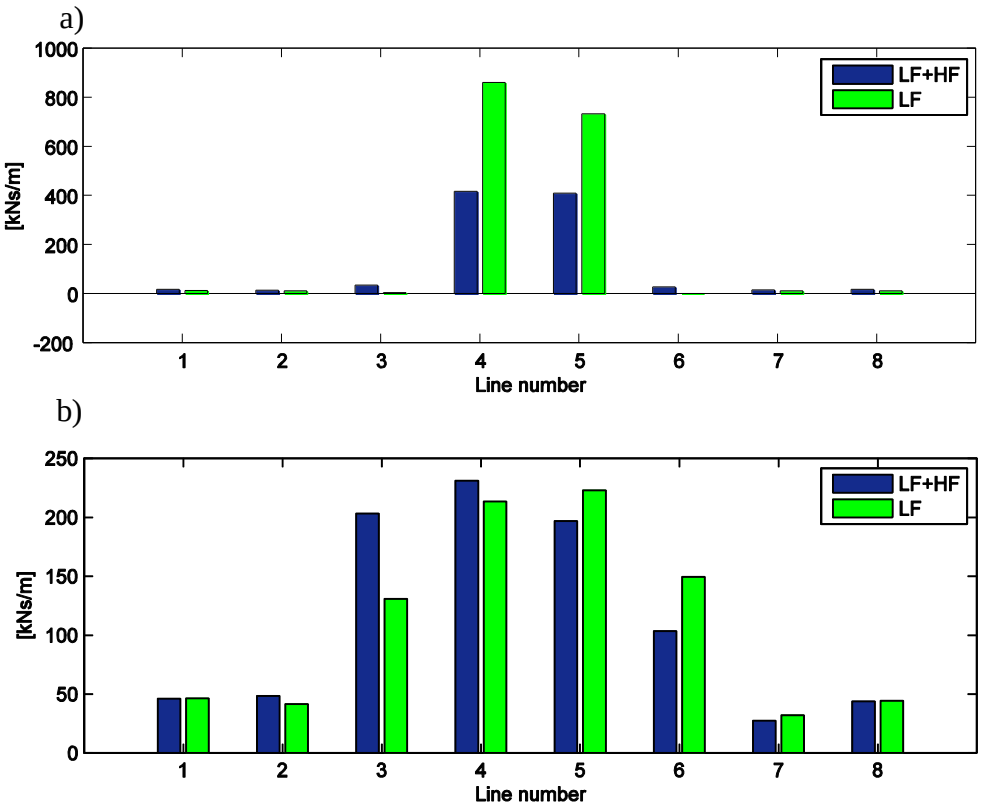

Figure 5.2 Line damping LF and LF+HF for 400m heading 0° in a) surge and b) sway.

The heading of 45° in Figure 5.3 shows large resemblances between the damping in surge and sway. Line no. 6 dominates the damping sway, followed by the two neighbouring lines, while the remaining lines have little influence. The same tendency is seen in surge with line no. 5 dominating, and worth observing is that line no. 7 in surge becomes negative. The surge and sway damping corresponds quite well, the damping from the lines is more evenly distributed and the values are a bit higher than in the case of 0°. The damping in surge and sway are of the same magnitude, which is to be expected since the platform has moved in the same order in both directions. Regarding the surge motion one should take line no. 7 into consideration as it is negative in many cases, which will give rise to a lower degree of damping.

The damping must be positive over the whole time series since the lines dissipate energy, and this can be negative for short time periods because of delays in the motions and phase lag. On the other hand, negative values would mean that the lines add energy to the system, which is not reasonable. The negative values could also be caused by a numerical error with the small but fast changing velocities, see Appendix C.2, which may give rise to negative values if they are out of phase with the line force. This could result in a negative number when adding the damping together for each time step.

The LF damping in 45° predicts a larger damping for most of the lines as can be seen in Figure 5.4. The lines contributing the most also show the largest overpredictions compared to LF+HF. Line no. 7 is negative in surge, but is less negative compared to the LF+HF.

In a heading of 90°, Figure 5.5 shows a large scatter in surge with lines no. 6 and 8 as the major contributors to the damping, while the other lines are small or even negative. This result is not to be considered reliable since line no. 6 is much larger than the second biggest line, which is significantly larger than the remaining lines. In sway, on the other hand, the line damping is more reasonable with lines no. 6 and 7 as the largest contributors followed by lines no. 5 and 8. The other lines do not contribute as much since they are in the same direction as the environmental loads and go slack.

The LF damping in 90° shows the same tendency as LF+HF in both surge and sway as can be seen in Figure 5.6. The lines in sway contributing the most to the line damping again predict a larger contribution by the LF method compared to LF+HF. The results in a surge of 90° cannot be considered reliable due to a scatter with the domination in lines no. 6 and 8 and large negative values in line nos. 4, 5 and 7. The large positive values in lines no. 6 and 8 are doubtful and the negative lines are not reasonable. This peculiar behaviour is present in all water depths for a surge of 90°.

In general, the negative line damping occurs in the same cases, 0° sway and 90° surge, for all water depths. These are the cases perpendicular to the environmental loads, and small but rapid platform motions are present, see Figure C.3, which could indicate and enhance a numerical error. At 0° the results are uncertain but have the same behaviour for all of the lines regardless of the water depth. The damping in sway is not as consistent as in surge - the platform velocities are very small as can be seen in Figure C.4 and there might be a numerical error. The surge motion at 90° is not of interest because of its small motion and of uncertainties.

In comparison, the LF method shows the same tendency as the LF+HF. It is difficult to see any pattern with the LF or LF+HF being larger than the other. The LF predicts a larger damping in the lines most exposed to the environmental loads, but for the other lines there is no clear trend.

The difference in the results between the methods could be explained by the variation in motions with larger LF motions than HF, in some cases the LF motion becomes greater than the LF+HF, which indicates that the HF part reduces the motion. From the results it is not clearly seen that the HF motion should either contribute or counteract to the damping. There might be a numerical error with phase-lag for the HF motion insofar as it increases and does not decrease the damping.

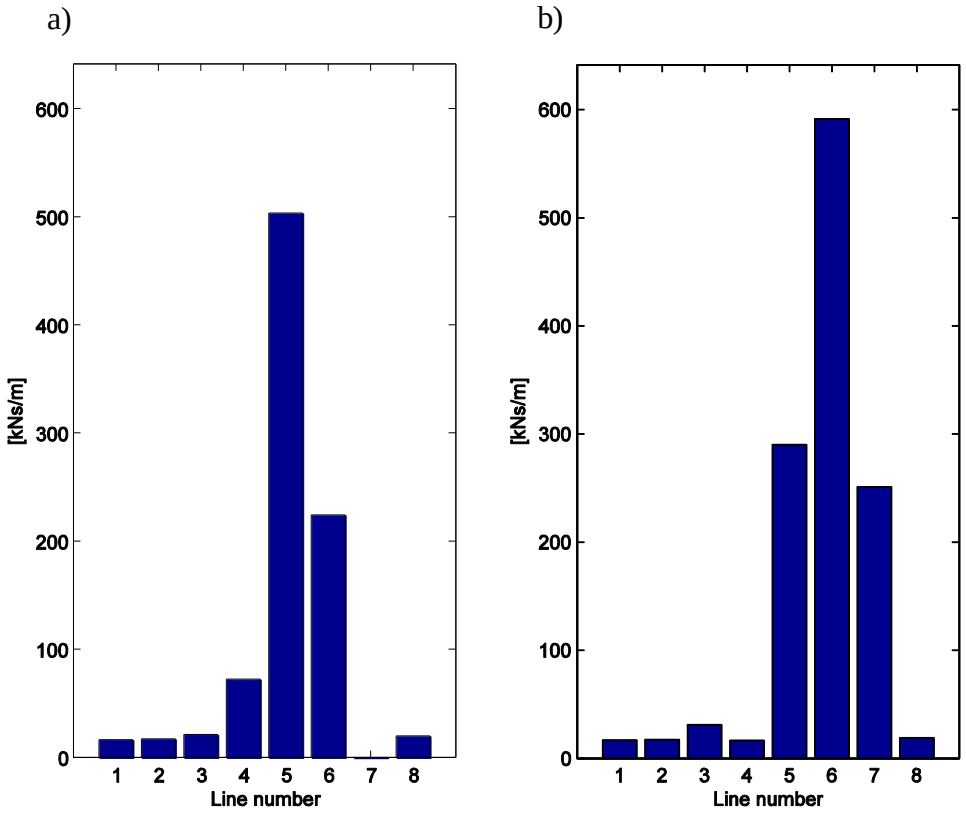

Figure 5.3 Line damping LF+HF for a 400m heading of 45° in a) surge and b) sway.

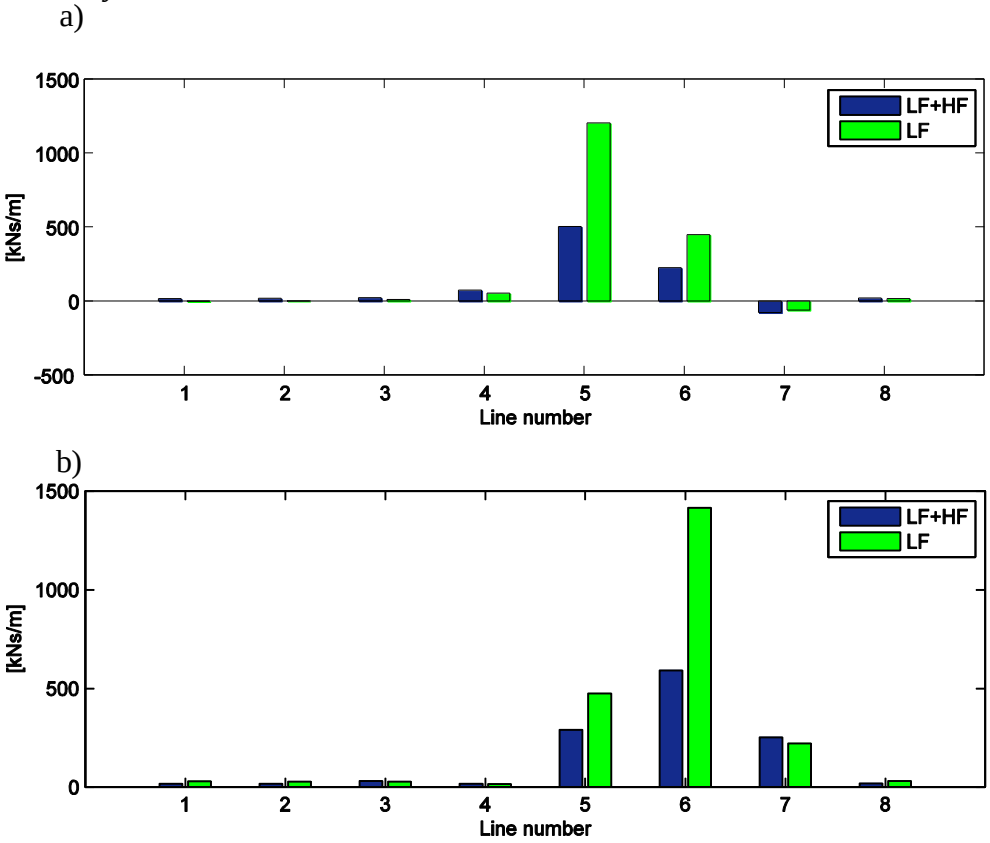

Figure 5.4 Line damping LF and LF+HF for a 400m heading of 45° in a) surge and b) sway.

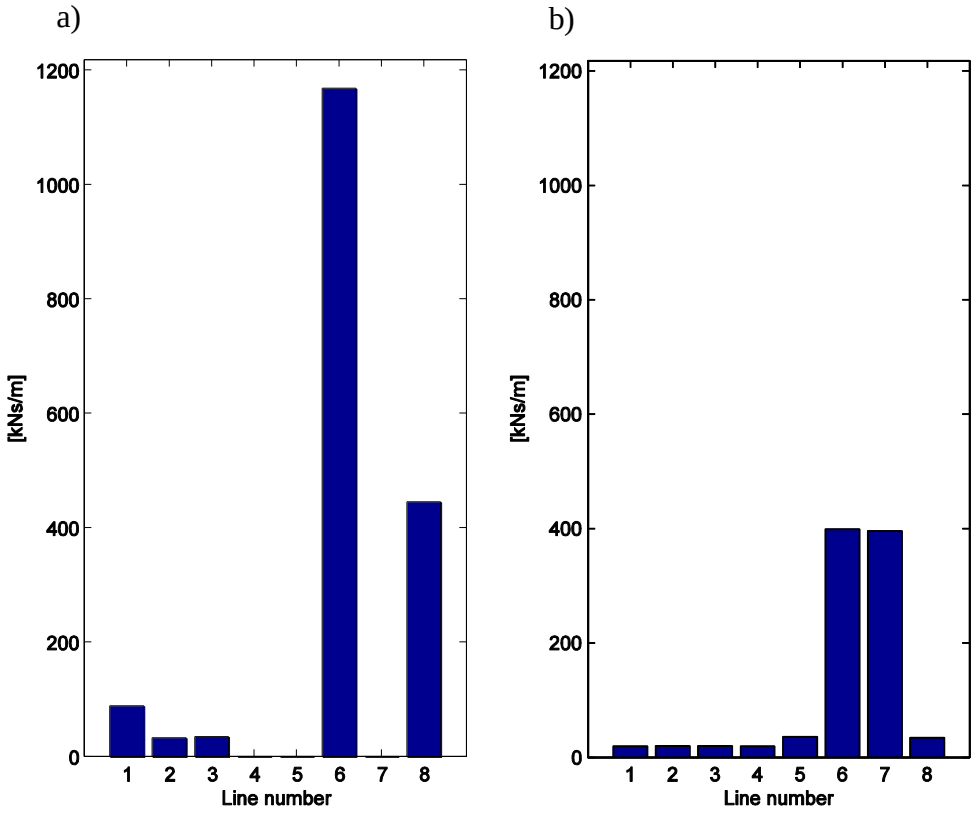

Figure 5.5 Line damping LF+HF for a 400m heading of 90° in a) surge and b) sway.

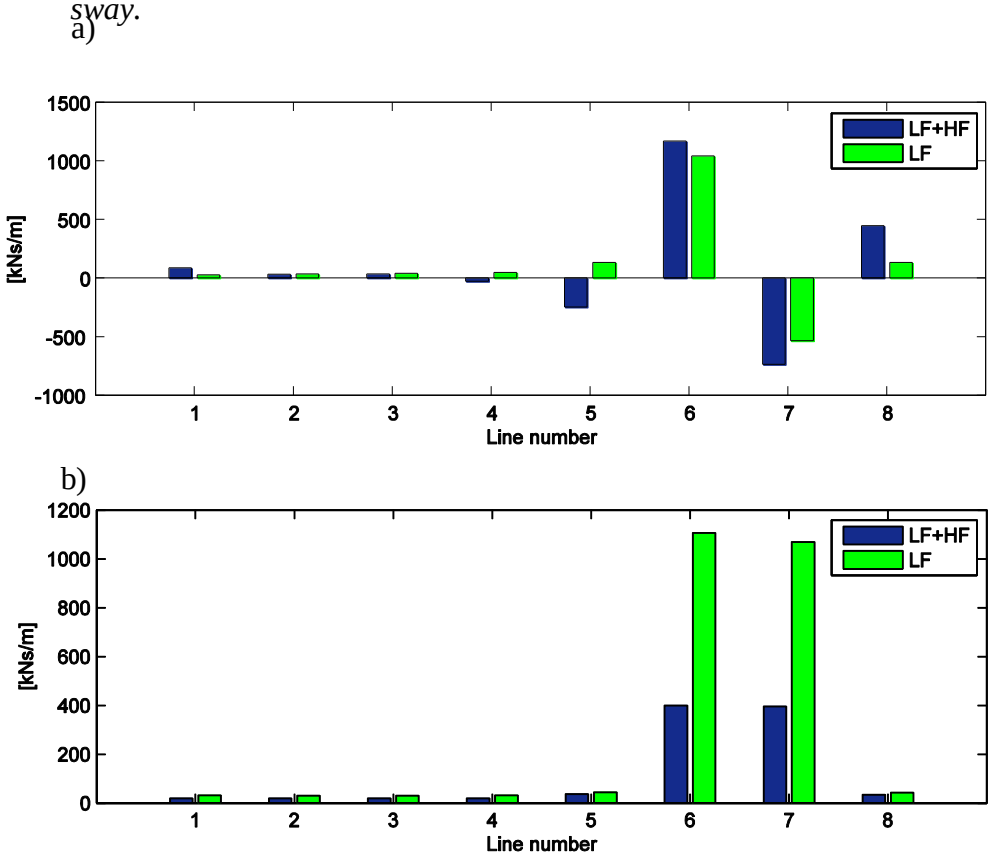

Figure 5.6 Line damping LF and LF+HF for a 400m heading of 90° in a) surge and b) sway.

5.2 Totalline damping

This section presents the total damping contribution from the mooring lines calculated in DeepC and MIMOSA v.5.7. The total damping is a sum of the lines' damping contributions, in surge and sway, as can be seen in Figure 5.7 and 5.8.

The calculated damping in DeepC is larger for all water depths and headings compared to the damping estimated in MIMOSA v.5.7. The trend in DeepC is that the total damping has its peak at 400m and then decreases with increasing water depth.

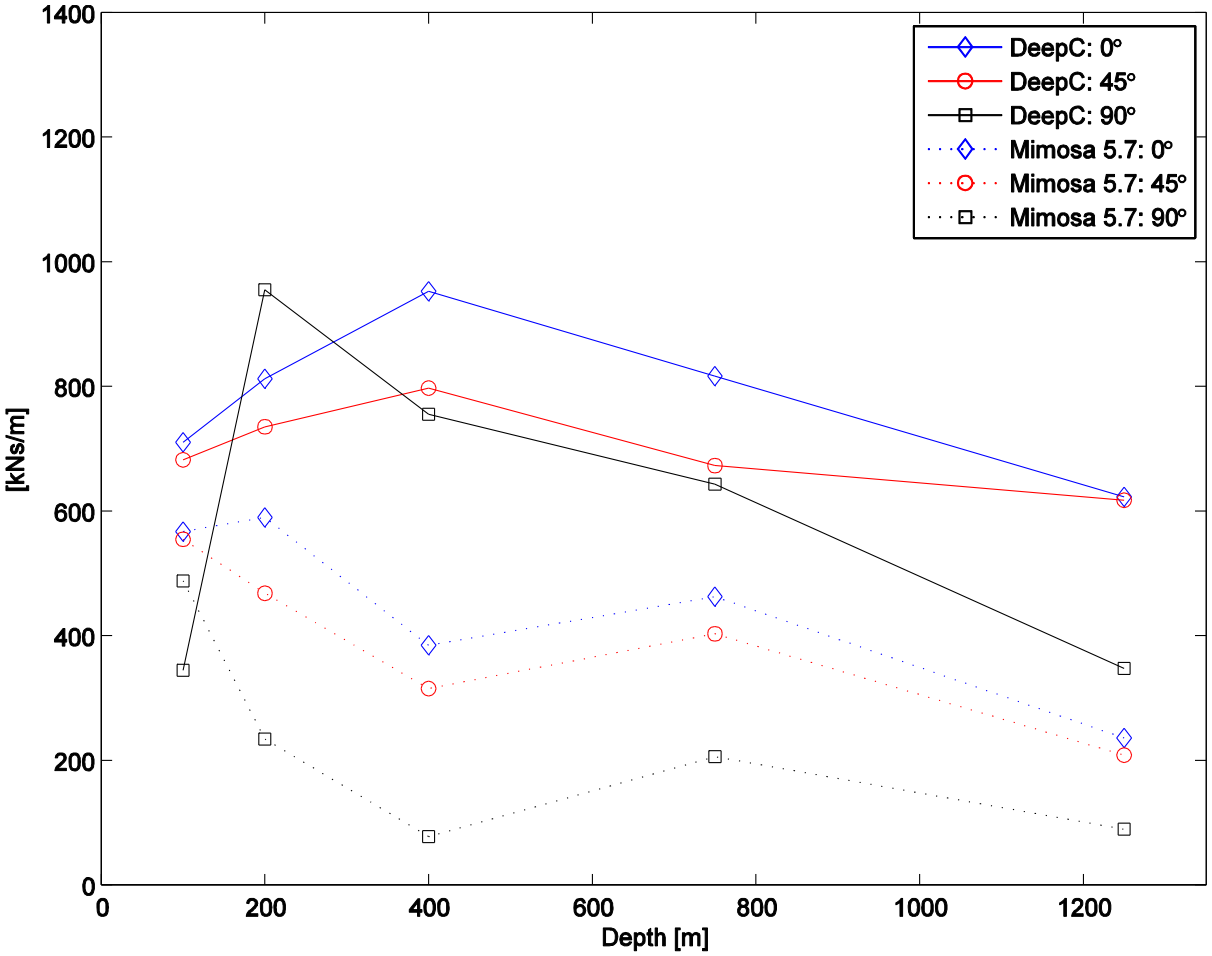

Figure 5.7 Total damping in surge for various water depths.

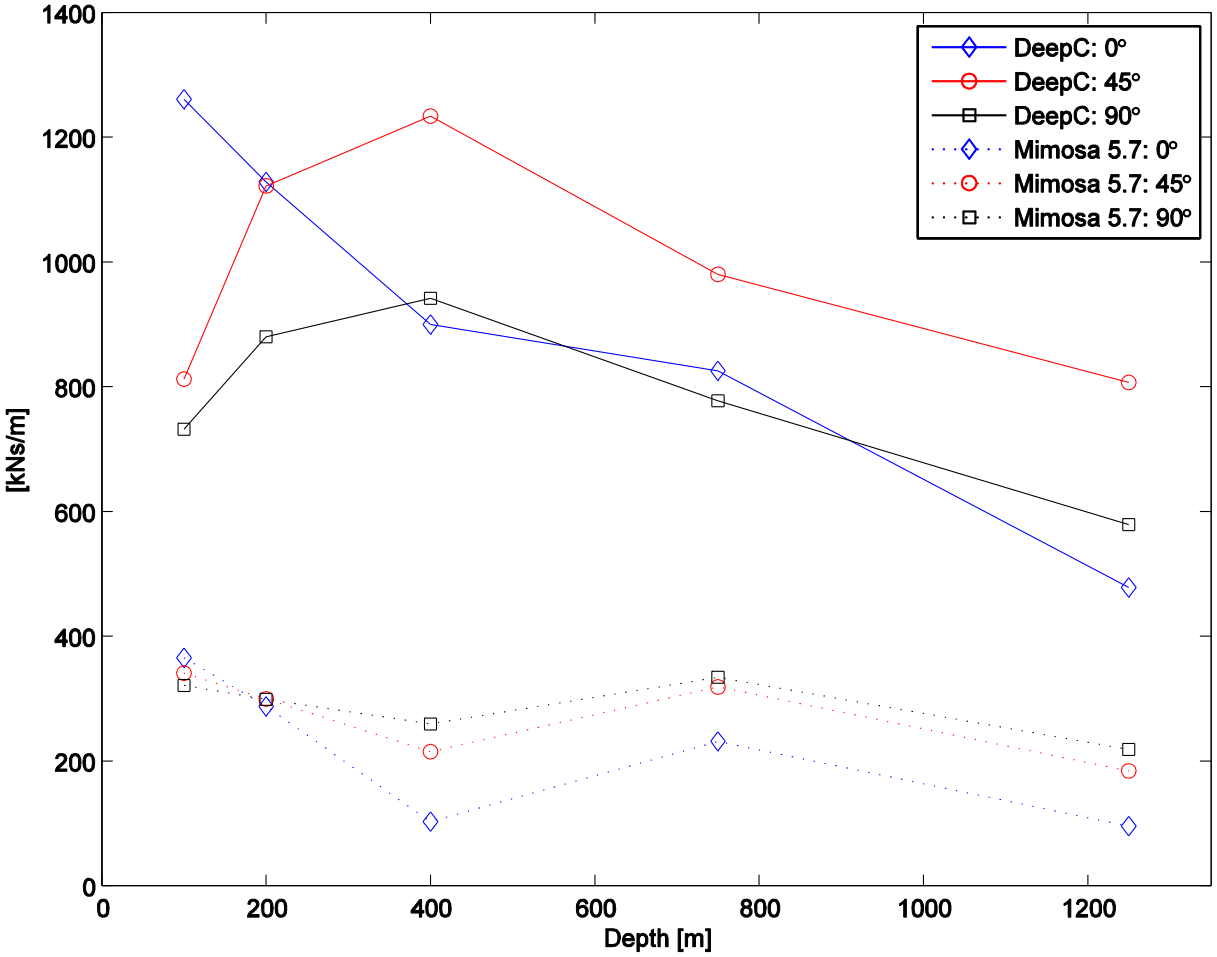

Figure 5.8 Total damping in sway for various water depths.

Table 5.1 shows an overview of the mooringline damping from DeepC as a ratio of the critical damping of the platform. The influence of the mooring lines is rather small at the most shallow depths, but increases with an increasing water depth. At 400m the damping force has its peak but as part of the critical damping it is relatively constant up to 1250m. The damping for cases at 0° and 45° shows the same tendency - - the damping in sway is larger than in surge. At 45° the damping ratio for surge and sway should possibly be more similar, since the influence from the negative values for line no. 7 in surge decreases the total damping. At 90° the values are not as consistent as at 45°, and in sway the damping is larger, and, considering, the unrealistic values in surge, it is not possible to draw any conclusions from this. Worth taking into account are the negative values for some of the mooring lines at 0° sway and surge at 90°, which will affect the total damping and hence decrease it. These two cases should not be considered reliable and the unrealistic damping affects the result to a large extent.

Table 5.1 Mooringline damping as part of critical damping.

Water depth [m]	Part of critical damp [%]					
	0°		45°		90°	
	Surge	Sway	Surge	Sway	Surge	Sway
100	8.0	14.5*	7.7	9.9	3.9*	8.2
200	15.3	22.7*	13.4	20.0	18.5*	15.2
400	27.2	34.3*	22.5	34.4	26.7*	23.2
750	24.9	30.4*	20.7	29.6	22.8*	21.6
1250	27.7	28.0*	28.0	36.0	19.2*	23.0

*Values should not be considered reliable

The damping ratio is quite constant over the water depths, and the damping in absolute values decreases with a decreased water depth. The stiffness of the system follows the same pattern and the factors affecting this are the mooringsystem configuration; pre-tension, line length and line type. The systems considered in this study are rather slack with a low pre-tension in the lines and thereby the static motions become large with increasing water depth. Also the pre-tension affect the damping in surge, such that the angle of the top end of the line becomes more vertical with an increasing water depth. This results in a smaller horizontal force component. With a more suspended line length the forces will be taken up as mechanical stretching and have less influence in the change of geometry, Huse (1991). The change in line material, at 750m to a combination of chain and wire, may have beneficial effects for the shape of the lines compared to chain for the shallower depths.

The mooring lines are taut at the larger water depths and the line shape is rather straight. With an increasing water depth the shape changes and at 400m the lines become more catenary and less taut. With more taut lines the influence of the current is smaller than for a slack line, and this is because a stiffer line will experience smaller motions and the energy dissipation will therefore be less, Liu (1998). This can explain why the mooring lines still contribute in the same range, in percentage, of the critical damping over the depth. The stiffness of the system and damping in absolute values decreases with an increasing depth.

The influence of different mooringline materials should be taken into consideration for the absolute line damping - at depths of 750 and 1250m wire is used for a major part of the mooring line. For a comparison of the software the choice of material is not an issue, as long as it is the same in all software.

5.3 Comparison of motion

In this section, the displacements for the different water depths are analysed and how this affects the mooringline damping. The comparison is carried out with frequency-domain and time-domain calculations in DeepC, MIMOSA v.5.7 and MIMOSA v.6.3. In MIMOSA v.6.3 the damping is divided into three cases; without line damping, with line damping from MIMOSA v.5.7 and the line damping from DeepC. In Figure 5.9-5.11 the dynamic motion in surge and sway is presented for the specified cases mentioned above. In Tables 5.2-5.4 the static equilibrium position in surge and sway is presented.

In Figure 5.9 the dynamic motion (maximum motion of 3.5h) in surge and sway is presented for the heading of 0°. For this heading the damping from DeepC in surge affects the dynamic motion more than for the other software, while the motion in sway for DeepC is higher than in the other cases. The damping predicted in DeepC is greater than in MIMOSA, which can explain the smaller motions in surge.

The dynamic motions for a 0° environmental heading are greater in surge than sway, which is expected due to head seas - the pontoons contribute more to the damping in head seas. Comparing the two cases MIMOSA v.5.7 and MIMOSA v.6.3 in surge with the same damping does not give the same response in motion as expected. The motions in surge coincide better than in sway except for the DeepC motion, which is lower. In head sea sway motions are not very reliable but still presented.

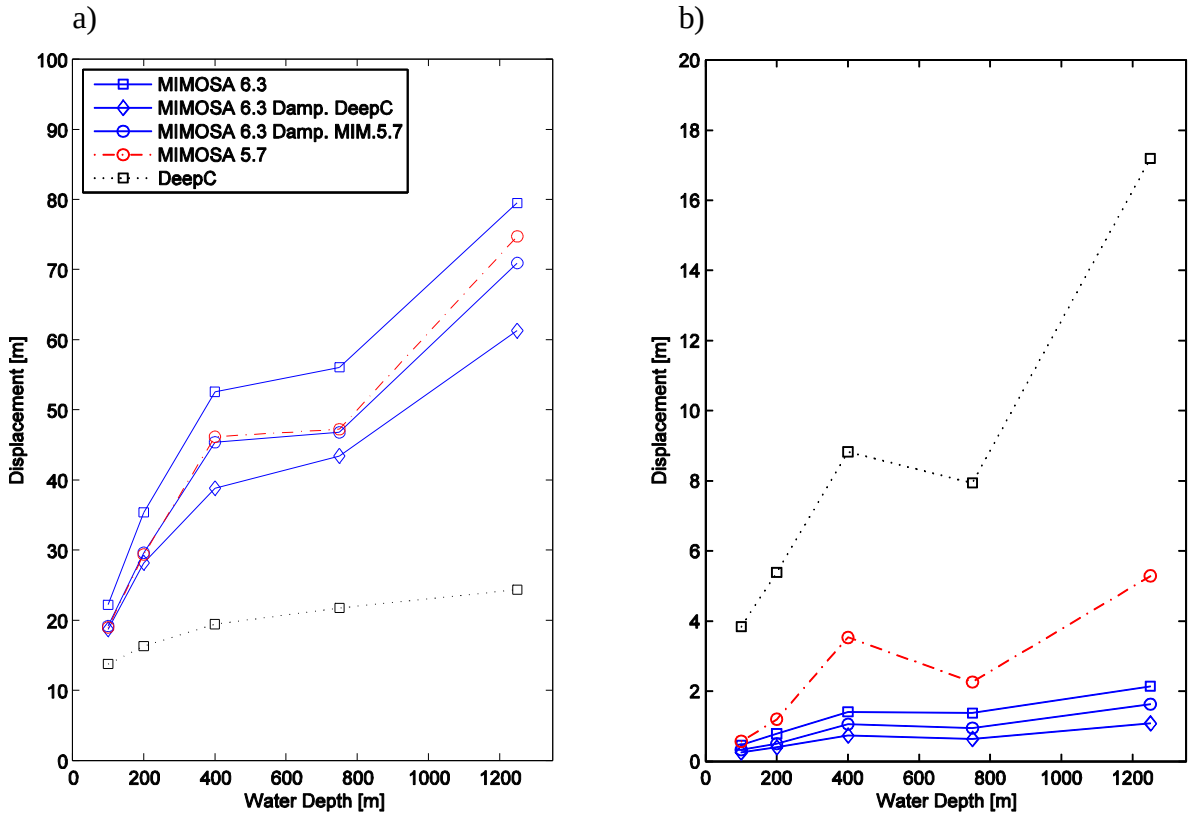

Figure 5.9 Dynamic motion in a) surge and b) sway for the platform at 0°.

The static motion (static equilibrium position) in surge and sway for the 0° environmental heading is presented in Table 5.2. It can be seen that the mooring systems used in the analyses are rather slack since there are large static displacements, especially for the larger depths. For the 0° heading the sway motion is small, which is expected as the weather is head sea and not beam sea.

Table 5.2 Static equilibrium position in surge and sway of the platform at 0°.

Water depth [m]	Static equilibrium 0° [m]					
	MIMOSA v.5.7		MIMOSA v.6.3		DeepC	
	Surge	Sway	Surge	Sway	Surge	Sway
100	1.4	-0.1	1.39	-0.28	3.36	-0.02
200	12.8	-0.6	12.82	-0.95	23.51	-0.05
400	98.2	-2.0	98.14	-3.39	135.9	-0.14
750	118.7	-1.0	118.65	-2.51	153.8	-0.14
1250	300.2	-3.2	300.03	-6.82	431.5	-0.33

The large difference in static equilibrium is not expected and is not reasonable. In Appendix D a further investigation and discussion is made, and the results from this is that the current and wind forces give rise to a large difference in offset, while the results coincide for the wave forces between the software.

Figure 5.10 presents the dynamic motion in surge and sway for the heading of 45°. The damping in surge from DeepC affects the dynamic motion more than the damping from the other software, while the motion in sway is lower and for some water depths even less than MIMOSA v.5.7. MIMOSA v.5.7 shows a larger displacement than MIMOSA v.6.3, which is peculiar since MIMOSA v.6.3 does not include any damping from the mooring lines which MIMOSA v.5.7 does.

The dynamic motions in surge and sway at 45° corresponds well and are of the same magnitude. This behaviour can be related to quartering seas giving the platform a similar displacement in both directions, although the surge motion is slightly larger than the sway due to the fact that the damping from the platform is not symmetrical. In Figure 5.9 a larger scatter between the cases in surge can also be seen than in sway.

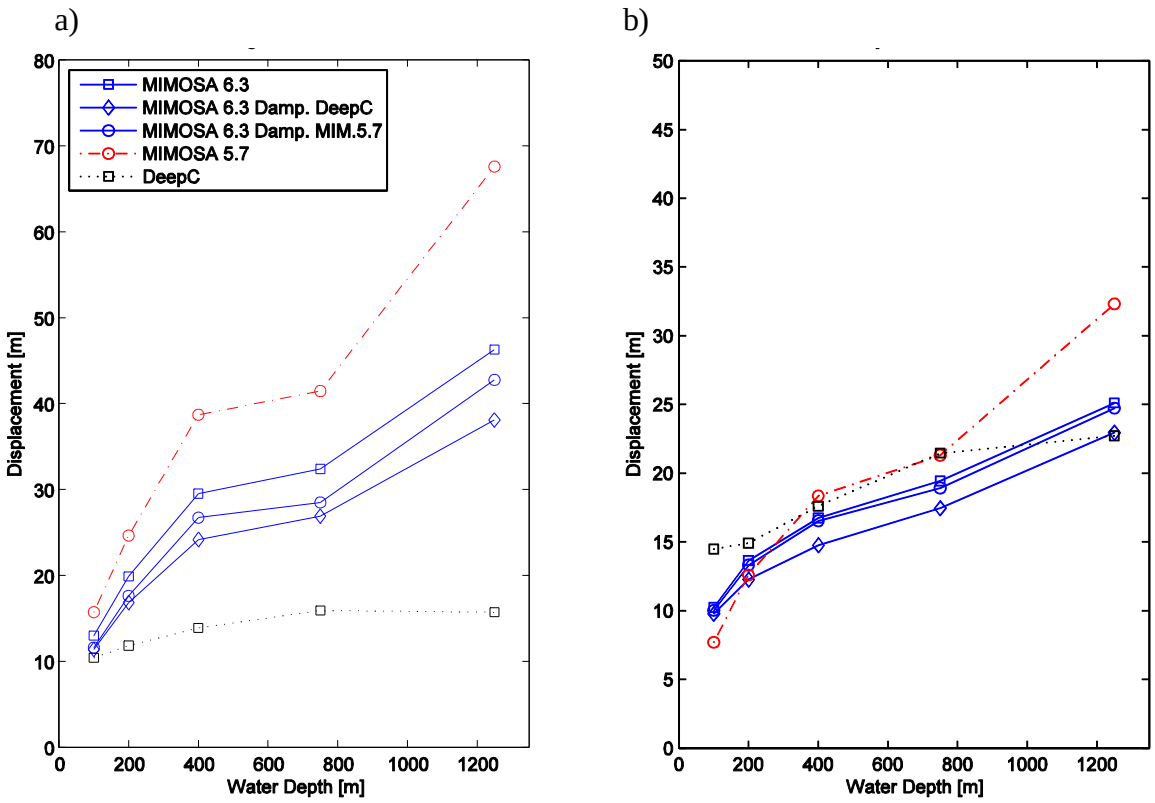

Figure 5.10 Dynamic motion in a) surge and b) sway for the platform at 45°.

Table 5.3 shows the static motion in surge and sway for the 45° environmental heading. The same behaviour as for 0° is observed with great displacements due to a slack mooring system.

Table 5.3 Static equilibrium position in surge and sway of the platform at 45°.

Water depth [m]	Static equilibrium 45° [m]					
	MIMOSA 5.7		MIMOSA 6.3		DeepC	
	Surge	Sway	Surge	Sway	Surge	Sway
100	2.9	2.9	2.88	4.35	5.07	8.62
200	13.9	17.8	13.85	17.77	20.19	28.62
400	77.4	89.3	77.35	89.35	95.21	118.30
750	93.6	107.6	93.57	107.64	114.50	138.11
1250	230.1	262.6	230.06	262.62	296.80	348.81

In Figure 5.11 the dynamic motions in surge and sway are presented for the 90° heading. The damping from DeepC in sway affects the dynamic motion more than the damping from MIMOSA. The surge motions for this heading are small compared to the sway motion, hence the rather small differences between the cases in surge, except for the case MIMOSA v.5.7.

The dynamic motions for a heading of 90° are larger in sway than surge due to beam sea. The motions in sway coincide better than in surge for the different software, with the exception of DeepC which predicts a lower motion. In beam sea surge motions are not very reliable but still presented.

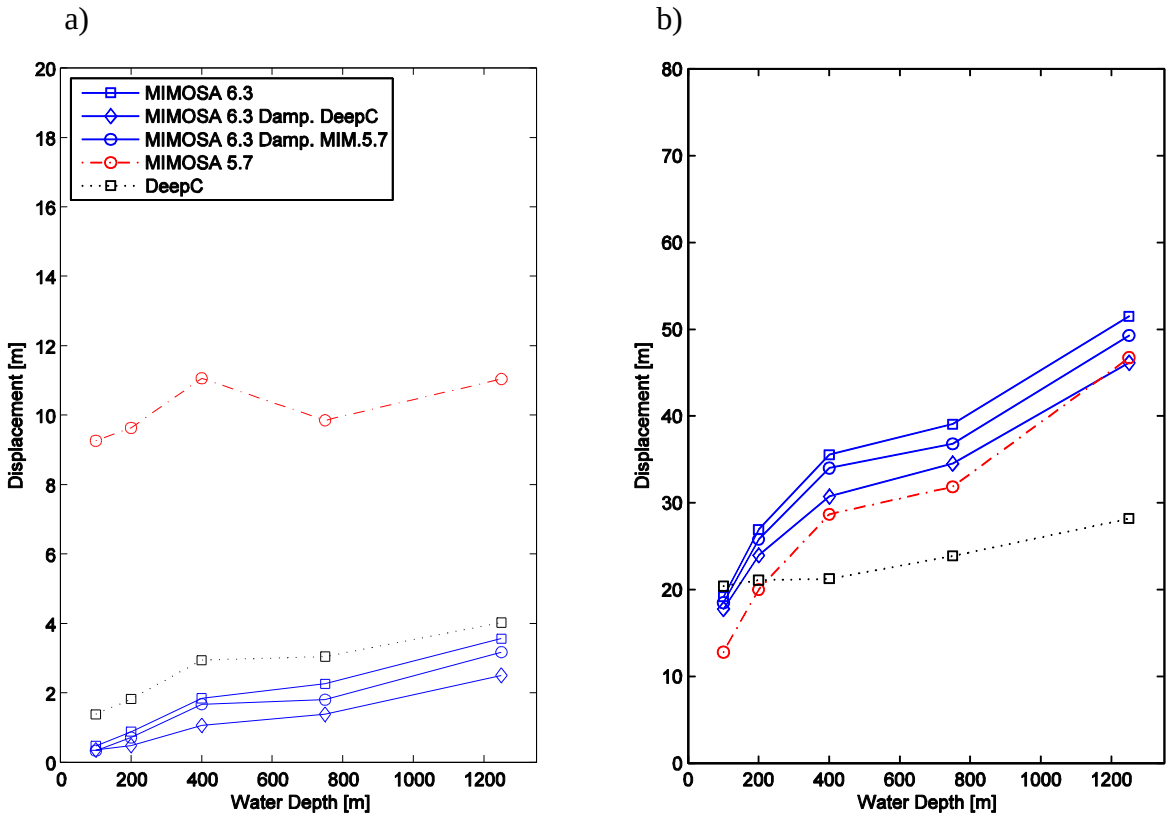

Figure 5.11 Dynamic motion in a) surge and b) sway for the platform at 90°.

The static motion in surge and sway for the heading of 90° is presented in Table 5.4. It can be seen that the mooring systems used in the analyses are rather slack and therefore experience a great offset. For the environmental heading at 90° the surge motion is small, which is expected as the weather is coming in as beam sea and not head sea.

Table 5.4 Static equilibrium position in surge and sway of the platform at 90°.

Water depth [m]	Static equilibrium 90° [m]					
	MIMOSA v.5.7		MIMOSA v.6.3		DeepC	
	Surge	Sway	Surge	Sway	Surge	Sway
100	-0.2	4.6	-0.2	4.62	0.08	9.055
200	-0.6	21.3	-0.59	21.26	0.17	33.58
400	-2.1	116.1	-2.07	116.07	0.44	150.1
750	-2.1	139.8	-2.08	139.76	0.53	176.7
1250	-5.1	343.8	-5.1	343.8	1.23	456.3

In order to verify the motion from DeepC, the damping is inserted into MIMOSA v.6.3. The motion in MIMOSA v.6.3 should decrease and the damped motion should correspond to the DeepC motion as a confirmation of the damping from DeepC. From the previous figures there is no clear connection between the motion in DeepC and MIMOSA v.6.3 including the DeepC damping, but a decrease in motion is observed when the damping is included.

Through the large displacements it is possible to see that the system is quite slack. The low pre-tension combined with the greater water depths results in a smaller line damping, as described in the previous section with the shape and angle of the lines. The motions in the same heading as the environmental loads are great for all the cases, i.e. surge and sway for head and beam sea, respectively .

Comparing the surge and sway motion at 0° and 90°, respectively, the heading motions should be in the same order, the motions correspond rather well, see Figures 5.9 and 5.11. The motions between the software show the same trend, while the magnitude differs to some extent, with DeepC predicting a higher motion in all the cases. The sway motion at 90° is slightly larger than the surge at 0°.

The results seem reasonable with large a surge motion of 0° and small sway motions, but with an uncertainty in sway, and the opposite for 90° with large sway motions and small surge motions also with an uncertainty due to small motions. While at 45° the motion is more equally distributed in surge and sway with roughly the same magnitude. There is a greater displacement in sway, which could be explained by the pontoon heading and the non-symmetric topside.

The motions in the shallow water depths are moderate even though the damping is small, the motion increases with the depth and after 400m the damping decreases in absolute numbers, but as a percentage of the critical damping it increases with the depth.

6 Conclusions

The viscous damping contribution has been studied in surge and sway for a mooringline system of a semi-submersible drilling platform with the influence of increasing water depth. Frequency- domain and time-domain analyses were performed for five water depths and three environmental headings; 0°, 45° and 90°.

The time-domain analysis shows that the damping contribution from the mooring system is nearly twice the damping calculated in the frequency-domain. There is a large scatter between the methods, with the time-domain predicting greater damping contributions for all water depths and headings. Results from the frequency-domain analysis will be more conservative than the results in the time-domain, since not all effects are included.

The damping in absolute numbers has its peak at around 400m and with an increasing water depth the damping decreases. The line damping as part of the critical damping shows a different behaviour and is rather constant over the water depths, even though the critical damping decreases with increasing depth. This can be explained by the mooring system becoming more slack with an increasing depth and therefore giving a decrease in system stiffness, which will result in a lower critical damping.

The study indicates that the damping contributions from the mooring lines are significantly higher than the guidelines stated in DNV-OS-E301. The line damping in surge and sway for the heading of 0° is 8-28 and 14-34 percent, respectively, of the critical damping. At a heading of 45° it is 8-28 and 10-36 percent for surge and sway, respectively, and at a heading of 90° it is between 4-27 and 8-23 percent. Due to numerical issues the results at 0° surge and 90° sway cannot be considered reliable. The conclusion is that further studies are needed to get a better overview of the line damping in deeper water.

The outcome from frequency-domain and time-domain analysis shows that the highest mooring- line tension and damping occurs in lines opposite the environmental loads. Therefore, damping in surge and sway motion differs among the cases. It is further concluded that the platform motion is decreased by the mooringline damping. The great differences in static equilibrium indicate that the environmental loads are different between the software with DeepC experiencing larger loads, hence the damping may be overestimated.

Finally, the study indicates that there is a significant viscous damping effect to consider when using mooring lines for stationkeeping and the damping should always be accounted for in the analysis. Moreover, there is insufficient information in classification rules as to how the line damping should be accounted for, regardless of calculation method in the mooring analysis.

7 Future work

The objective was to establish realistic damping levels from the mooring lines with an increasing water depth. The damping levels concluded are uncertain since the mooring systems used throughout the analyses were rather slack and as a result the platform motions were quite large, which are not feasible for a real platform. For further investigations it would therefore be favourable to have a stiffer system. This can be achieved with larger pre-tensions or an automatic dynamic positioning system, which would not allow for as large static displacements. A study regarding the contribution or counteraction of the highfrequency motion to the mooring line damping is needed.

Moreover, the risers were not considered in this study, but would contribute to the damping of the platform. To what extent risers, fixed or flexible, would contribute to the damping is difficult to state, but flexible risers are similar to mooring lines and it is recommended to investigate this.

The number of mooring lines is an important factor for the damping and it would be of interest to analyse a platform with more than 8 lines and a different anchor pattern. Therefore, further study of the effects of using buoys and clump weights to have different line shapes is suggested.

With decreased water depth the use of synthetic fibre rope is becoming more common and therefore this would be of interest to study. The damping would be affected with this change in material due to different drag forces and stiffness as well as geometry change.

Finally, since the mooring line damping is dependent on sea state it is of interest to examine the damping levels for other cases rather than the extreme conditions used in this study.

8 References

Bai Y. and Bai Q. (2005): *Subsea Pipeline and Risers*. Elsevier, Oxford.

Chakrabarti, Subrata K, (2005): *Handbook of offshore engineering*. Vol. 1. Elsevier Science & Technology, Amsterdam, 2005.

Dercksen A., Huijsmans R.H.M, and Wichers J.E.W. (1992): An Improved Method for Calculating the Contributon of Hydrodynamic Chain Damping on Low-Frequency Vessel Motions (OTC6967). In: Proceedings of OTC 24th annual Offshore Technology Conference, Houston, Texas, May 4-7, 1992, pp. 209-218.

DNV [Det Norske Veritas] (2010): *Offshore Standard DNV-OS-E301 Position mooring*, Det Norske Veritas, Høvik, Norway.

DNV [Det Norske Veritas] (2010): *Sesam user manual; DeepC*, DNV, Høvik, Norway.

DNV [Det Norske Veritas] (2005): *Sesam user manual; DeepC theory*, DNV, Høvik, Norway.

Faltinsen O.M (1993): *Sea loads on ships at offshore structures*. Cambridge University, Cambridge.

Huse E. (1986): Influence of mooring line damping upon rig motions (OTC5204). In: Proceedings of OTC 18th annual Offshore Technology Conference, Houston, Texas, May 5-8, 1986, pp. 433-436.

Huse E. (1988): Practical estimation of mooring line damping. (OTC5676). In: Proceedings of OTC 20th annual Offshore Technology Conference, Houston, Texas, May 2-5, 1988, pp. 543-552.

Huse E. (1991): New developments in prediction of mooring system damping. (OTC6593). In: Proceedings of OTC 23rd annual Offshore Technology Conference, Houston, Texas, May 6-9, 1991, pp. 291-298.

Huse E. (1991): *A note on time-domain simulations of vessel motions including mooring system damping.* MARINTEK Project Report No. 513006.10.01, Trondheim, 1991.

Huse E. (1992): *Mooring line damping summary and recommendations.* MARINTEK Project Report No. 513003.00.05, Trondheim, 1992.

International Standard [ISO] (2005): *Petroleum and natural gas industries- Specific requirements for offshore structures, Part 7: Stationkeeping systems for floating offshore structures and mobile offshore units*, ISO, ISO 19901-7:2005(E), Geneva, Switzerland.

Journèe J.M.J, Massie W.W (2001): *Offshore Hydromechanics*. Delft University of Technology, Delft.

Lie H, Gao Z, Moan T (2007): Mooring line damping estimation by a simplified dynamic model (OMAE2007-29155). In: Proceedings of the 26th International Conference on Offshore Mechanics and Arctic Engineering, San Diego, California, USA, June 10-15, 2007, pp. 1-8

Liu Y. (1998): *Dynamics and Extreme Value Problems for Moored Platforms*. Report Series A:29. Department of hydraulics Chalmers University of Technology, Gothenburg.

MARINTEK [Norwegian Marine Technology Research Institute] (2010a): *MIMOSA V6.3- User's Documentation*, MARINTEK, Trondheim, Norway.

MARINTEK [Norwegian Marine Technology Research Institute] (2007): *SIMO-User's Manual Version 3.6*, MARINTEK, Trondheim, Norway.

MARINTEK [Norwegian Marine Technology Research Institute] (2008): *RIFLEX-Theory Manual Version 3.6*, MARINTEK, Trondheim, Norway.

MARINTEK [Norwegian Marine Technology Research Institute] (2010b): *RIFLEX-User's Manual Version 3.6*, MARINTEK, Trondheim, Norway.

Moberg G. (1988): *Wave forces on a vertical slender cylinder*. Department of Hydraulics Chalmers University of Technology, Gothenburg.

Norwegian Maritime Directorate (NMD) (2009): *Regulation of positioning- and anchoring systems on mobile offshore units* (Forskrift om posisjonerings- og ankringssystemer på flyttbare innretninger (Ankringsforskriften 09)), NMD, Norge.

Sjöberg A, Bergdahl L (1981): *Förankringar och förankringskrafter*. Department of Hydraulics Chalmers University of Technology, Gothenburg.

Vasudevan S, Westlake P (2012): Investigation on the use of different approaches to mooring analysis and appropriate safety factors. (OMAE2012). In: Proceedings of ASME 2012 31st International Conference on Ocean, Offshore and Artic Engineering, Rio de Janeiro, Brazil, July 1-6, 2012, pp. 1-6.

Wilson James F. (2003): *Dynamics of Offshore Structures (2nd edition)*. New Jersey, USA.

Appendix A: Program interactions

DeepC is a graphical software using the two programs RIFLEX and SIMO, developed by MARINTEK. RIFLEX is a program for analysis of slender structures, mainly flexible riser systems but can be applied to all forms of slender structures, i.e. mooring lines MARINTEK (2010b). SIMO is a program for motion and stationkeeping for floating vessels and suspended loads MARINTEK (2007). RIFLEX and SIMO consist of different modules for performing the calculations as can be seen in Figure A.1. Below is a short description of the modules for RIFLEX;

- INPMOD reads the input data and it organizes it for further analyses.
- STAMOD performs static analyses and the results are used for defining the initial configuration for the dynamic analyses and element mesh as well as creating the required data for finite element analysis.
- DYNMOD performs time-domain dynamic analyses. Time series are generated with the desired data.

The modules in SIMO are INPMOD, STAMOD and DYNMOD. They have the same function as in RIFLEX, and INPMOD reads the input data; STAMOD is the initial condition and static equilibrium; DYNOD is the time-domain simulation.

For post-processing, two modules are used in each software. In SIMO the modules are S2XMOD and PLOMOD and in RIFLEX OUTMOD and PLOMOD. S2XMOD and OUTMOD make it possible to export the time series and PLOMOD is an animation tool for visualizing the dynamic behaviour of, for example, the mooring lines.

For further analysis, the time series is exported to MATLAB in order to calculate the damping coefficient and statistical data of the time series.

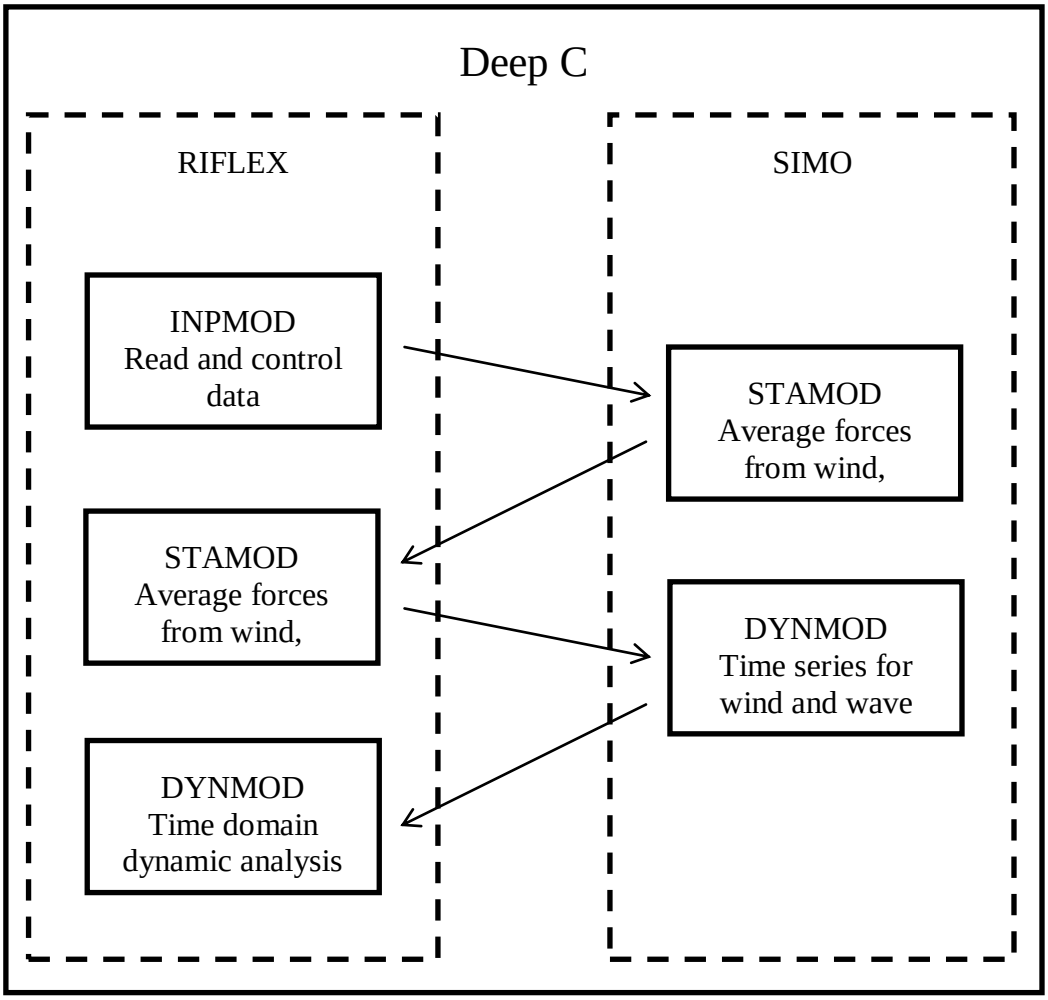

Figure A.1 RIFLEX and SIMO modules used in DeepC.

Appendix B: Mooringsystem configuration

This section presents the different mooringline setups for the five water depths. The configurations are governed by the line pre-tension and line length. The safety factor is the limiting factor and has to be at least 1.50 according to NMD (2009).

In Table B.1, a summary of the chosen configuration's safety factors for the different depths is shown. For further details, see Section B.2.

Table B.1 Safety factors for the chosen mooring- system configuration

Heading	Water depths [m]				
	100	200	400	750	1250
0°	1.57	1.69	1.79	1.84	2.03
30°	1.6	1.51	1.52	1.6	1.73
45°	1.79	1.8	1.79	1.78	1.85
60°	1.65	1.63	1.53	1.56	1.64
90°	1.5	1.61	1.72	1.75	1.88

B.1. Initial set-up of the mooringsystem calculations

The mooring lines have pre-tension in order to decrease the motion of the platform. The system is defined in calm weather, and when the environmental forces are applied the platform will have a new equilibrium position. The displacement to the new equilibrium position can be seen in Tables B.2-B.6. The surge and sway displacement stated in the tables are the amplitude motions, oscillating around the equilibrium position. The length on the seabed is the minimum and maximum length of the mooring line lying on the seabed. The safety factor for tension is according to Equation (B.1).

$$SF = \frac{Max\,tension}{MBL} \tag{B.1}$$

Table B.2 Result of mooring- system calculations at a water depth of 100m, 45°.

Water depth of 100 m, Heading: 45°								
Length of mooring line: 1800 m			Thruster: 3400 kN			Line type: Chain		
Pre-tension [kN]	EquilibriumX [m]	EquilibriumY [m]	Safety factor	Max Tension [kN]	Length on seabed [m]	Surge [m]	Sway [m]	Yaw [deg]
700	3.43	5.14	1.78	3375.4	1406-1555	13.87	10.52	1.77
800	2.88	4.35	1.79	3365.1	1390-1531	12.98	10.24	1.73
900	2.48	3.79	1.77	3404.7	1375-1508	12.27	10	1.7
1000	2.2	3.37	1.72	3488.4	1359-1486	11.71	9.79	1.67
1100	1.98	3.06	1.68	3582	1344-1466	11.24	9.61	1.65
1200	1.82	2.82	1.63	3686	1330-1446	10.99	9.46	1.63
1300	1.7	2.63	1.58	3795	1315-1427	10.8	9.33	1.61
1400	1.6	2.49	1.54	3913	1301-1409	10.64	9.21	1.6
1500	1.52	2.35	1.49	4034	1287-1392	10.51	9.11	1.59

Table B.3 Result of mooring- system calculations at a water depth of 200m, 45°.

Water depth 200 m, Heading: 45°								
Length of mooring line: 1600 m			Thruster: 2700 kN			Line type: Chain		
Pre-tension [kN]	EquilibriumX [m]	EquilibriumY [m]	Safety factor	Max Tension [kN]	Length on seabed [m]	Surge [m]	Sway [m]	Yaw [deg]
700	16.97	21.52	1.8	3334	978-1289	21.26	14.04	1.9
800	13.85	17.77	1.8	3349	962-1257	19.89	13.64	1.86
900	11.62	15.04	1.78	3382	945-1225	18.68	13.2	1.82
1000	9.98	13.01	1.75	3432	928-1195	17.63	12.76	1.78
1100	8.72	11.43	1.72	3494	910-1166	16.71	12.33	1.75
1200	7.27	10.16	1.69	3566	892-1138	15.91	11.92	1.73
1300	6.93	9.15	1.65	3647	874-1111	15.21	11.53	1.7
1400	6.28	8.31	1.61	3735	856-1084	14.59	11.17	1.68
1500	5.73	7.61	1.57	3829	838-1059	14.04	10.84	1.66

Table B.4 Result of mooring- system calculations at a water depth of 400m, 45°.

Water depth of 400 m, Heading: 45°								
Length of mooring line: 1600 m			Thruster: 1500 kN			Line type: Chain		
Pre-tension [kN]	EquilibriumX [m]	EquilibriumY [m]	Safety factor	Max Tension [kN]	Length on seabed [m]	Surge [m]	Sway [m]	Yaw [deg]
700	99.8	113.8	113.8	113.8	551-1214	30.78	16.61	2
800	77.36	89.36	89.36	89.36	545-1169	29.51	16.74	1.96
900	62.69	72.08	72.08	72.08	535-1134	28.2	16.17	1.93
1000	52.34	61.41	61.41	61.41	521-1097	26.93	16.56	1.9
1100	44.64	52.63	52.63	52.63	505-1060	25.71	16.32	1.86
1200	38.69	45.77	45.77	45.77	488-1024	24.57	16.02	1.83
1300	33.96	40.29	40.29	40.29	470-987	23.5	15.69	1.81
1400	30.13	35.84	35.84	35.84	451-951	22.51	15.33	1.79
1500	26.99	32.16	32.16	32.16	432-916	21.59	14.96	1.75

Table B.5 Result of mooring- system calculations at a water depth of 750m, 45°.

Water depth of 750 m, Heading: 45°								
Length of mooring line: 1300+700 m			Thruster: 800 kN			Line type: Chain+Wire		
Pre-tension [kN]	EquilibriumX [m]	EquilibriumY [m]	Safety factor	Max Tension [kN]	Length on seabed [m]	Surge [m]	Sway [m]	Yaw [deg]
700	122.5	140.11	1.8	3339.3	283-1189	34.42	19.38	1.94
800	106.37	122.06	1.79	3351.5	276-1155	33.41	19.46	1.92
900	93.57	107.64	1.78	3371	265-1119	32.38	19.43	1.9
1000	83.22	95.92	1.76	3411.9	253-1081	31.35	19.33	1.88
1100	74.64	86.16	1.74	3462	238-1042	30.34	19.15	1.85
1200	67.39	77.92	1.71	3520.6	221-1022	29.34	18.92	1.83
1300	61.27	70.91	1.68	3574	202-963	28.39	18.64	1.81
1400	56.01	64.88	1.64	3663.7	183-923	27.49	18.36	1.79
1500	51.45	59.66	1.6	3746.5	162-893	26.63	18.04	1.77

Table B.6 Result of mooring- system calculations at a water depth of 1250m, 45°.

Water depth of 1,250 m, Heading: 45°								
Length of mooring line: 1500+1100 m			Thruster: 800 kN			Line type: Chain+Wire		
Pre-tension [kN]	EquilibriumX [m]	EquilibriumY [m]	Safety factor	Max Tension [kN]	Length on seabed [m]	Surge [m]	Sway [m]	Yaw [deg]
700	321.35	363.44	1.85	3252	N/A	N/A	N/A	N/A
800	268.13	304.85	1.86	3231.4	275-1344	47.57	24.80	2.04
900	230.06	262.62	1.85	3243.4	267-1317	46.27	25.11	2.02
1000	200.71	229.87	1.84	3265.9	257-1284	44.95	25.27	2.00
1100	177.29	203.56	1.82	3295.8	243-1247	43.62	25.27	1.97
1200	158.11	181.92	1.83	3289.7	227-1204	42.29	25.19	1.95
1300	142.08	163.82	1.78	3382.8	208-1165	40.99	24.98	1.92
1400	128.54	148.44	1.75	3439.8	188-1121	39.72	24.72	1.90
1500	117.09	135.38	1.72	3503.9	165-1076	38.51	24.39	1.87

Appendix C: Results

This section sums up the data from the simulations in MIMOSA and DeepC. The data presented are amplitudes in LF, HF, LF+HF-motion, equilibrium position, critical damping, maximum line tension and safety factor.

C.1. Results from frequency-domain simulations (MIMOSA)

Table C.1 Output data from MIMOSA v.6.3 foran environmental heading of 0°.

Water depth [m]	LF- motion [m]				HF-motion [m]				LF+HF motion [m]		Equilibrium pos. [m]		Stiffness [N/m]		Critical damping [Ns/m]		Damping Coeff. [kNs/m]		Max line tension [kN]	Safety factor
	Surge		Sway		Surge		Sway		Surge	Sway										
	Max amp.	Std.	Max amp.	Std.	Max amp.	Std.	Max amp.	Std.	Max amp.	Std	Surge	Sway	Surge	Sway	Surge	Sway	Surge	Sway		
100	17.37	4.98	0.43	0.13	9.14	2.42	0.05	0.01	22.21	0.46	1.39	-0.28	2.67E+05	2.56E+05	8.89E+06	8.70E+06	710.4	1260.6	3828.9	1.57
200	30.51	9.25	0.75	0.24	9.14	2.42	0.08	0.02	35.35	0.79	12.82	-0.95	9.55E+04	8.39E+04	5.32E+06	4.98E+06	812.4	1128.6	3551.9	1.69
400	47.74	15.2	1.35	0.42	9.13	2.42	0.11	0.03	52.57	1.41	98.14	-3.39	4.15E+04	2.33E+04	3.50E+06	2.62E+06	952.53	899.83	3365.5	1.79
750	51.22	16.44	1.34	0.45	9.14	2.42	0.08	0.02	56.05	1.38	118.65	-2.51	3.64E+04	2.50E+04	3.28E+06	2.72E+06	710.98	736.29	3259.5	1.84
1250	74.65	25.24	2.09	0.71	9.13	2.42	0.1	0.03	79.49	2.14	300.03	-6.82	1.71E+04	9.87E+03	2.25E+06	1.71E+06	622.58	478.18	2958.9	2.03

Table C.2 Output data from MIMOSA v.6.3 for an environmental heading of 45°.

Water depth [m]	LF- motion [m]				HF-motion [m]				LF+HF motion [m]		Equilibrium pos. [m]		Stiffness [N/m]		Critical damping [Ns/m]		Damping Coeff. [kNs/m]		Max line tension [kN]	Safety factor
	Surge		Sway		Surge		Sway		Surge	Sway										
	Max amp.	Std.	Max amp.	Std.	Max amp.	Std.	Max amp.	Std.	Max amp.	Max amp.	Surge	Sway	Surge	Sway	Surge	Sway	Surge	Sway		
100	9.45	2.85	6.86	2.09	6.66	1.76	6.07	1.61	12.98	10.24	2.88	4.35	2.65E+05	2.69E+05	8.85E+06	8.91E+06	682.11	812.31	3365.1	1.79
200	16.34	5.2	10.45	3.36	6.71	1.78	6.01	1.59	19.89	13.64	13.85	17.77	1.02E+05	1.06E+05	5.49E+06	5.60E+06	735.23	1121.83	3349.6	1.80
400	25.89	8.67	13.65	4.57	6.84	1.81	5.84	1.55	29.51	16.74	77.35	89.35	4.23E+04	4.34E+04	3.54E+06	3.58E+06	796.91	1233.9	3360.5	1.79
750	28.79	9.78	16.29	5.61	6.77	1.79	5.93	1.57	32.38	19.43	93.57	107.64	3.57E+04	3.70E+04	3.25E+06	3.31E+06	672.94	980.1	3376.2	1.78
1250	42.65	15.27	22.01	7.98	6.83	1.81	5.85	1.55	46.27	25.11	230.06	262.62	1.65E+04	1.70E+04	2.21E+06	2.24E+06	617.22	806.49	3243.4	1.85

Table C.3 Output data from MIMOSA v.6.3 for an environmental heading of 90°.

Water depth [m]	LF- motion [m]				HF-motion [m]				LF+HF motion [m]		Equilibrium pos. [m]		Stiffness [N/m]		Critical damping [Ns/m]		Damping Coeff. [kNs/m]		Max line tension [kN]	Safety factor
	Surge		Sway		Surge		Sway		Surge	Sway										
	Max amp.	Std.	Max amp.	Std.	Max amp.	Std.	Max amp.	Std.	Max amp.	Max amp.	Surge	Sway	Surge	Sway	Surge	Sway	Surge	Sway		
100	0.46	0.14	14.59	3.79	0.02	0.01	8.66	2.29	0.47	19.17	-0.2	4.62	2.58E+05	2.71E+05	8.73E+06	8.95E+06	344.62	731.81	4017	1.50
200	0.87	0.28	22.33	6.23	0.03	0.01	8.65	2.29	0.88	26.91	-0.59	21.26	8.95E+04	1.13E+05	5.15E+06	5.78E+06	954.92	880.15	3736.3	1.61
400	1.83	0.62	30.97	9.23	0.02	0	8.66	2.29	1.84	35.55	-2.07	116.07	2.70E+04	5.59E+04	2.83E+06	4.07E+06	754.99	941.91	3500.8	1.72
750	2.24	0.77	34.48	10.54	0.02	0.01	8.66	2.29	2.26	39.06	-2.08	139.76	2.70E+05	4.39E+04	8.94E+06	3.60E+06	578.55	737.62	3434.5	1.75
1250	3.55	1.29	46.92	15.43	0.02	0.01	8.66	2.29	3.56	51.51	-5.1	343.8	1.10E+04	2.15E+04	1.81E+06	2.52E+06	347.22	579.17	3200.6	1.88

Table C.4 Mooring- line damping estimates from MIMOSA v.5.7 [kNs/m].

Heading	Water depth [m]									
	100m		200m		400m		750m		1250m	
	Surge	Sway	Surge	Sway	Surge	Sway	Surge	Sway	Surge	Sway
0°	567.3	365.6	589.8	287.7	384.2	102.4	462.4	231.4	235.8	95.6
45°	554.5	340.7	468.3	299.7	315.2	214.8	403.0	318.8	208.3	184.0
90°	487.9	321.0	234.1	298.9	77.6	259.5	205.9	334.1	89.4	218.3

Table C.5 Output data from MIMOSA v.5.7 for an environmental heading of 0°.

Water depth [m]	LF- motion [m]				HF-motion [m]				LF+HF motion [m]		Equilibrium pos. [m]		Stiffness [N/m]		Critical damping [Ns/m]		Damping Coeff. [kNs/m]		Max line tension [kN]	Safety factor
	Surge		Sway		Surge		Sway		Surge	Sway										
	Max amp.	Std.	Max amp.	Std.	Max amp.	Std.	Max amp.	Std.	Max amp.	Max amp.	Surge	Sway	Surge	Sway	Surge	Sway	Surge	Sway		
100	14.12	4.09	0.53	0.17	9.14	2.42	0.07	0.02	18.96	0.57	1.4	-0.1	2.53E+05	2.52E+05	8.65E+06	8.63E+06	567.30	365.60	3866.5	1.56
200	24.53	7.8	1.15	0.38	9.13	2.42	0.11	0.03	29.36	1.21	12.8	-0.6	8.96E+04	8.19E+04	5.15E+06	4.92E+06	589.80	287.70	4027.9	1.49
400	41.3	14.1	3.45	1.22	9.12	2.41	0.16	0.04	43.13	3.53	98.2	-2	3.93E+04	2.29E+04	3.41E+06	2.60E+06	384.20	102.40	4167.7	1.44
750	42.41	14.6	2.2	0.79	9.13	2.42	0.11	0.03	47.24	2.26	118.7	-1	3.57E+04	2.48E+04	3.25E+06	2.71E+06	462.40	231.40	4126.4	1.46
1250	69.91	25.7	5.21	1.99	9.12	2.41	0.14	0.04	74.73	5.29	300.2	-3.2	1.68E+04	9.76E+03	2.23E+06	1.70E+06	235.80	95.60	3638.8	1.65

Table C.6 Output data from MIMOSA v.5.7 for an environmental heading of 45°.

Water depth [m]	LF- motion [m]				HF-motion [m]				LF+HF motion [m]		Equilibrium pos. [m]		Stiffness [N/m]		Critical damping [Ns/m]		Damping Coeff. [kNs/m]		Max line tension [kN]	Safety factor
	Surge		Sway		Surge		Sway		Surge	Sway										
	Max amp.	Std.	Max amp.	Std.	Max amp.	Std.	Max amp.	Std.	Max amp.	Max amp.	Surge	Sway	Surge	Sway	Surge	Sway	Surge	Sway		
100	10.68	3.27	7.71	2.41	9.16	2.42	0.01	0	15.7	7.71	2.9	2.9	2.62E+05	2.67E+05	8.81E+06	8.89E+06	554.50	340.70	4319.6	1.39
200	19.78	6.43	12.59	4.18	9.16	2.42	0.01	0	24.63	12.6	13.9	17.8	9.94E+04	1.04E+05	5.42E+06	5.55E+06	468.30	299.70	5121.5	1.17
400	33.85	11.6	18.33	6.32	9.16	2.42	0.01	0	38.7	18.34	77.4	89.3	4.14E+04	4.27E+04	3.50E+06	3.55E+06	315.20	214.80	5205	1.16
750	36.6	12.7	21.31	7.55	9.16	2.42	0.01	0	41.45	21.31	93.6	107.6	3.54E+04	3.68E+04	3.24E+06	3.30E+06	403.00	318.80	4891.1	1.23
1250	62.73	23	32.3	12.02	9.16	2.42	0.01	0	67.58	32.31	230.1	262.6	1.64E+04	1.69E+04	2.20E+06	2.24E+06	208.30	184.00	4315.5	1.39

Table C.7 Output data from MIMOSA v.5.7 for an environmental heading of 90°.

Water depth [m]	LF- motion [m]				HF-motion [m]				LF+HF motion [m]		Equilibrium pos. [m]		Stiffness [N/m]		Critical damping [Ns/m]		Damping Coeff. [kNs/m]		Max line tension [kN]	Safety factor
	Surge		Sway		Surge		Sway		Surge	Sway										
	Max amp.	Std.	Max amp.	Std.	Max amp.	Std.	Max amp.	Std.	Max amp.	Max amp.	Surge	Sway	Surge	Sway	Surge	Sway	Surge	Sway		
100	0.17	0.05	12.79	3.69	9.16	2.42	0.01	0	9.26	12.79	-0.2	4.6	2.57E+05	2.67E+05	8.72E+06	8.89E+06	487.90	321.00	3170.4	1.90
200	0.73	0.24	19.99	6.29	9.16	2.42	0.01	0	9.63	19.99	-0.6	21.3	8.86E+04	1.10E+05	5.12E+06	5.70E+06	234.10	298.90	3319.1	1.81
400	2.78	0.95	28.68	9.67	9.16	2.42	0.01	0	12.49	30.09	-2.1	116.1	2.67E+04	5.48E+04	2.81E+06	4.02E+06	77.60	259.50	3687.1	1.63
750	0.99	0.35	31.84	11.1	9.16	2.42	0.01	0	9.85	31.84	-2.1	139.8	2.70E+04	4.35E+04	2.82E+06	3.59E+06	205.90	334.10	3819.6	1.57
1250	2.55	0.94	46.72	17.38	9.16	2.42	0.01	0	11.04	46.72	-5.1	343.8	1.10E+04	2.14E+04	1.81E+06	2.52E+06	89.40	218.30	3752.2	1.60

C.2. Time series (DeepC)

This section presents examples of the time series for the case of 400m at 0°. Figure C.1 shows the platform displacement for an extract of the total time series, from 2,000s to 7,000s. The filtered displacement, in LF and HF, is presented in Figures C.2 and C.3. The platform velocity, line forces and the multiplication of the force can be seen in Figures C.4-8. These are extracts from the total time series from 2,000s to 2,200s (10 000 to 11 000 time steps).

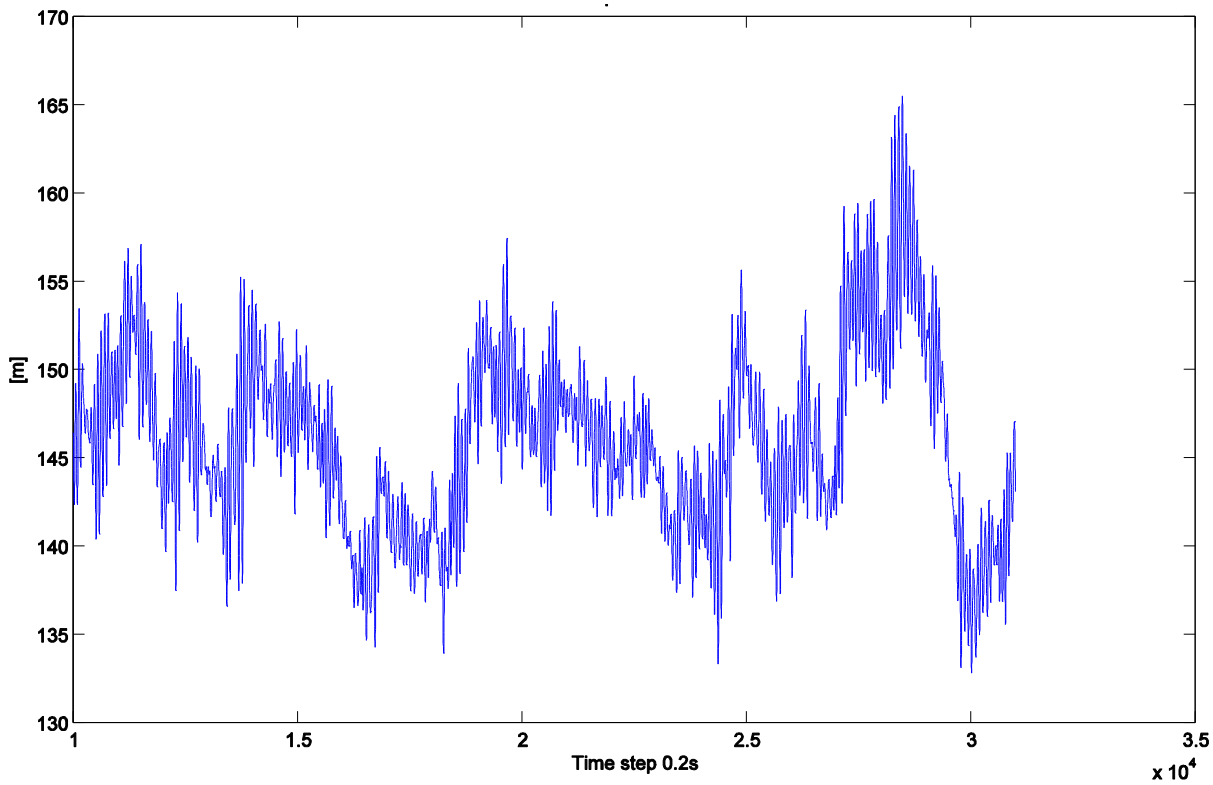

Figure C.1 Platform displacement for 400m,at 0°.

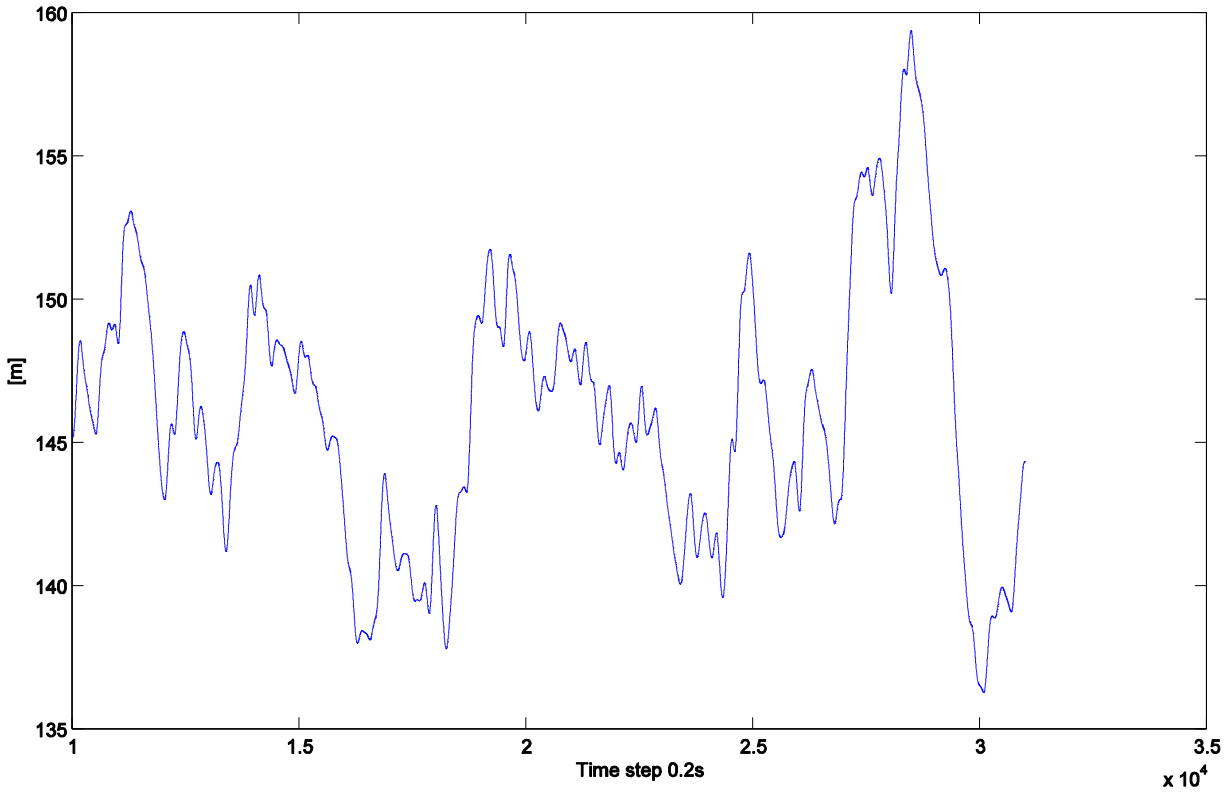

Figure C.2 LF-filtered platform displacement for 400m, at 0°.

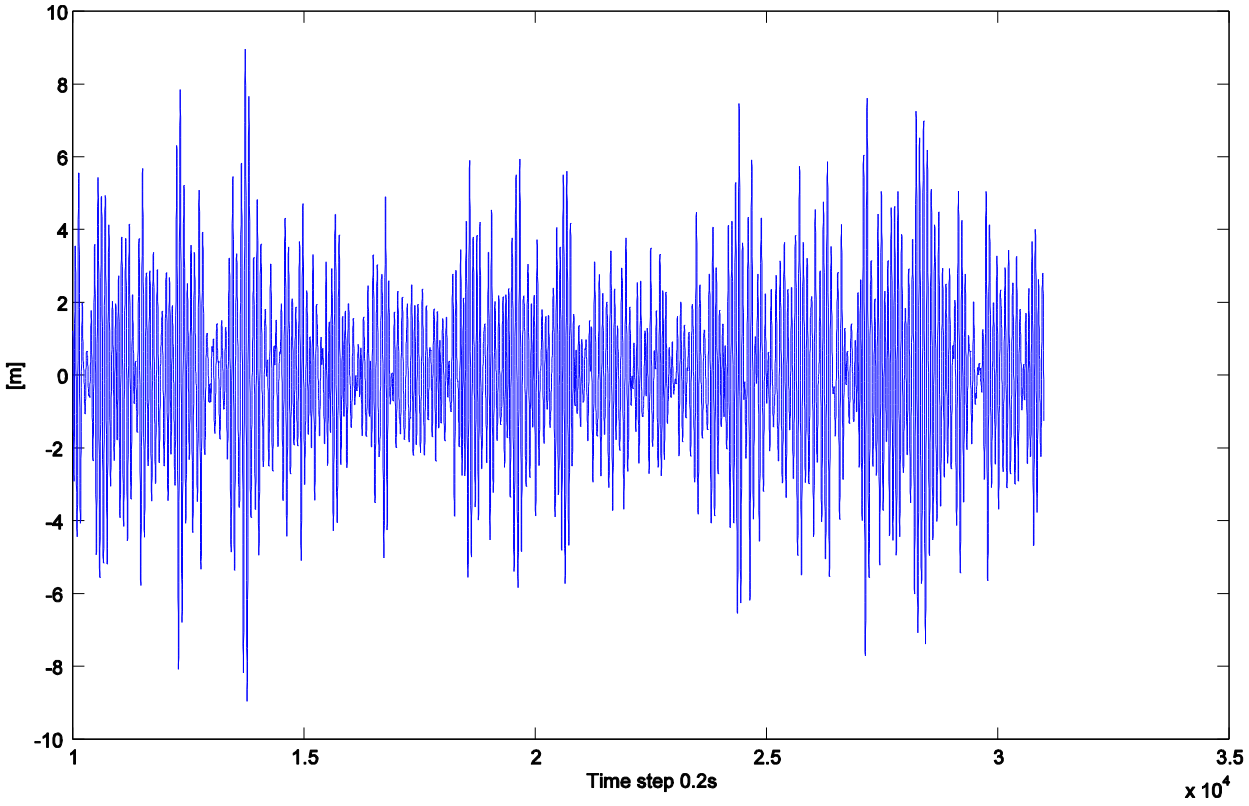

Figure C.3 HF-filtered platform displacement for 400m, at 0°.

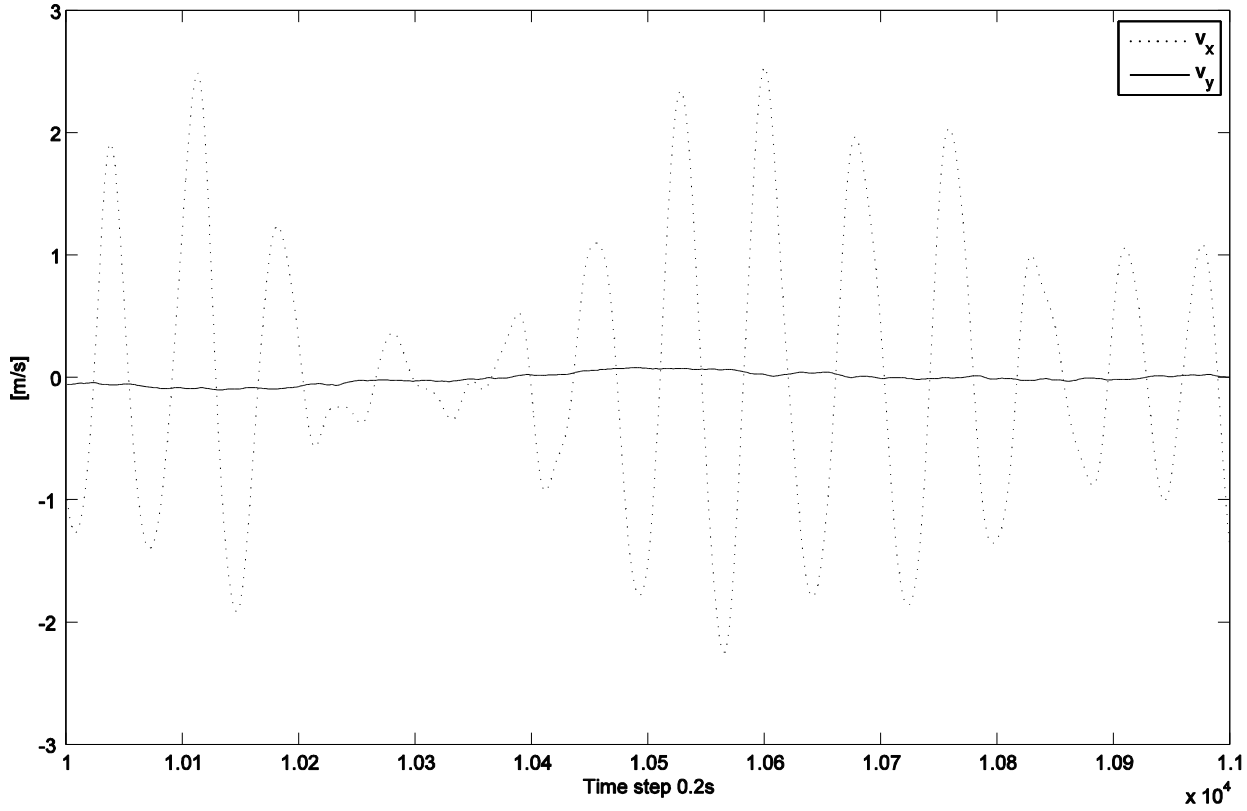

Figure C.4 Platform velocity in surge (x) and sway (y) for 400m, at 0°.

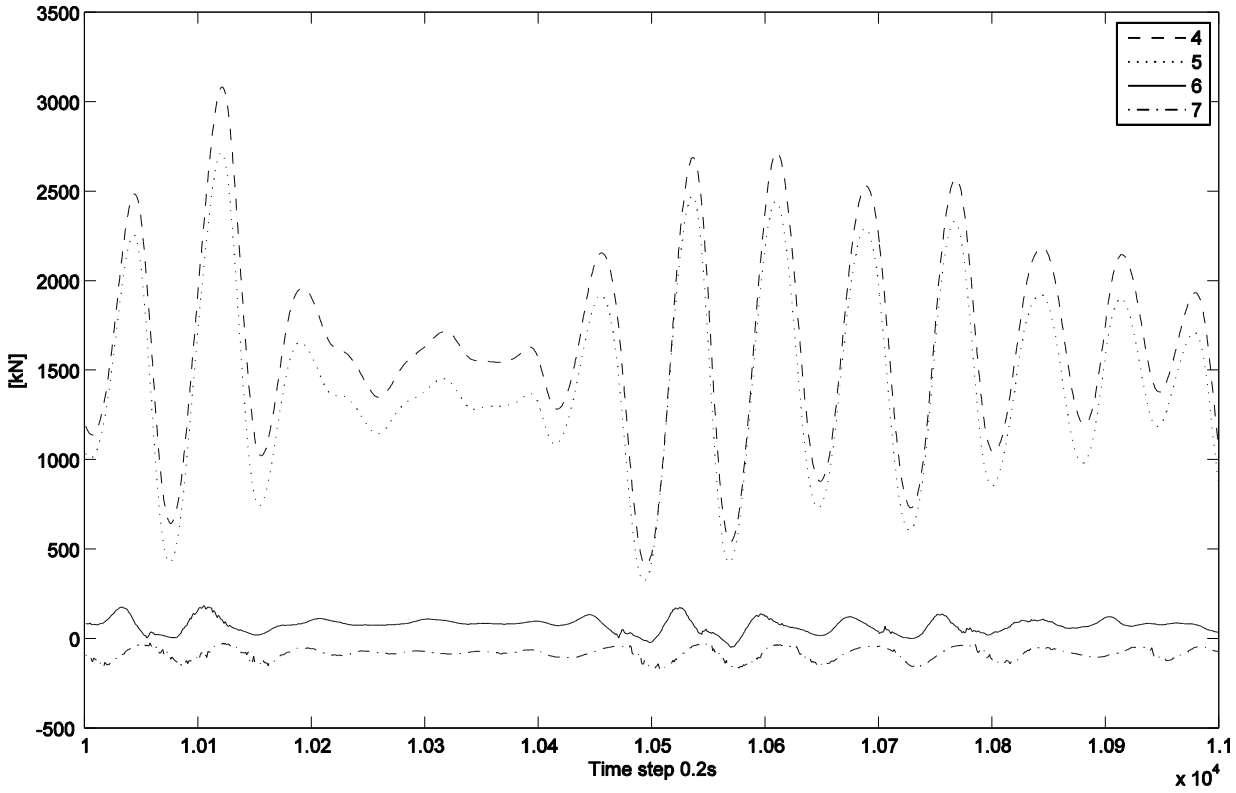

Figure C.5 Line forces for line no. 4, 5, 6, and 7 in surge for 400m, at 0°.

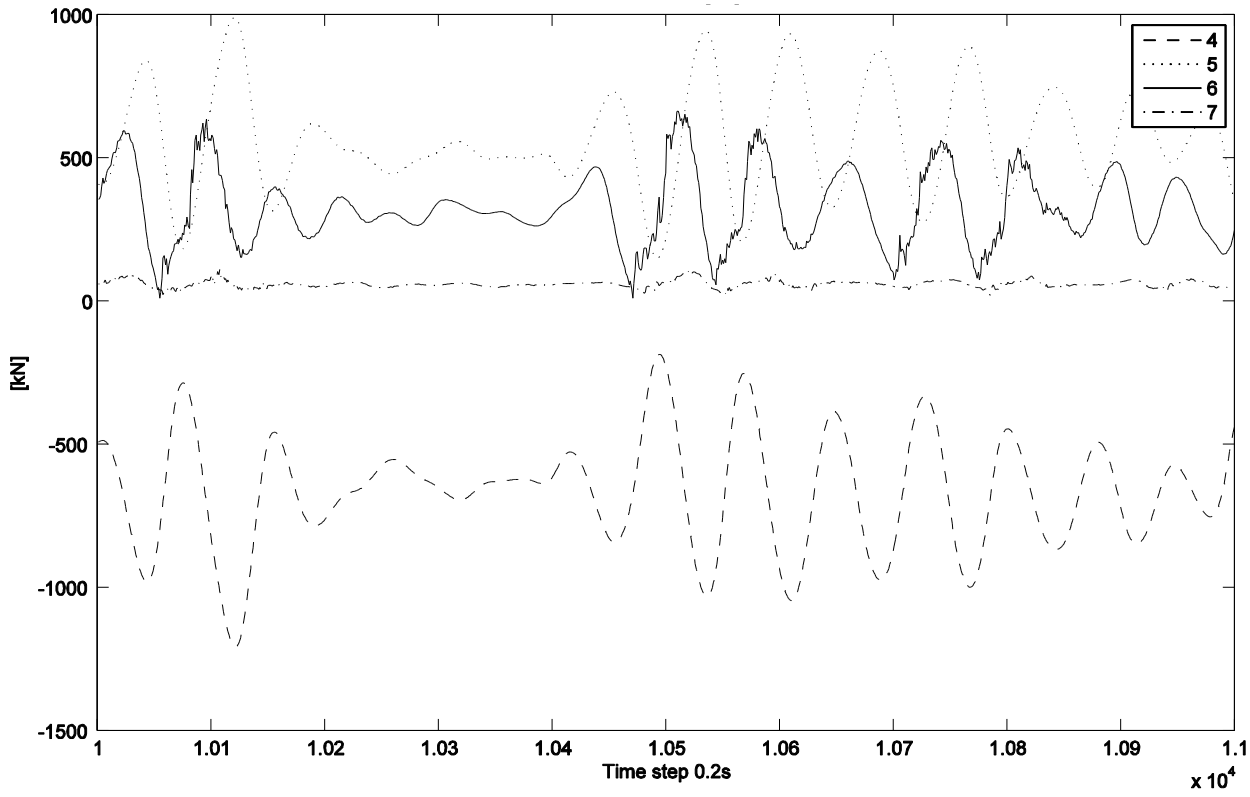

Figure C.6 Line forces for line no. 4, 5, 6, and 7 in sway for 400m, at 0°.

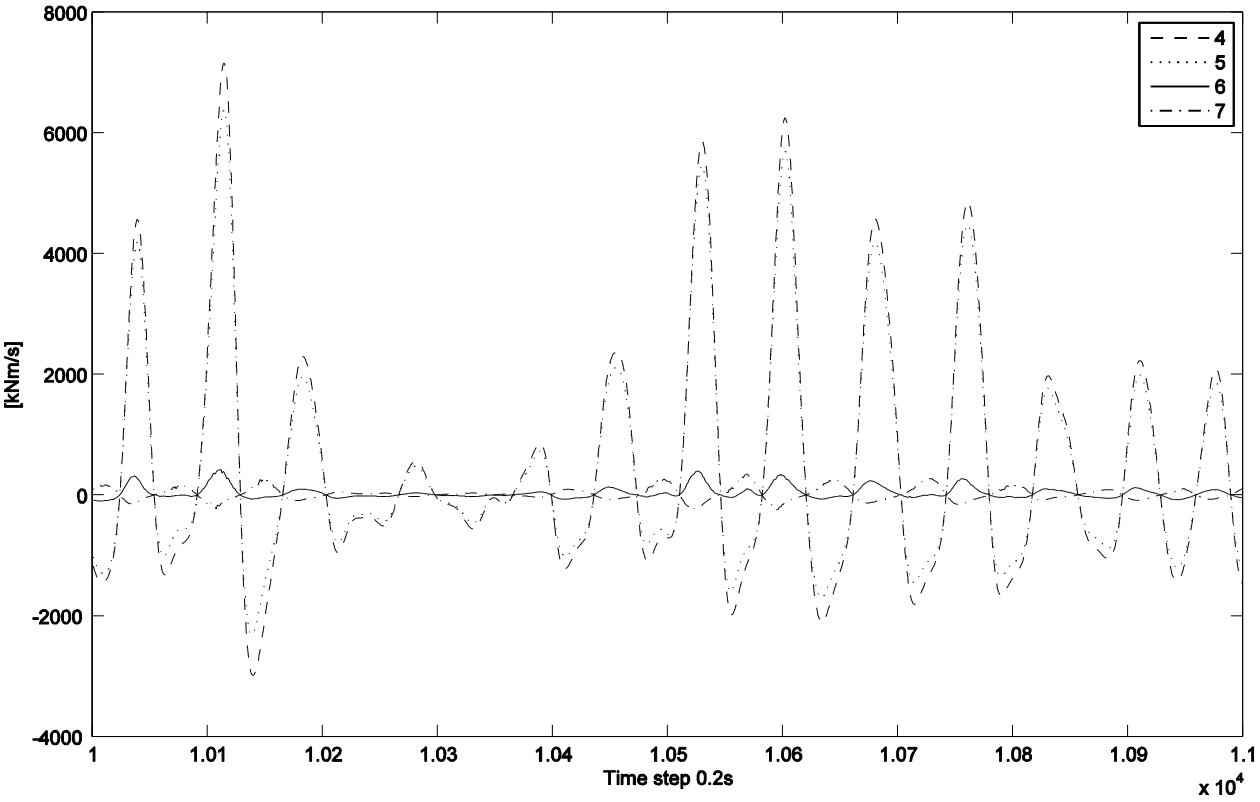

Figure C.7 Line forces for line no. 4, 5, 6, and 7 in surge for 400m, at 0°.

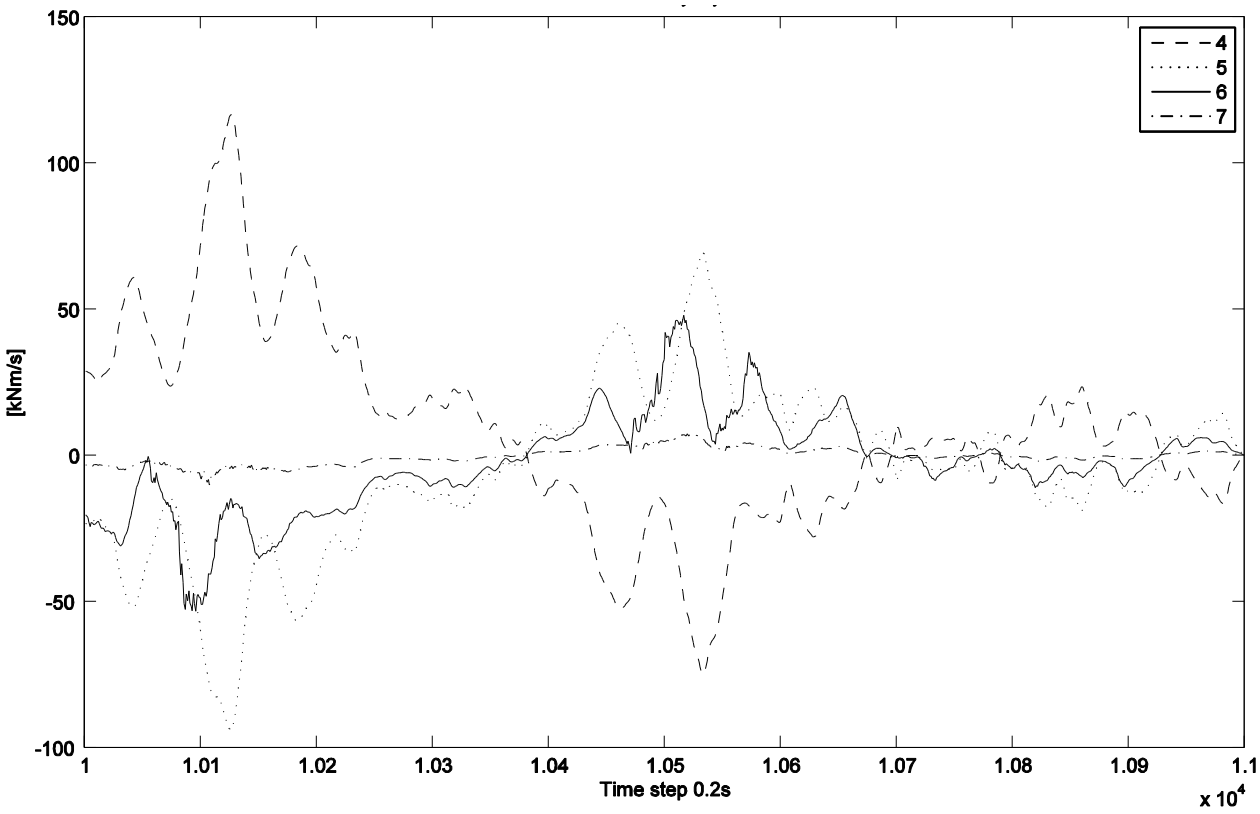

Figure C.8 Line forces for line no. 4, 5, 6, and 7 in sway for 400m, at 0°.

C.3. Results from time-domain simulations (DeepC)

This section presents the total line damping and the line damping in each mooring line.

C.3.1. Total line damping

In Tables C.8 and C.9, the total line damping in absolute numbers and as a percentage of the critical damping, LF+HF cases and LF case, respectively, are shown.

Table C.8 Summation of total line damping (LF+HF)

Water depth [m]	Heading											
	0°				45°				90°			
	Surge		Sway		Surge		Sway		Surge		Sway	
	Damping [kNs/m]	%	Damping [kNs/m]	%	Damping [kNs/m]	%	Damping [kNs/m]	%	Damping [kNs/m]	%	Damping [kNs/m]	%
100	710.40	7.99	1260.60	14.48	682.11	7.71	812.31	9.91	344.62	3.95	731.81	8.18
200	812.40	15.29	1128.60	22.66	735.23	13.39	1121.83	20.05	954.92	18.53	880.15	15.22
400	952.53	27.20	899.83	34.29	796.91	22.53	1233.90	34.45	754.99	26.71	941.91	23.16
750	816.41	24.90	825.62	30.37	672.90	20.70	980.10	29.64	643.22	22.76	777.01	21.57
1250	622.58	27.70	478.18	28.00	617.22	27.98	806.49	36.02	347.22	19.22	579.17	22.96

Table C.9 Summation of total line damping (LF)

Water depth [m]	Heading											
	0°				45°				90°			
	Surge		Sway		Surge		Sway		Surge		Sway	
	Damping [kNs/m]	%	Damping [kNs/m]	%	Damping [kNs/m]	%	Damping [kNs/m]	%	Damping [kNs/m]	%	Damping [kNs/m]	%
100	1439.80	16.19	1249.80	14.36	1663.40	18.80	1519.70	17.05	1184.62	13.57	1467.72	16.41
200	1440.10	27.11	1084.20	21.77	1778.52	32.40	2139.90	38.24	1511.15	22.33	2056.06	35.56
400	1641.40	46.87	880.94	33.57	1660.05	46.95	2243.00	62.62	922.71	32.64	2387.88	58.71
750	1579.20	48.17	803.88	29.57	1390.50	42.78	1643.40	49.70	807.67	28.58	2039.44	56.61
1250	1245.10	55.40	463.51	27.14	960.26	43.54	1379.88	61.63	449.88	24.91	1534.62	60.83

C.3.2. Line damping

In this section, the line damping from each line is presented for the different water depths and headings. Each case is presented with two graphs ;the first shows only the LF+HF damping, and the second the LF+HF and LF damping. For each water depth the line damping in the headings of 0°, 45° and 90° are presented.

Water depth of 100 m at 0°

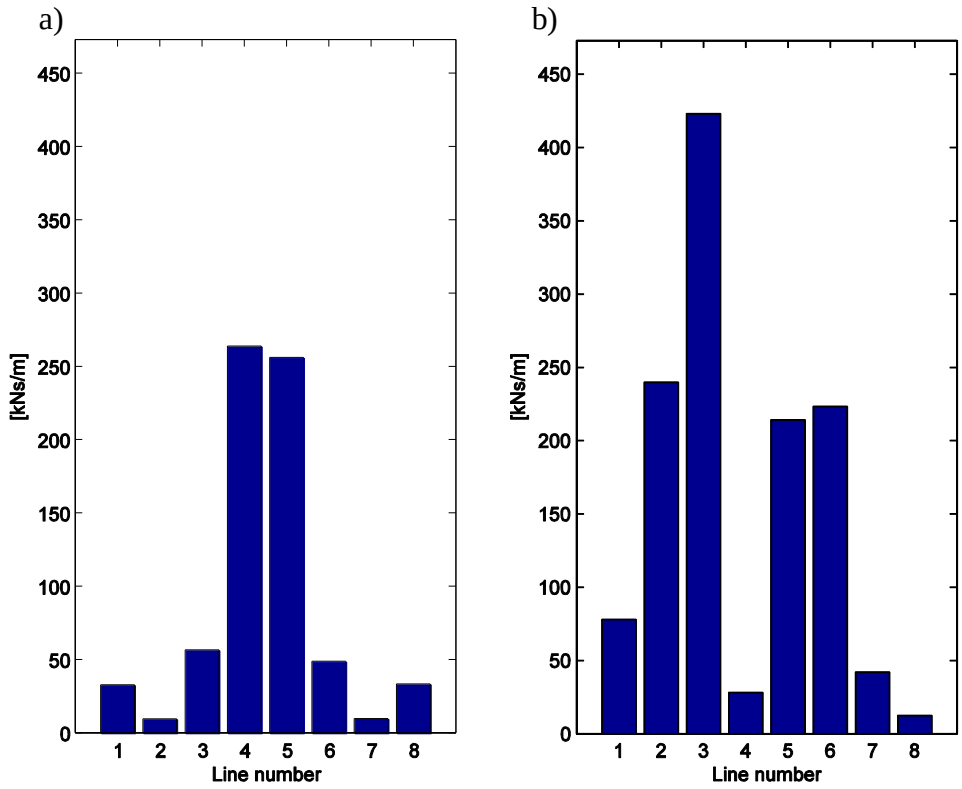

Figure C.9 Line damping LF+HF for 100m heading at 0° in a) surge and b) sway.

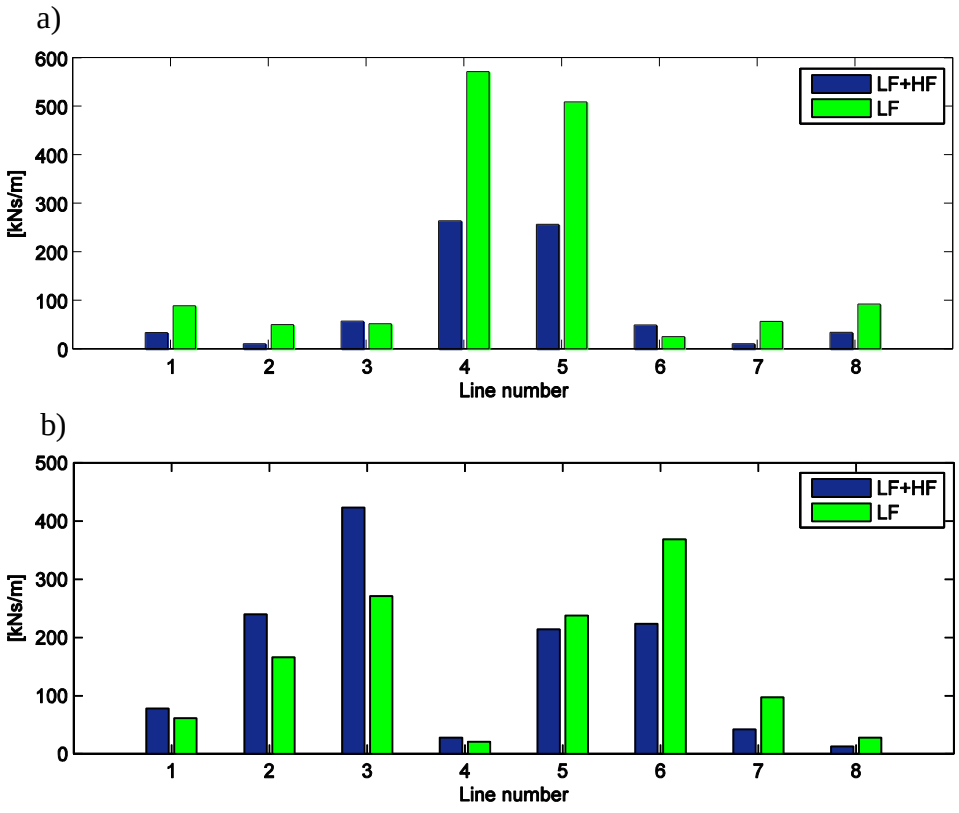

Figure C.10 Line damping for 100m heading at 0° in a) surge and b) sway.

Water depth of 100 m at 45°

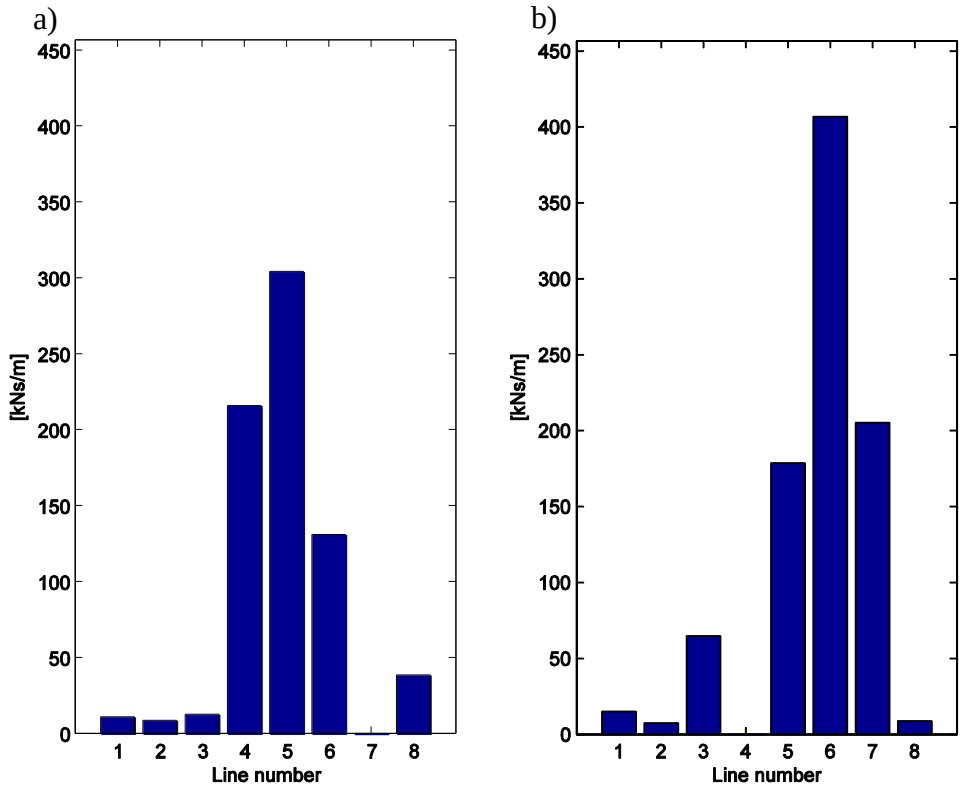

Figure C.11 Line damping LF+HF for 100m heading at 45° in a) surge and b) sway.

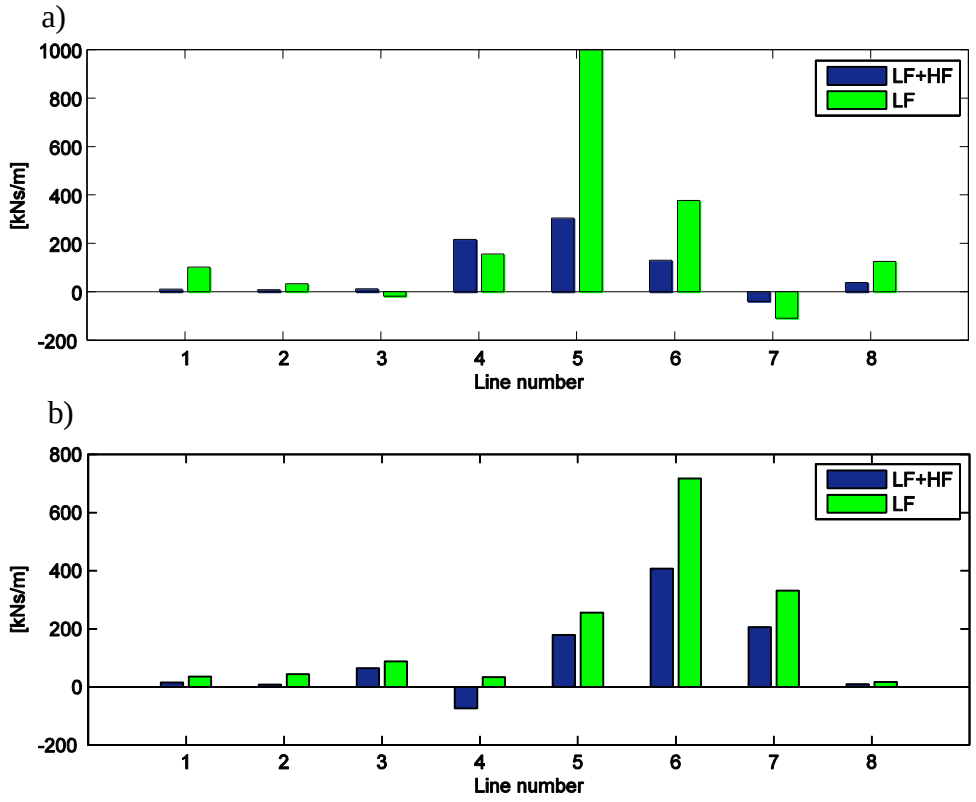

Figure C.12 Line damping for 100m heading at 45° in a) surge and b) sway.

Water depth of 100 m at 90°

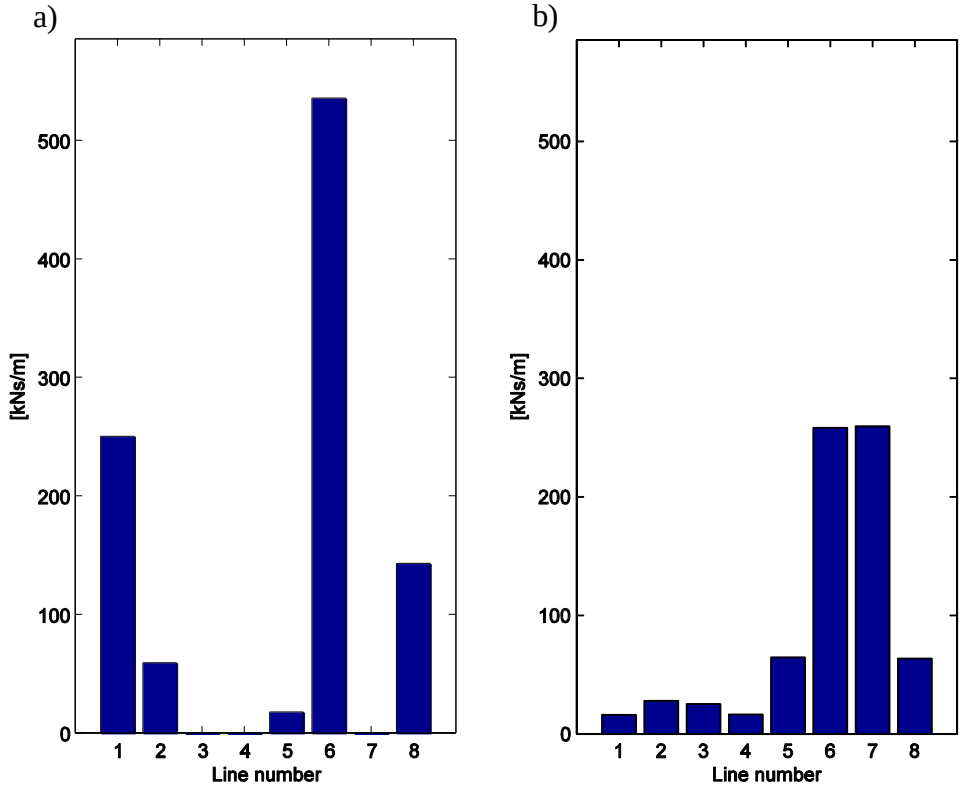

Figure C.13 Line damping LF+HF for 100m heading at 90° in a) surge and b) sway.

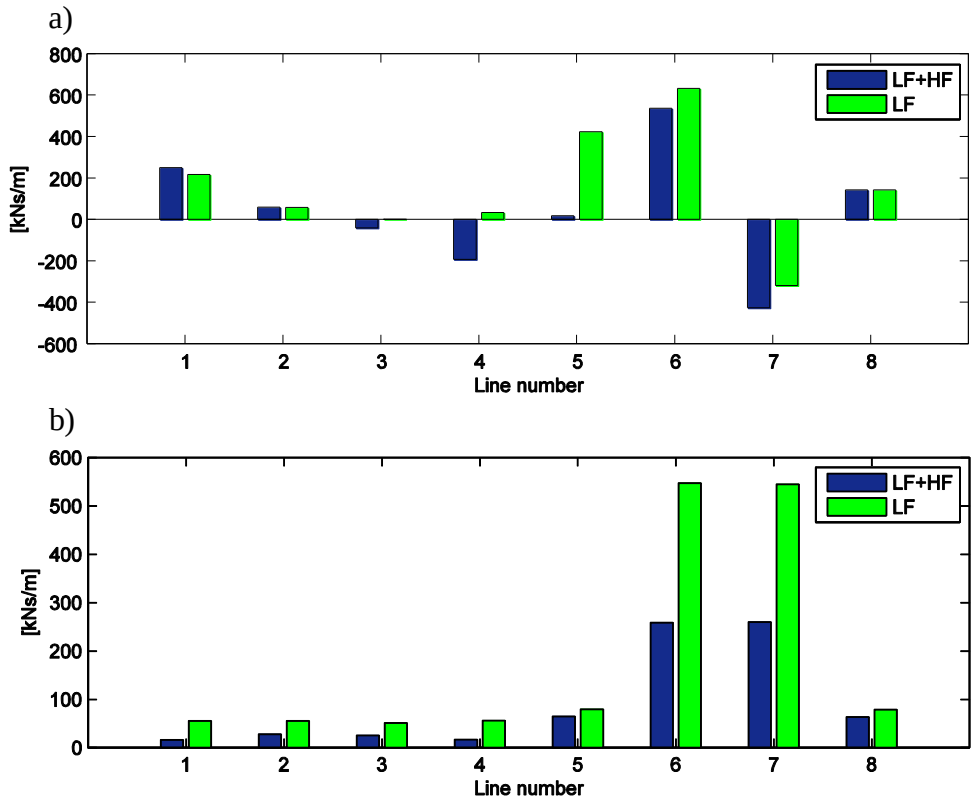

Figure C.14 Line damping for 100m heading at 90° in a) surge and b) sway.

Water depth of 200 m at 0°

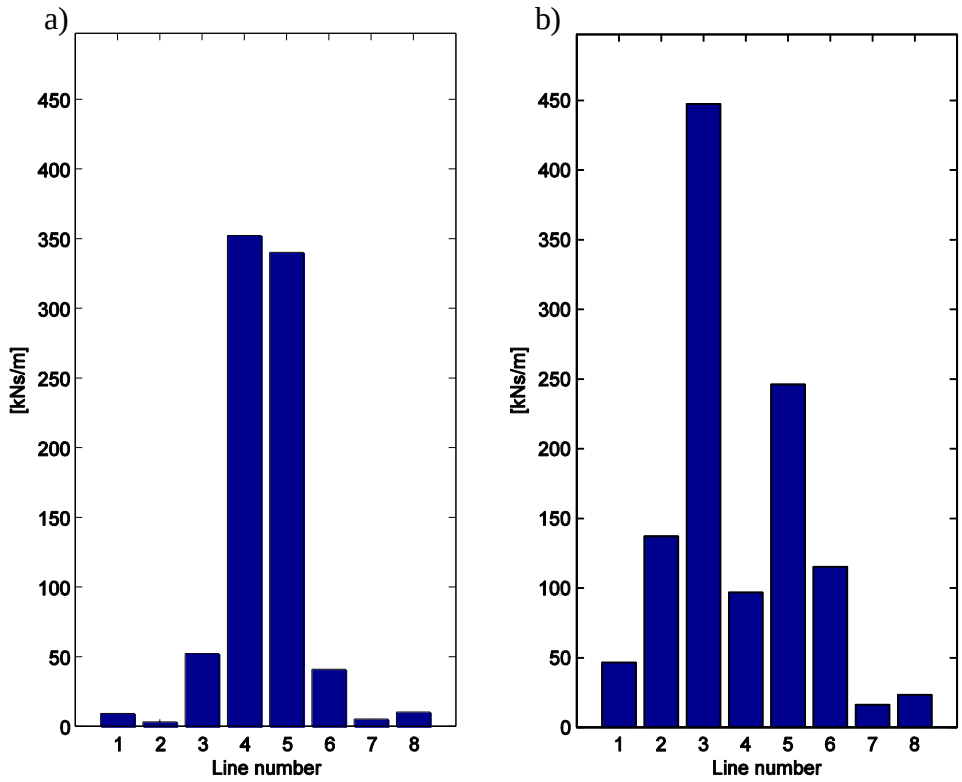

Figure C.15 Line damping LF+HF for 200m heading at 0° in a) surge and b) sway.

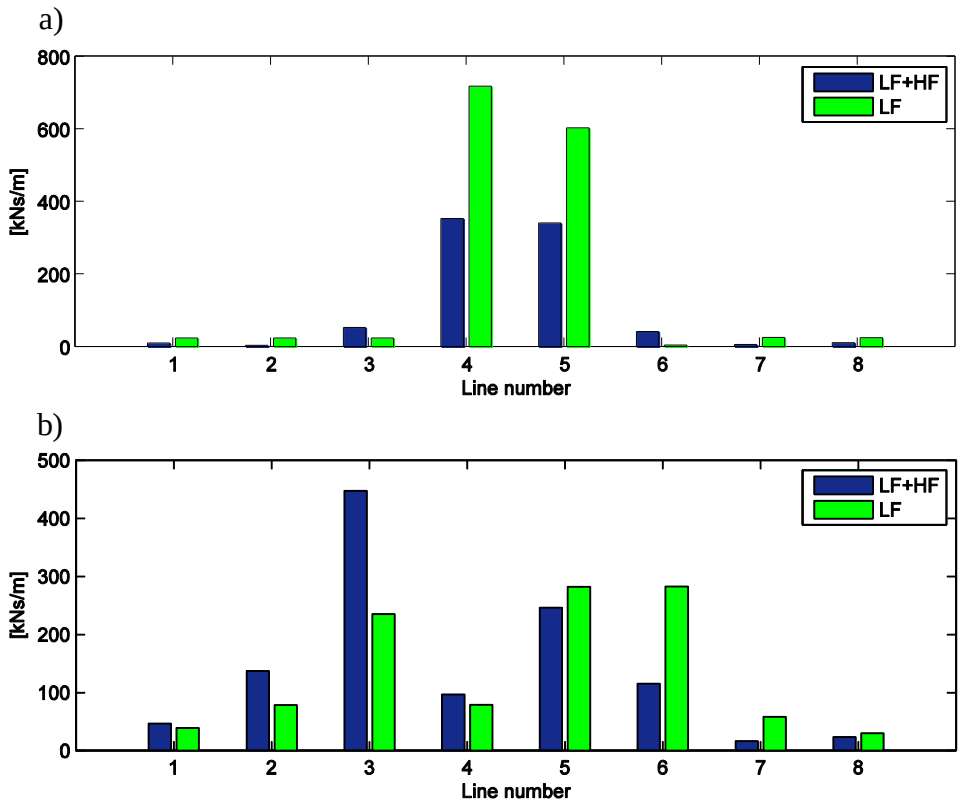

Figure C.16 Line damping 200m heading at 0° in a) surge and b) sway.

Water depth of 200 m at 45°

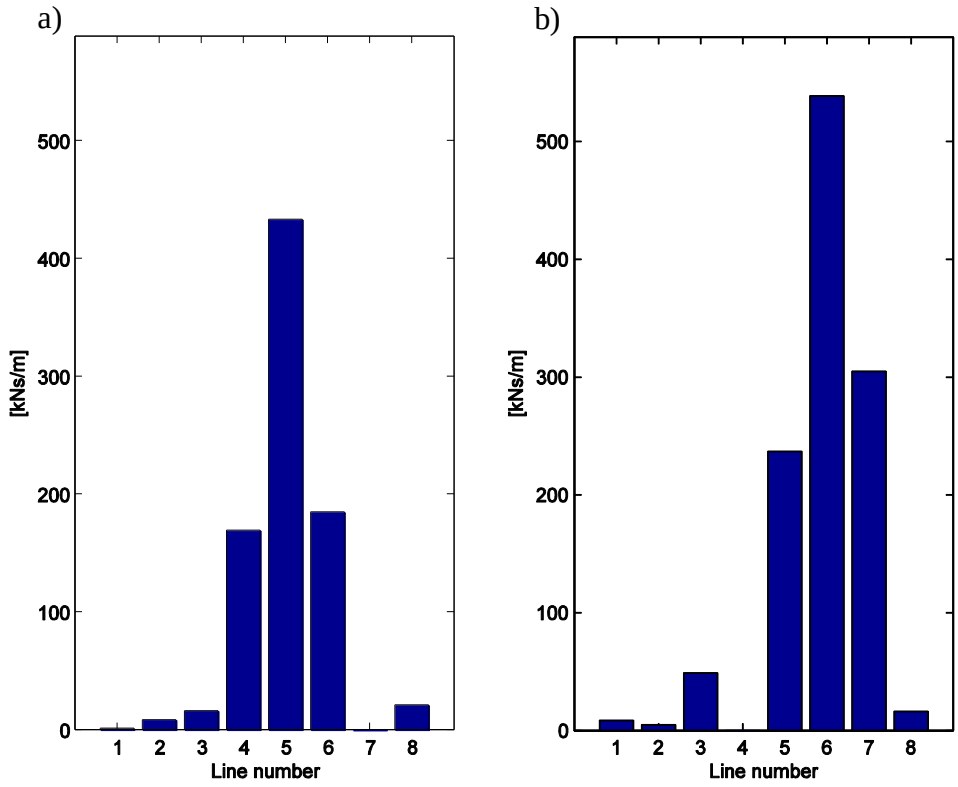

Figure C.17 Line damping LF+HF for 200m heading 45° in a) surge and b) sway.

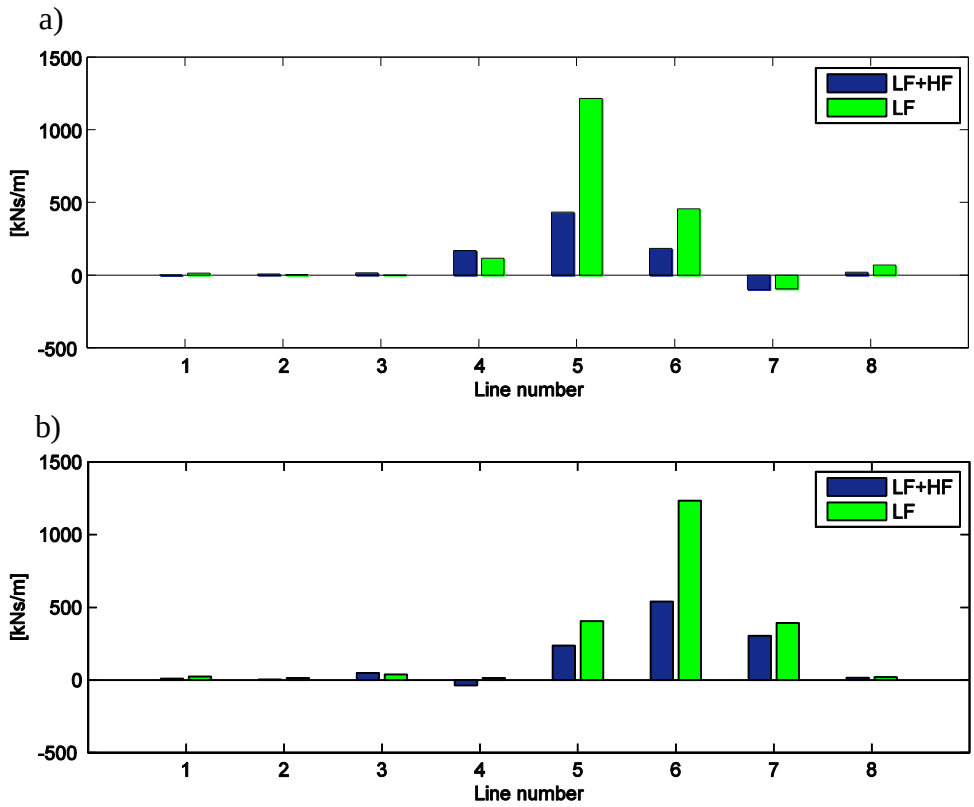

Figure C.18 Line damping for a 200m heading at 45° in a) surge and b) sway.

Water depth of 200 m at 90°

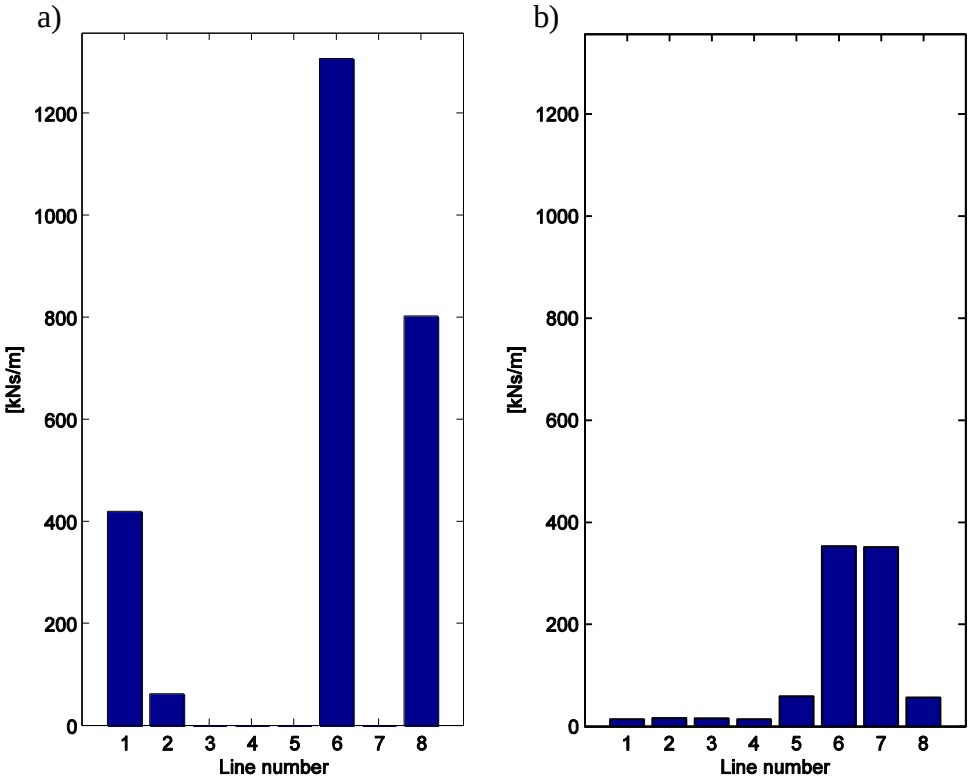

Figure C.19 Line damping LF+HF for a 200m heading at 90° in a) surge and b) sway.

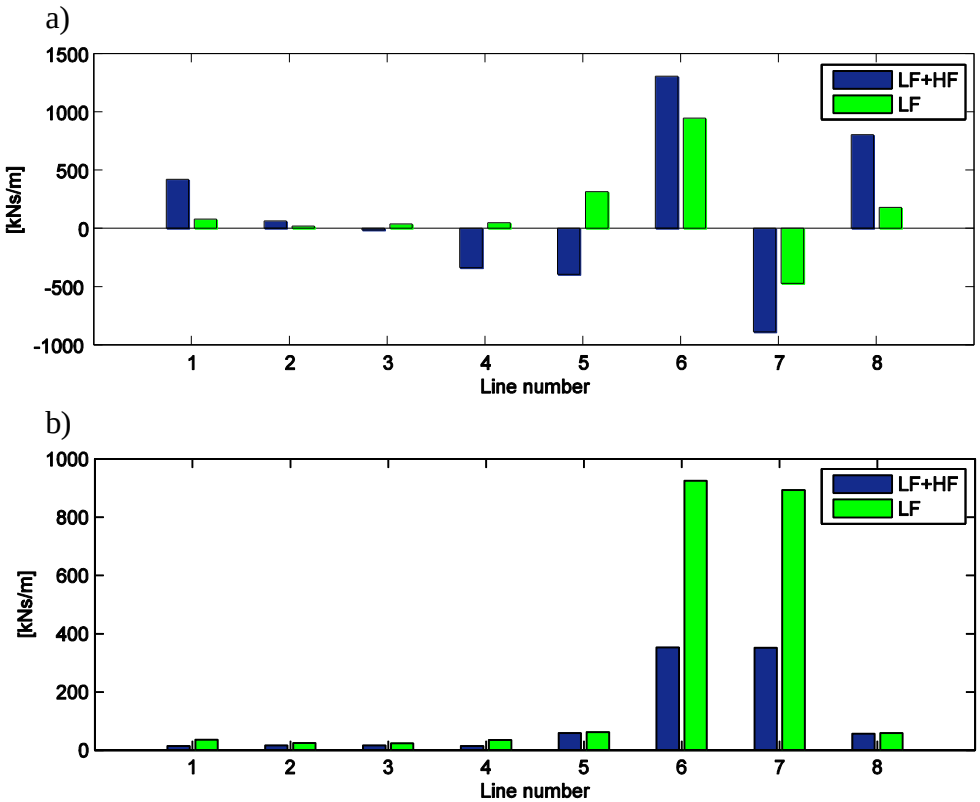

Figure C.20 Line damping for a 200m heading at 90° in a) surge and b) sway.

Water depth of 400 m at 0°

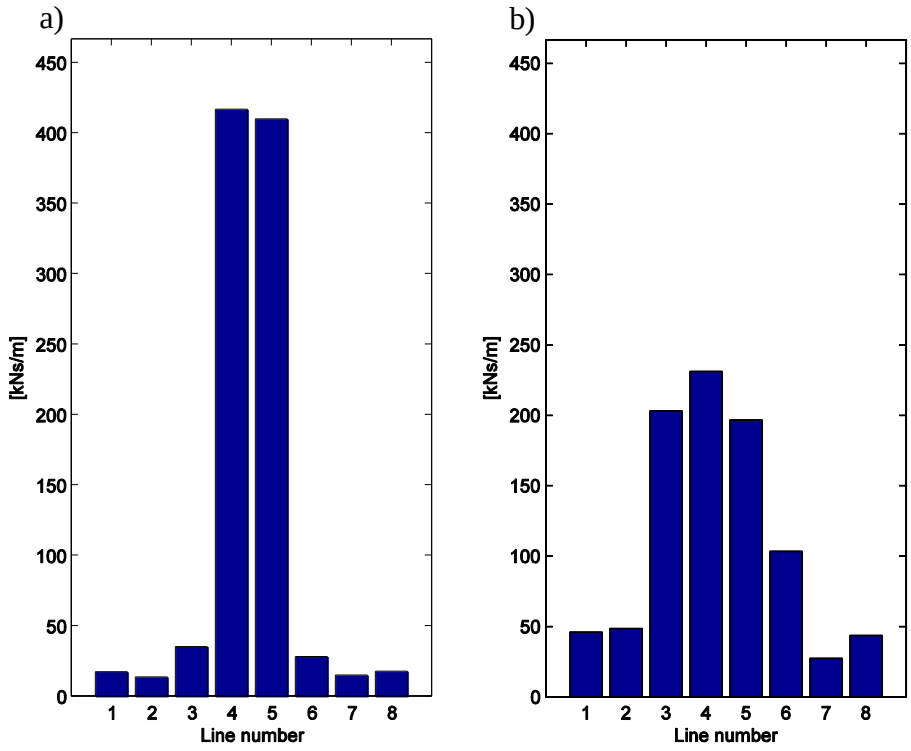

Figure C.21 Line damping LF+HF for a 400m heading at 0° in a) surge and b) sway.

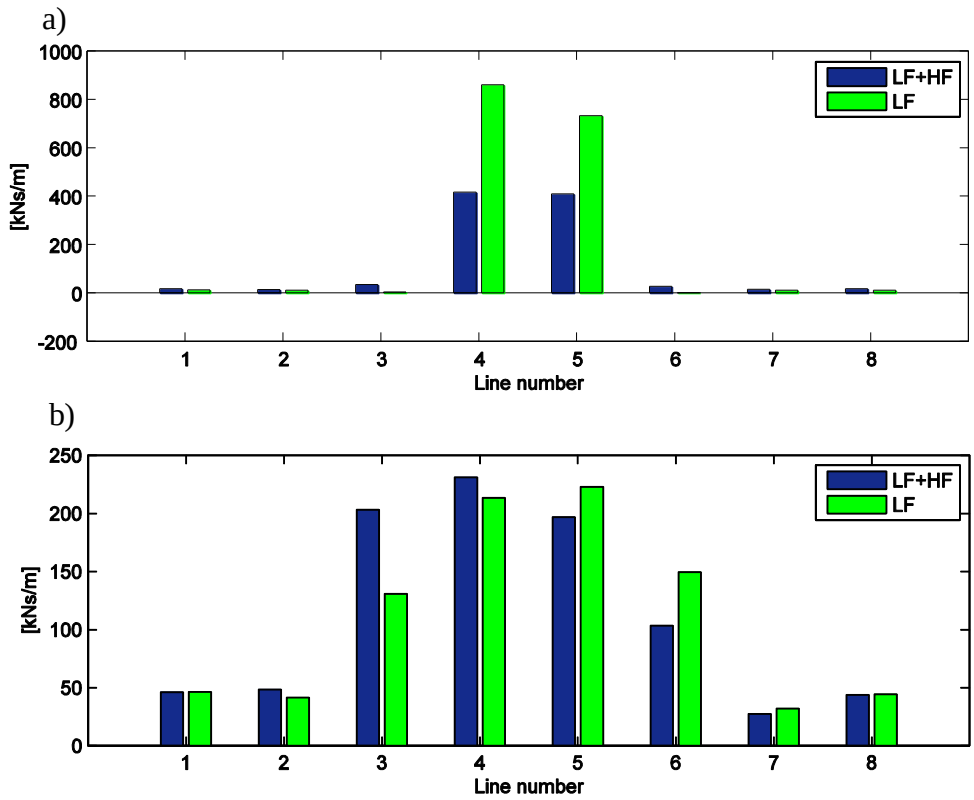

Figure C.22 Line damping LF+HF for a 400m heading at 0° in a) surge and b) sway.

Water depth of 400 m at 45°

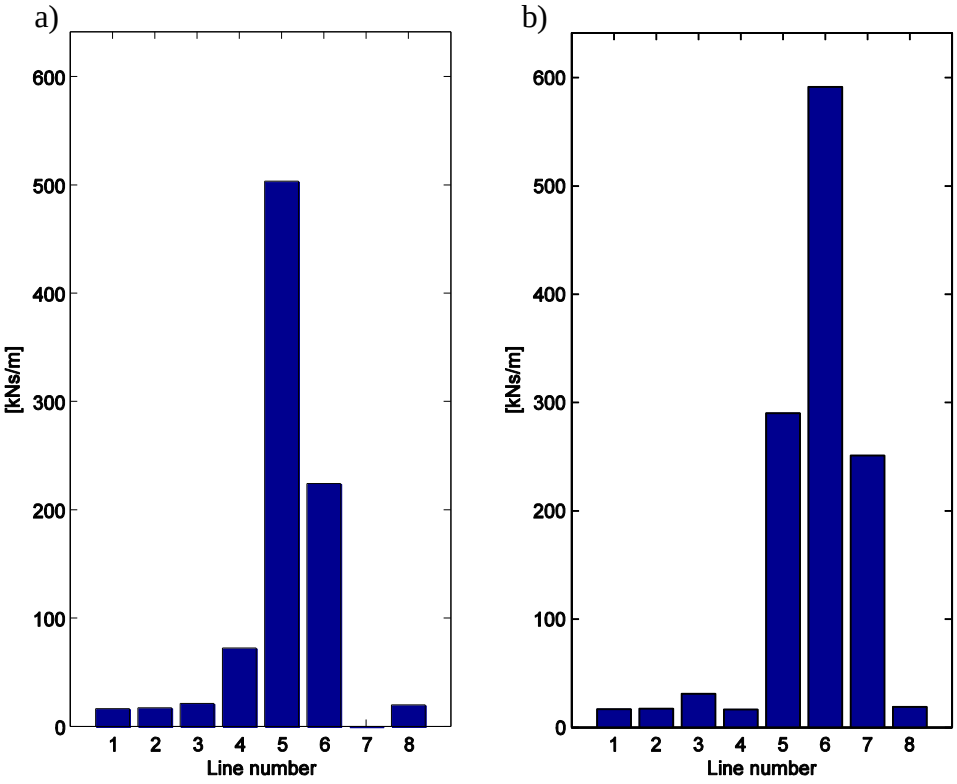

Figure C.23 Line damping LF+HF for a 400m heading at 45° in a) surge and b) sway.

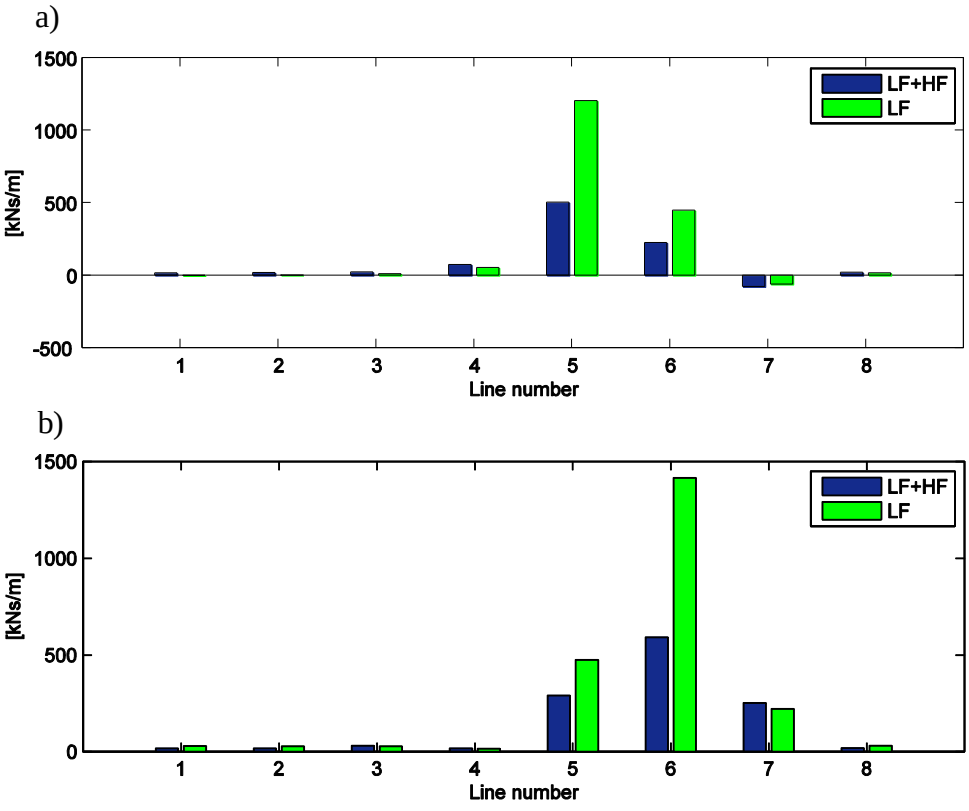

Figure C.24 Line damping for a 400m heading at 45° in a) surge and b) sway.

Water depth of 400 m at 90°

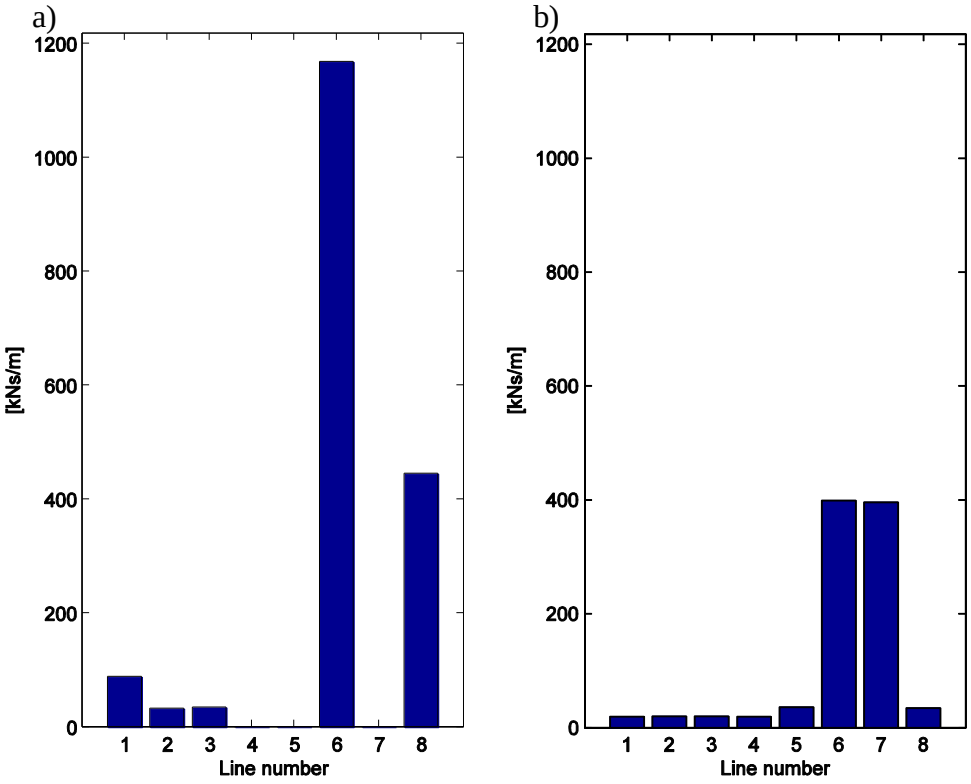

Figure C.25 Line damping LF+HF for a 400m heading at 90° in a) surge and b) sway.

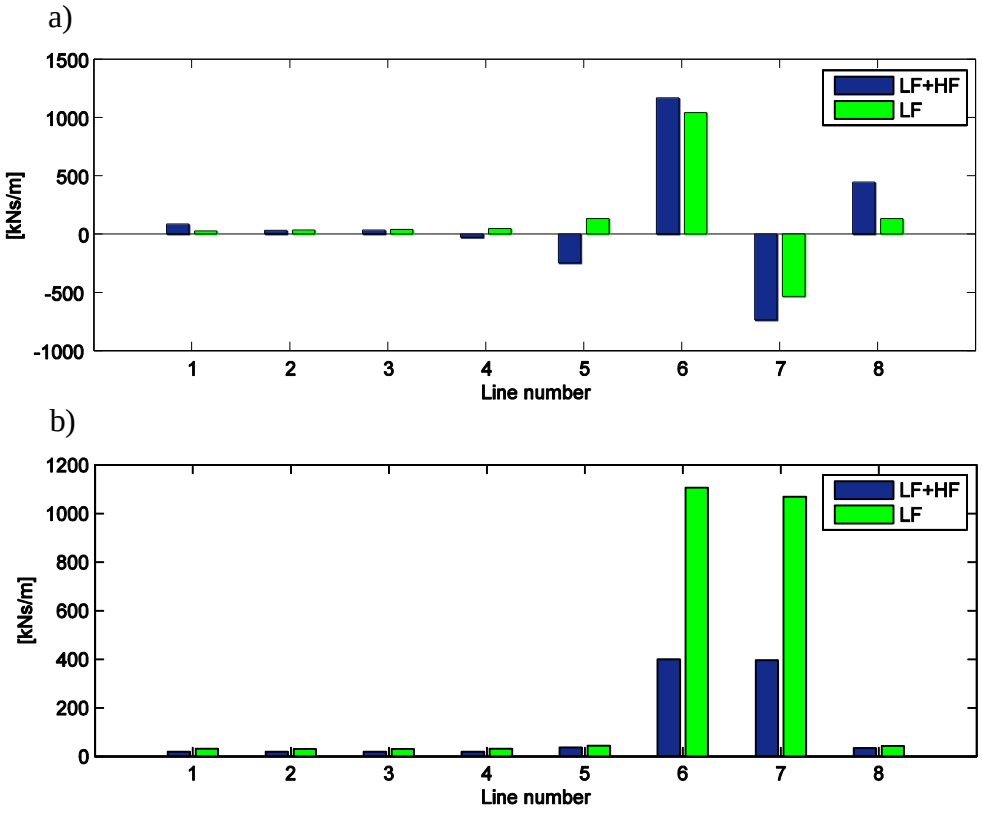

Figure C.26 Line damping for a 400m heading at 90° in a) surge and b) sway.

Water depth of 750 m at 0°

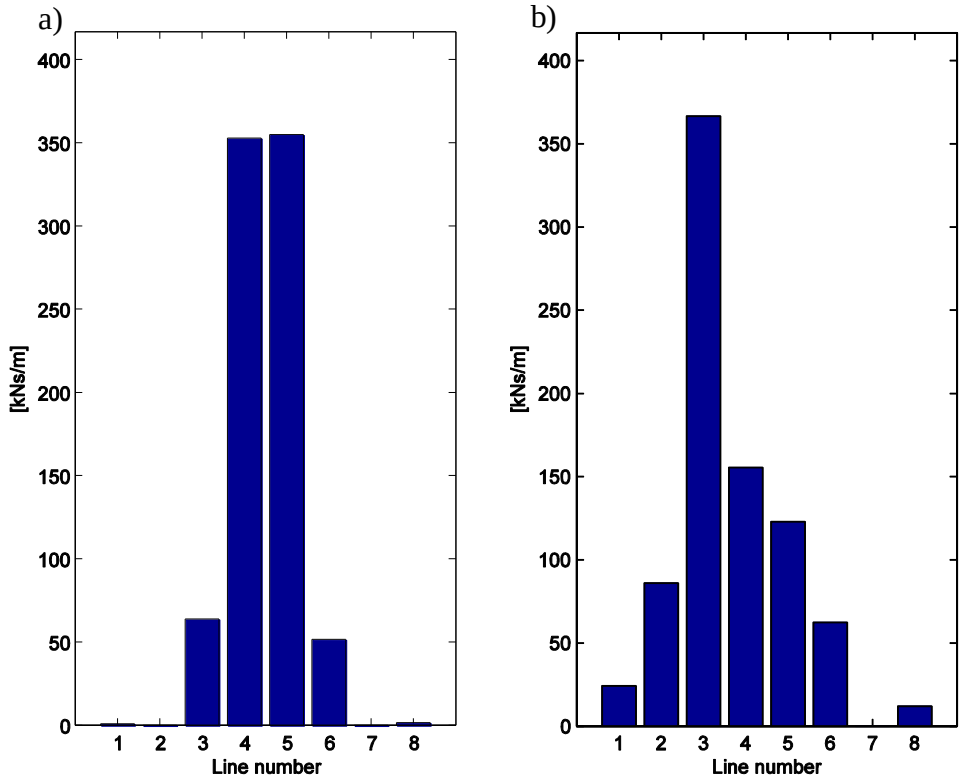

Figure C.27 Line damping LF+HF for a 750m heading at 0° in a) surge and b) sway.

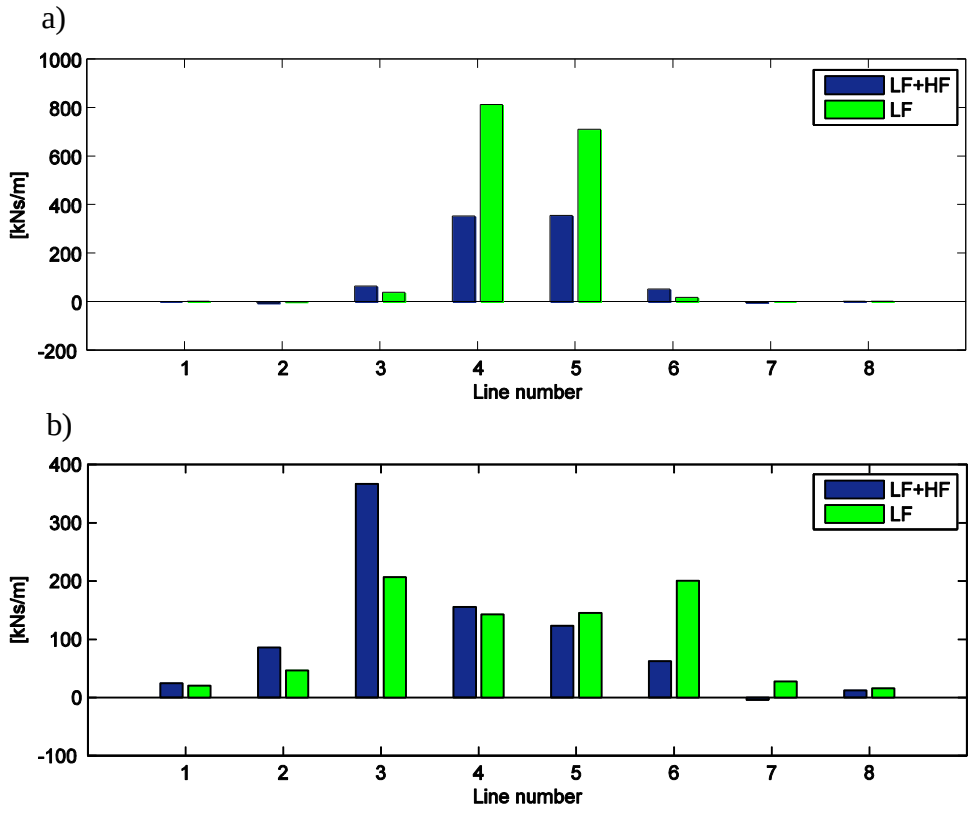

Figure C.28 Line damping for a 750m heading at 0° in a) surge and b) sway.

Water depth of 750 m at 45°

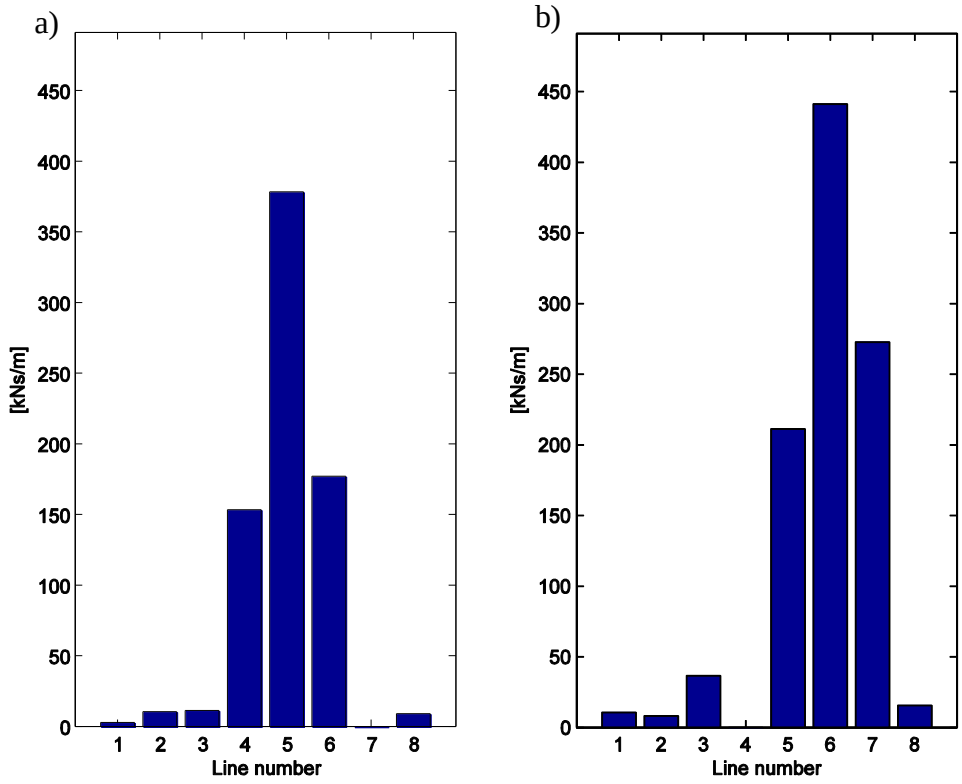

Figure C.29 Line damping LF+HF for a 750m heading at 45° in a) surge and b) sway.

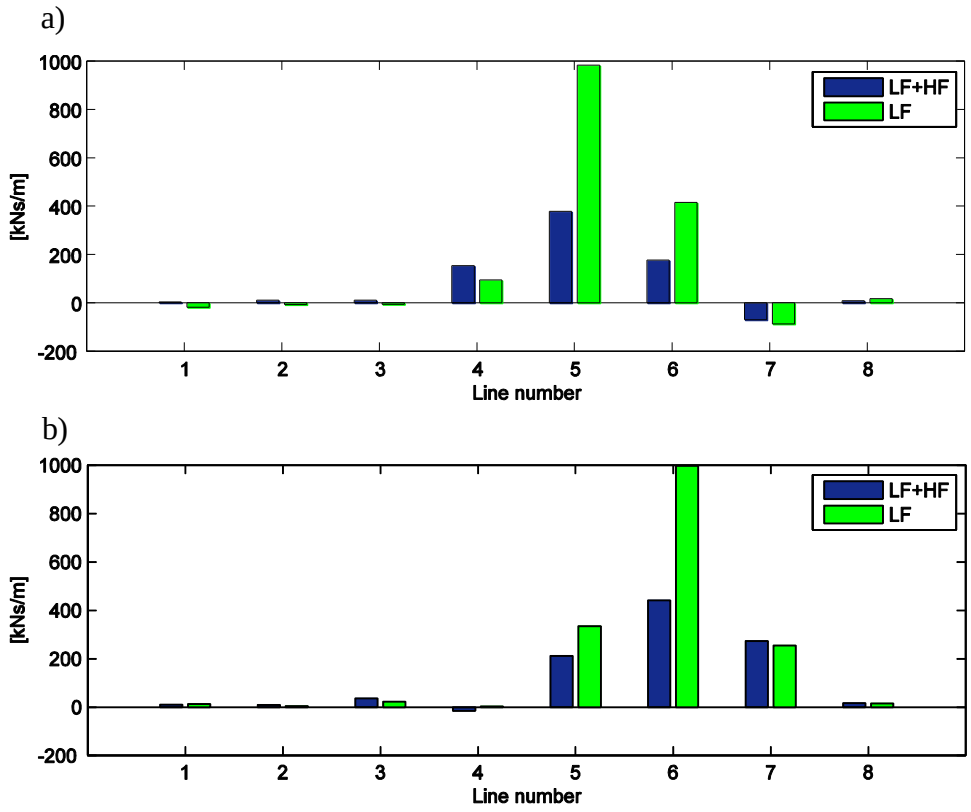

Figure C.30 Line damping LF+HF for a 750m heading at 45° in a) surge and b) sway.

Water depth of 750 m at 90°

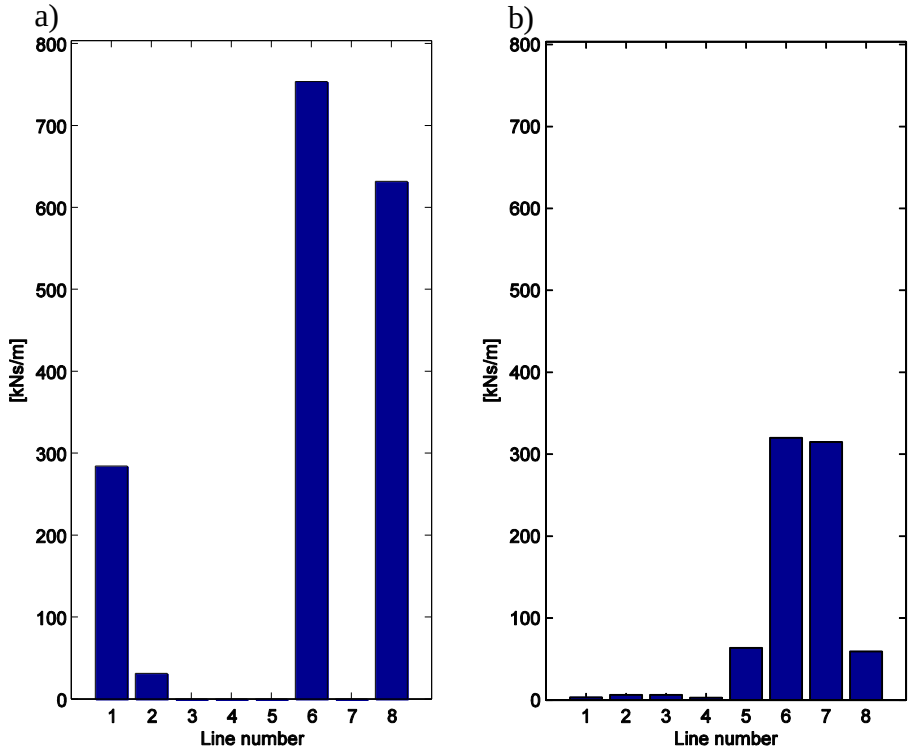

Figure C.31 Line damping LF+HF for a 750m heading at 90° in a) surge and b) sway.

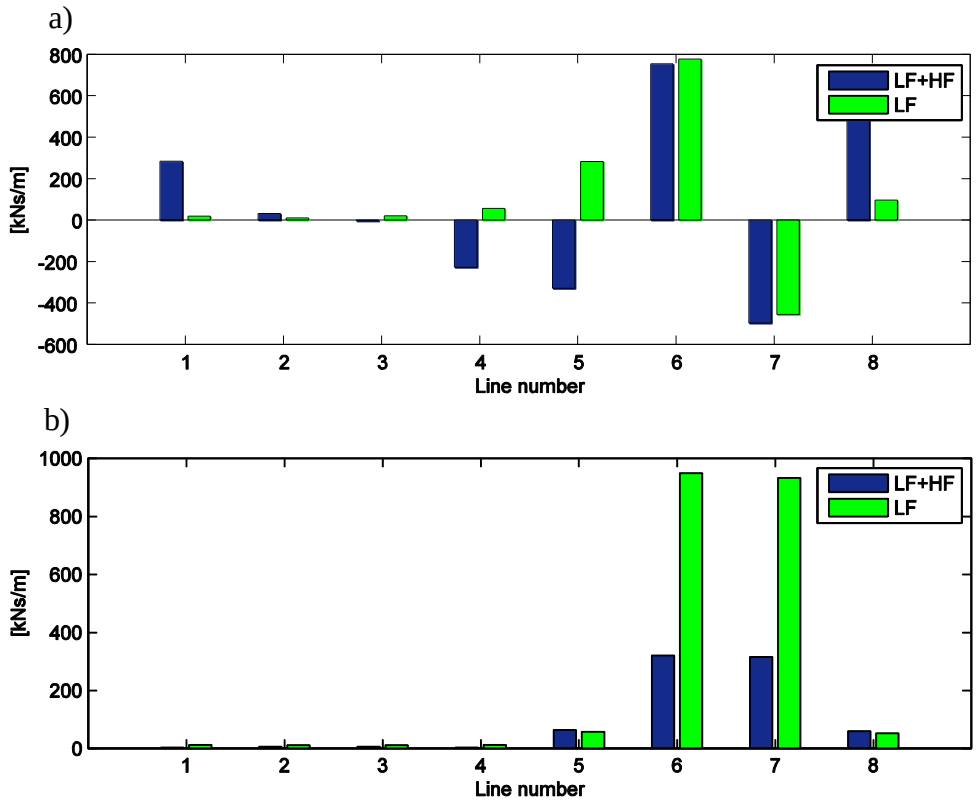

Figure C.32 Line damping LF+HF for a 750m heading at 90° in a) surge and b) sway.

Water depth of 1,250 m at 0°

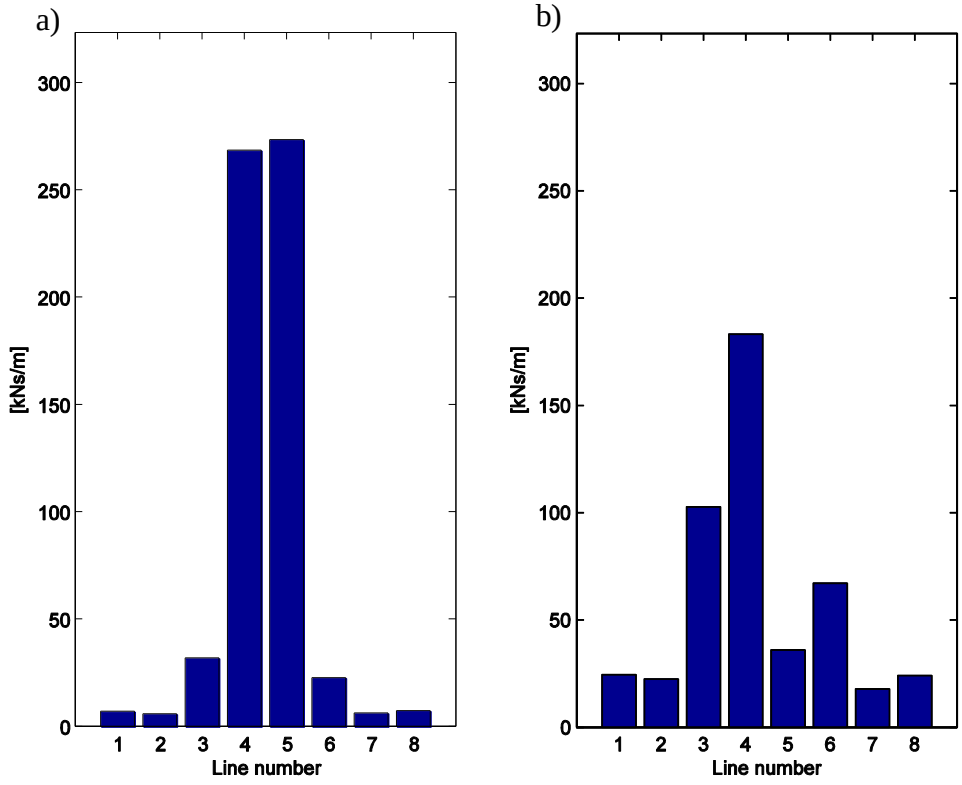

Figure C.33 Line damping LF+HF for a 1,250m heading at 0° in a) surge and b) sway.

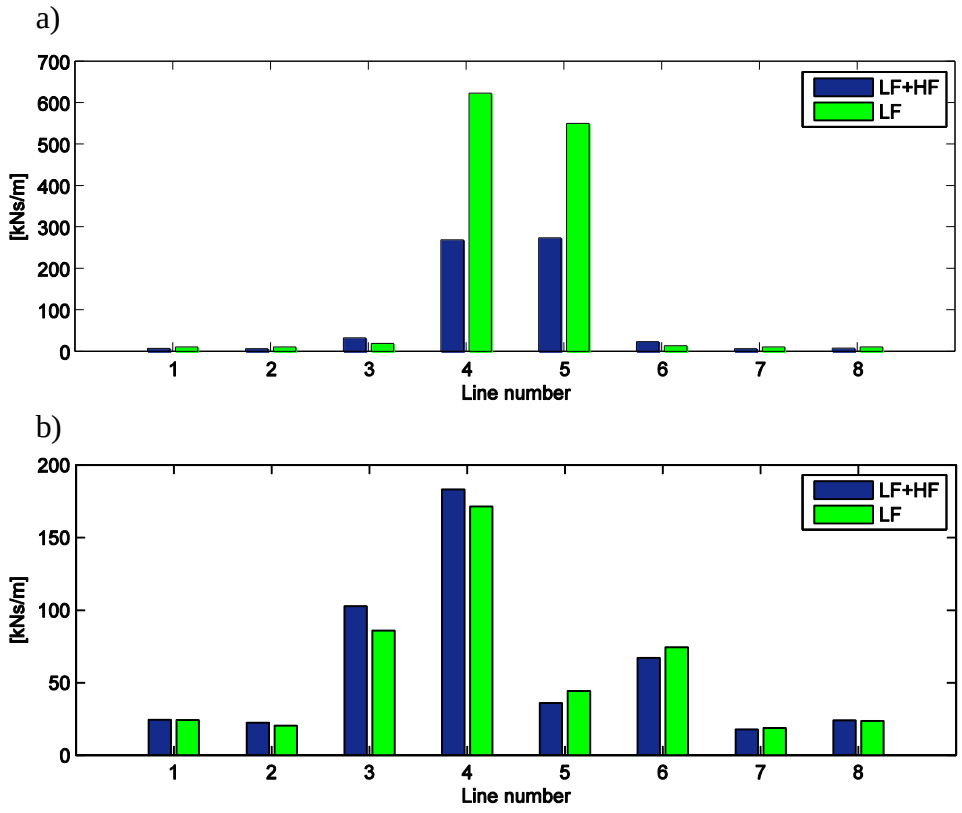

Figure C.34 Line damping for a 1,250m heading at 0° in a) surge and b) sway.

Water depth of 1,250 m at b45°

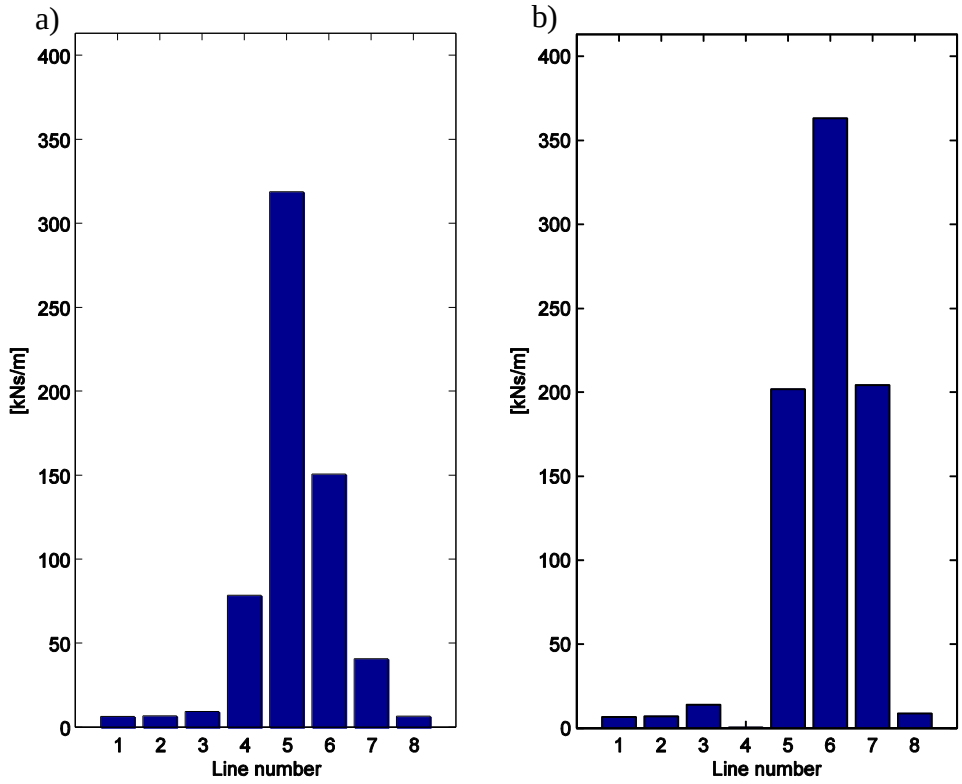

Figure C.35 Line damping LF+HF fora 1,250m heading at 45° in a) surge and b) sway.

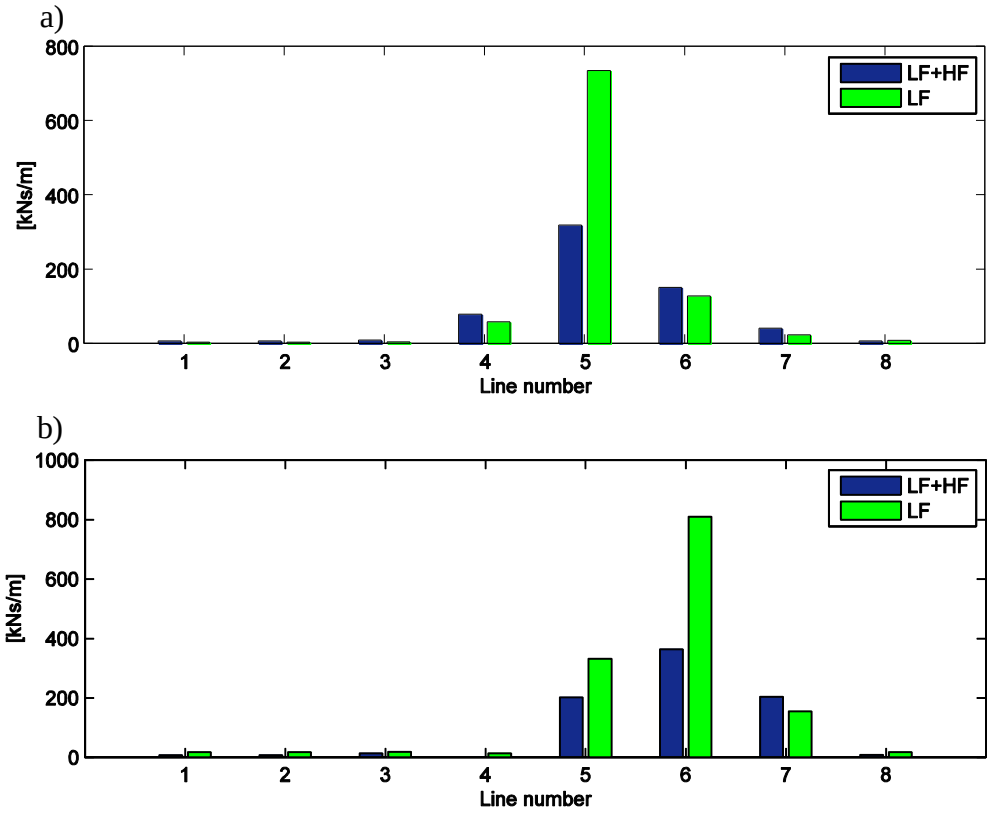

Figure C.36 Line damping for a 1,250m heading at 45° in a) surge and b) sway.

Water depth of 1,250 m at 90°

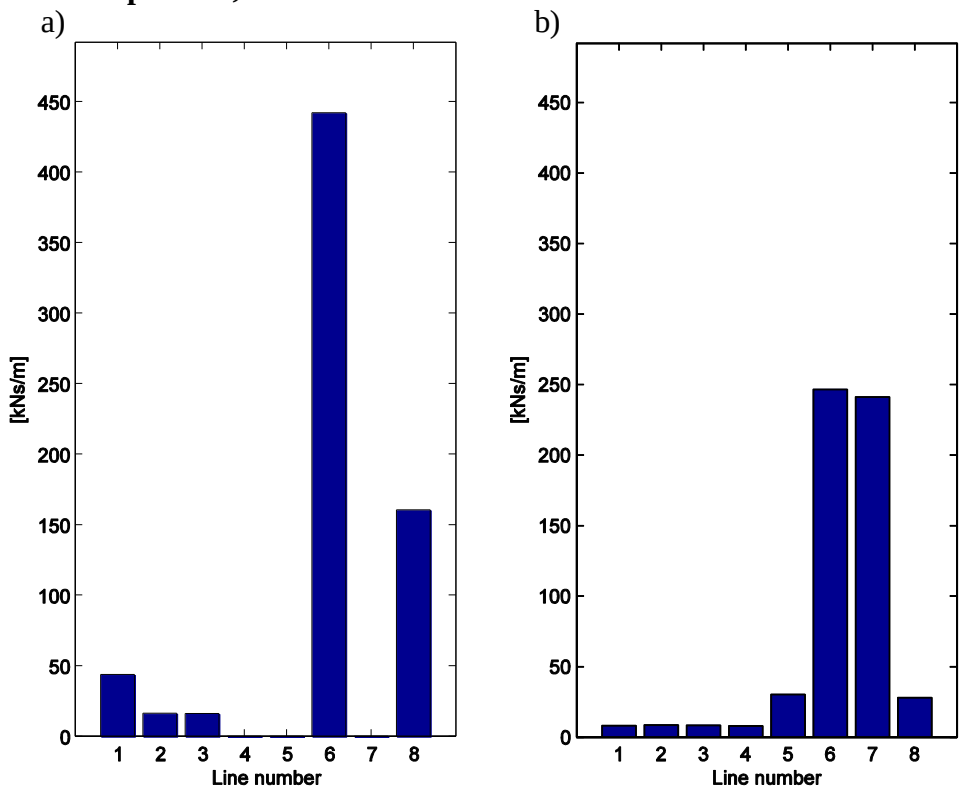

Figure C.37 Line damping LF+HF for a 1,250m heading of 90° in a) surge and b) sway.

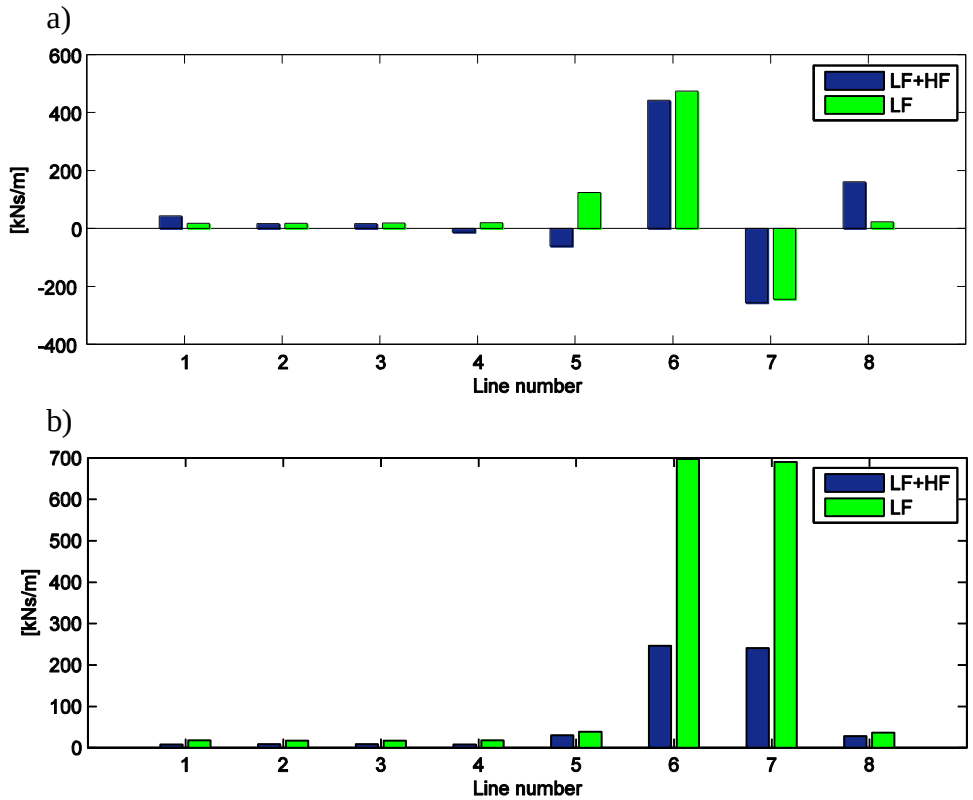

Figure C.38 Line damping for a 1,250m heading at 90° in a) surge and b) sway.

Appendix D: Software verification

This section is a summary of the verification of MIMOSA v.6.3 and DeepC with regard to line tension and standard deviation. The test case is 400m at 0° with no drag, and the results are divided into LF, HF and LF+HF, which can be seen in Tables D.1-D.3 and Figures D1-D3.

Table D.1 LF line tension and standard deviation

Line no.	MIMOSA v.6.3		DeepC	
	Max [kN]	Std	Max [kN]	Std
1	662	19.1	316	3.6
2	742	13.2	419	9.1
3	1221	52.9	968	46.3
4	3104	319.5	3069	227.6
5	3025	311.7	2508	191.6
6	1165	50.6	919	38.4
7	720	10.8	391	7.9
8	655	18.1	311	3.6

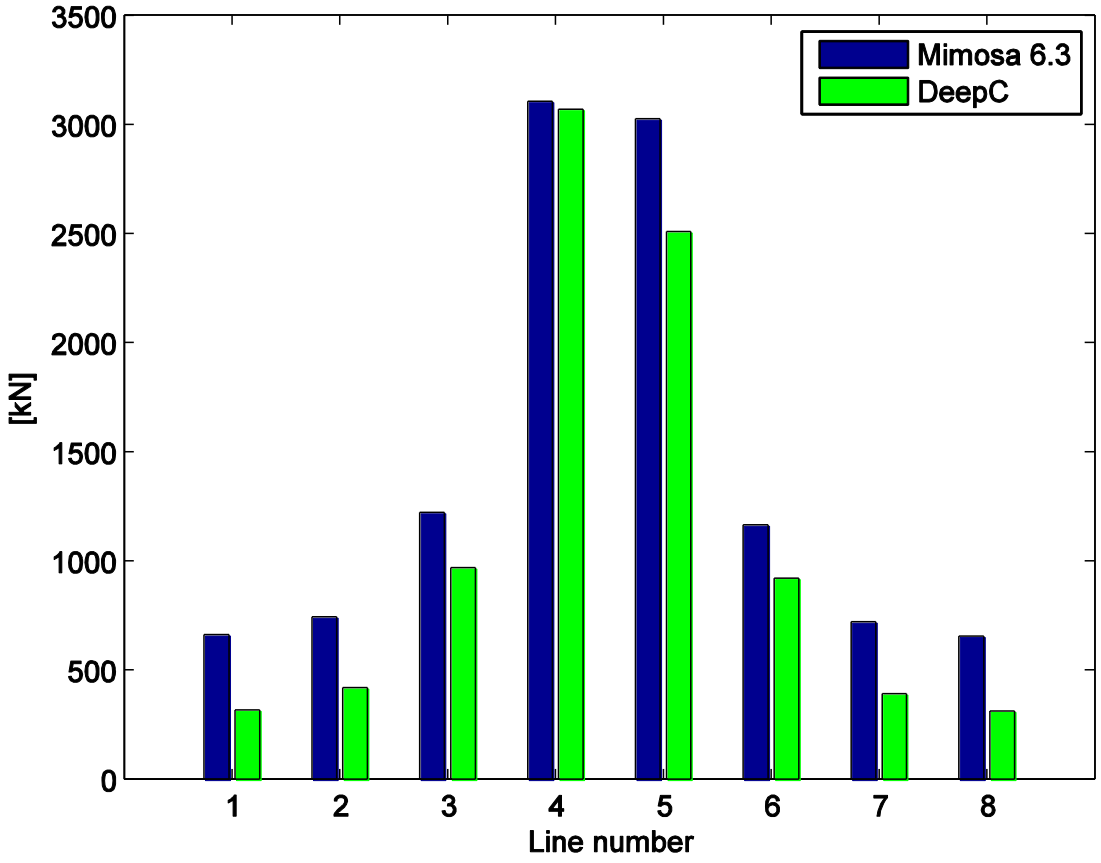

Figure D.1 LF line tensions for 400m at 0° with no drag.

Table D.2 HF line tension and standard deviation

Line no.	MIMOSA v.6.3		DeepC	
	Max [kN]	Std	Max [kN]	Std
1	615	17.5	189	42.8
2	709	9.4	471	76.8
3	1084	44.2	1223	247.3
4	2114	471.0	2217	570.5
5	2058	452.3	2051	551.1
6	1033	40.8	1185	225.1
7	695	8.4	439	68.0
8	610	16.5	178	42.2

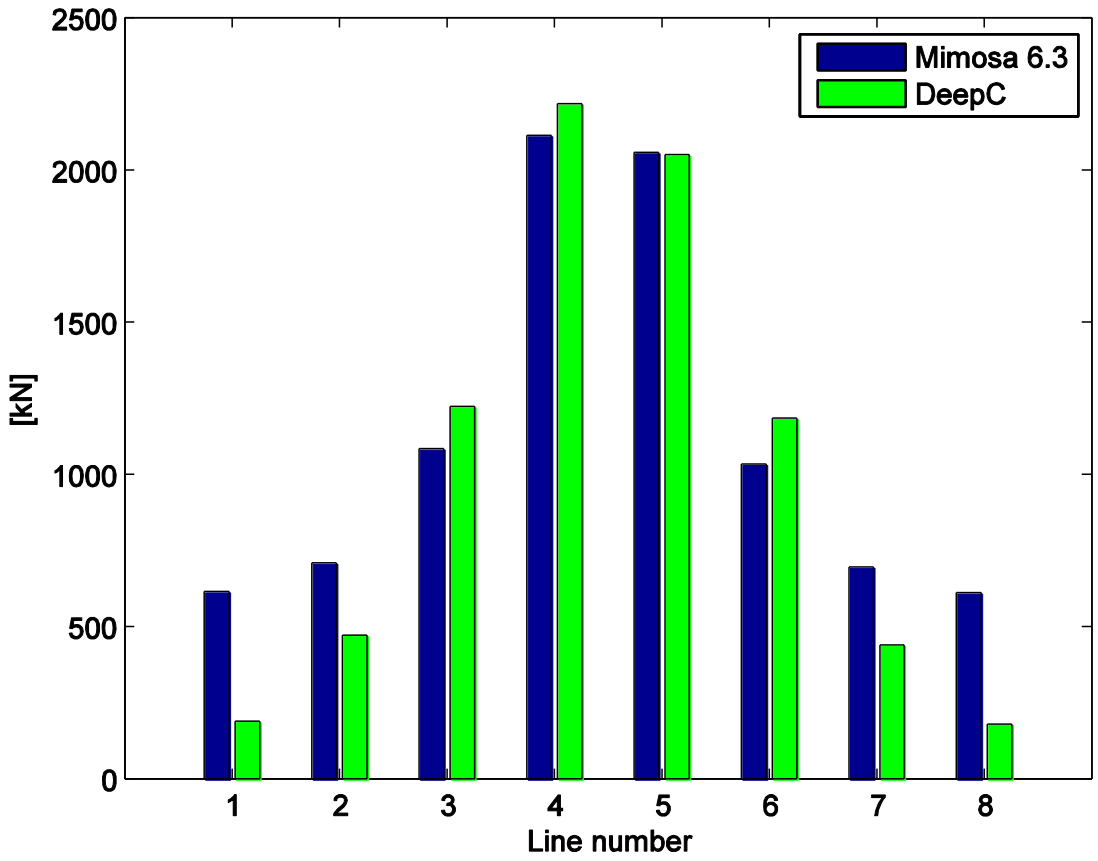

Figure D.2 HF line tensions for 400m at 0° with no drag.

Table D.3 Maximum line tension

Line no.	MIMOSA v.5.7	MIMOSA v.6.3	DeepC
1	868	671	489
2	1015	747	852
3	1642	1245	2128
4	4168	3366	4778
5	4117	3276	4260
6	1551	1187	2030
7	1020	725	803
8	873	664	476

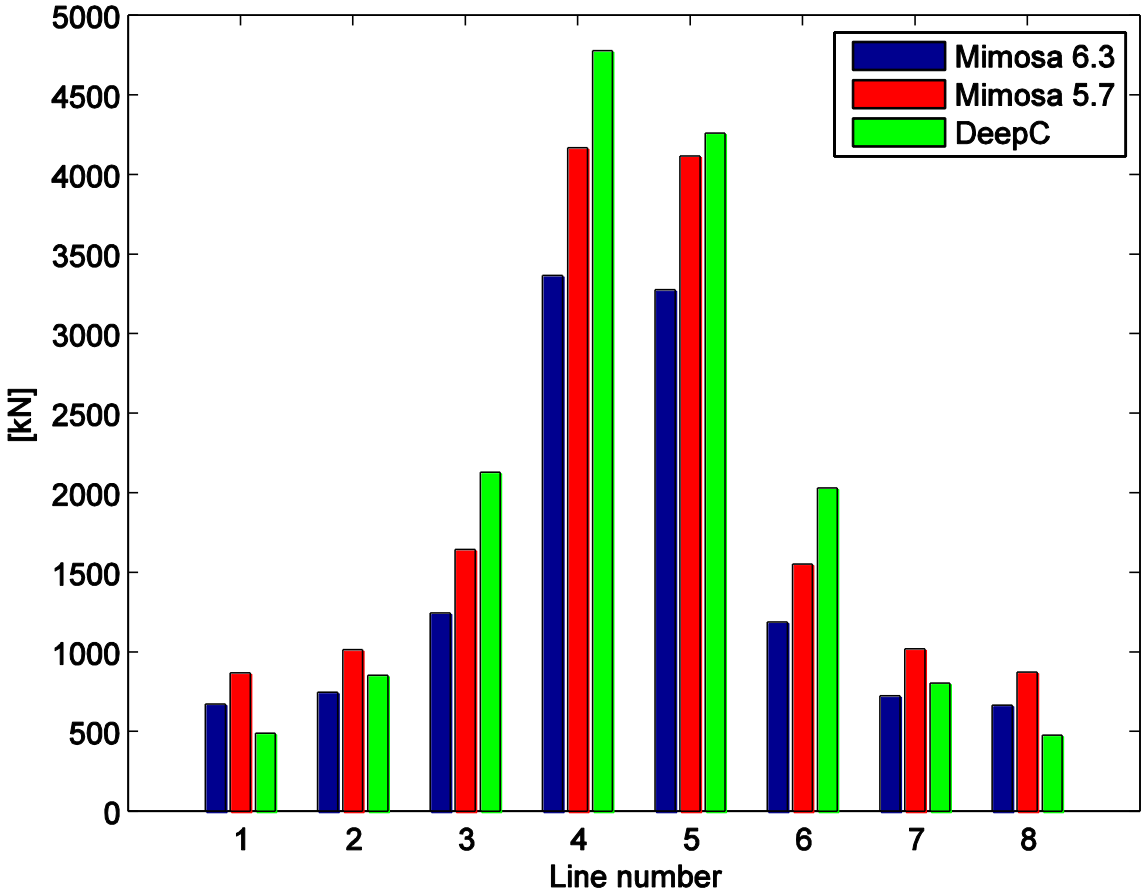

Figure D.3 Maximum line tensions for 400m at 0° with no drag.

The great differences in offset for static equilibrium is not feasible - the software should generate a more similar static equilibrium for the same environment. To find an explanation for this, two tests were performed at 400m at 0°; in the first case the waves remained as in the previous analyses but the current and wind is set to small values; 0.1 m/s and 2 m/s, respectively, and in the second case the significant wave height was set to 0.1m, while the current and wind was unchanged. In MIMOSA, the static equilibrium (surge) was -42m in the first case and 76m in the second, while in DeepC it was -41m and 122 m, respectively .

In the first case, the values correspond well and the wave forces are modelled in the same way. The negative equilibrium position is a result of the thruster force, which is still applied in the opposite direction of the environmental loads.

The second case shows an unsatisfactory behaviour with a large difference in static offset, the DeepC position is 1.5 times larger than in MIMOSA. This case indicates that the there is a difference in the software for the current and wind forces and implies larger loads in DeepC, hence the damping calculated in DeepC may be overestimated because of the larger motions.

In Table D.4 the forces are presented from the two cases with small waves, current and wind forces, respectively.

Table D.4 No drag comparison and influence of environmental loads

Line no.	MIMOSA 6.3 No waves		DeepC No waves		MIMOSA 6.3 No curr/wind		DeepC No curr/wind	
	Max force [kN]	Std	Max force [kN]	Std	Max force [kN]	Std	Max force [kN]	Std
1	681.2	16.50	309.7	1.56	1332.6	83.14	1580.6	156.46
2	753.5	10.80	390.3	5.19	960.7	24.06	1472.4	144.07
3	1077.5	33.30	734.4	25.90	792.8	12.71	1257.4	115.76
4	1811.6	144.50	1599.0	95.48	804.4	25.08	1179.9	91.82
5	1756.0	138.30	1427.1	73.00	804.4	25.20	1165.0	92.82
6	1007.2	27.40	636.7	17.43	793.2	12.88	1339.3	118.32
7	729.0	9.50	371.9	4.68	959.0	23.74	1472.0	142.63
8	672.4	16.10	307.4	1.81	1332.2	83.00	1561.0	155.18

Appendix E: Convergence test

The RIFLEX User's Manual Marintek (2010b) defines the mooring line as the suspended structure between supernodes - two points with specified boundary conditions. The line is divided into segments in order to have the possibility of different properties for different parts of the line ; a segment has uniform element length and cross section properties. For the FE-analysis, the segments are divided into smaller elements as can be seen in Figure E.1.

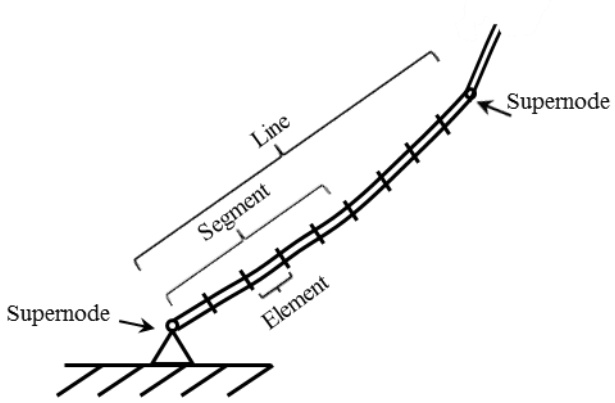

Figure E.1 Overview of how DeepC handles a mooring line (Marintek 2010)

In the convergence test the mooring lines are divided into 4 segments (fairlead, middle, touch-down and seabed), see Figure E.2, in order not to have to use more elements than necessary in the further calculations.

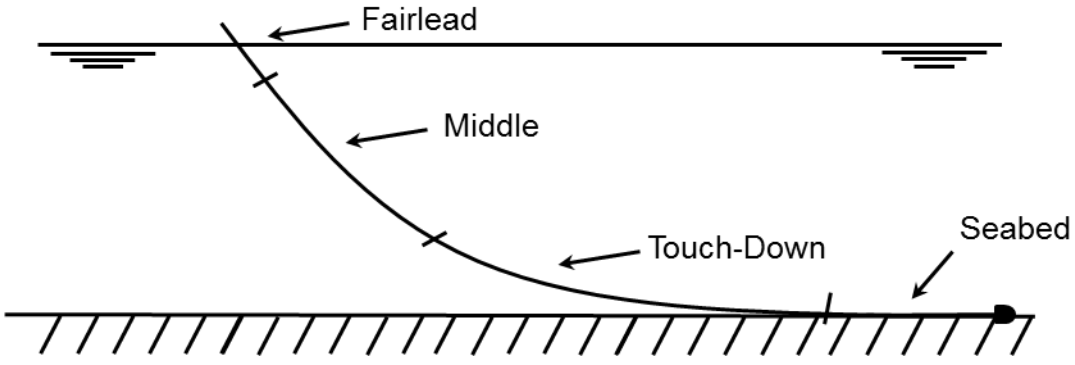

Figure E.2 Overview of the mooringline segments

The convergence tests were carried out at a water depth of 400 m. The length of the elements does not depend on the length of the mooring line, hence it is sufficient to do the test only for one water depth. The length of the segments will change when using a different water depth, but the element length will be the same. The properties of interest are the mean force experienced by the mooring line and the standard deviation

of the force. The force in the mooring lines will affect the motion of the platform, hence it is necessary to have as little error effects from the mesh as are reasonably possible. The standard deviation is to see the scatter of the mean force between the elements on the segment.

The areas that require a finer element length are the touchdown point on the seabed and the fairlead part near the water surface. The part lying on the seabed, not in the perimeter of the touch-down point, will not affect the calculations significantly, hence a coarse mesh is sufficient.

The conclusion from the convergence test is that the element length may vary along the lines. It is necessary to have a smaller element length for the fairlead and touchdown segments, while having a coarser one for middle and seabed segments. Hence, the element lengths to be used in the analyses are then 10m for fairlead, 20m middle, 10m touchdown and 30m for the seabed segment.

E.1. Fairlead segment

For the fairlead segment the element length will vary while the element length for the other segments are held fixed in order not to affect the results. The set-up is seen in Table E.1. The convergence for the force and standard deviation can be seen in Figures E.2 and E.3 - the properties are rather constant throughout the changes in element length. The graphs are normalized against the result for an element size of 0.5m.

Table E.1 Convergence test set-up for the fairlead segment

Segment	Length [m]	Element length [m]
Fairlead	50	X
Middle	300	10
Touch-down	950	10
Seabed	300	10

a)

b)

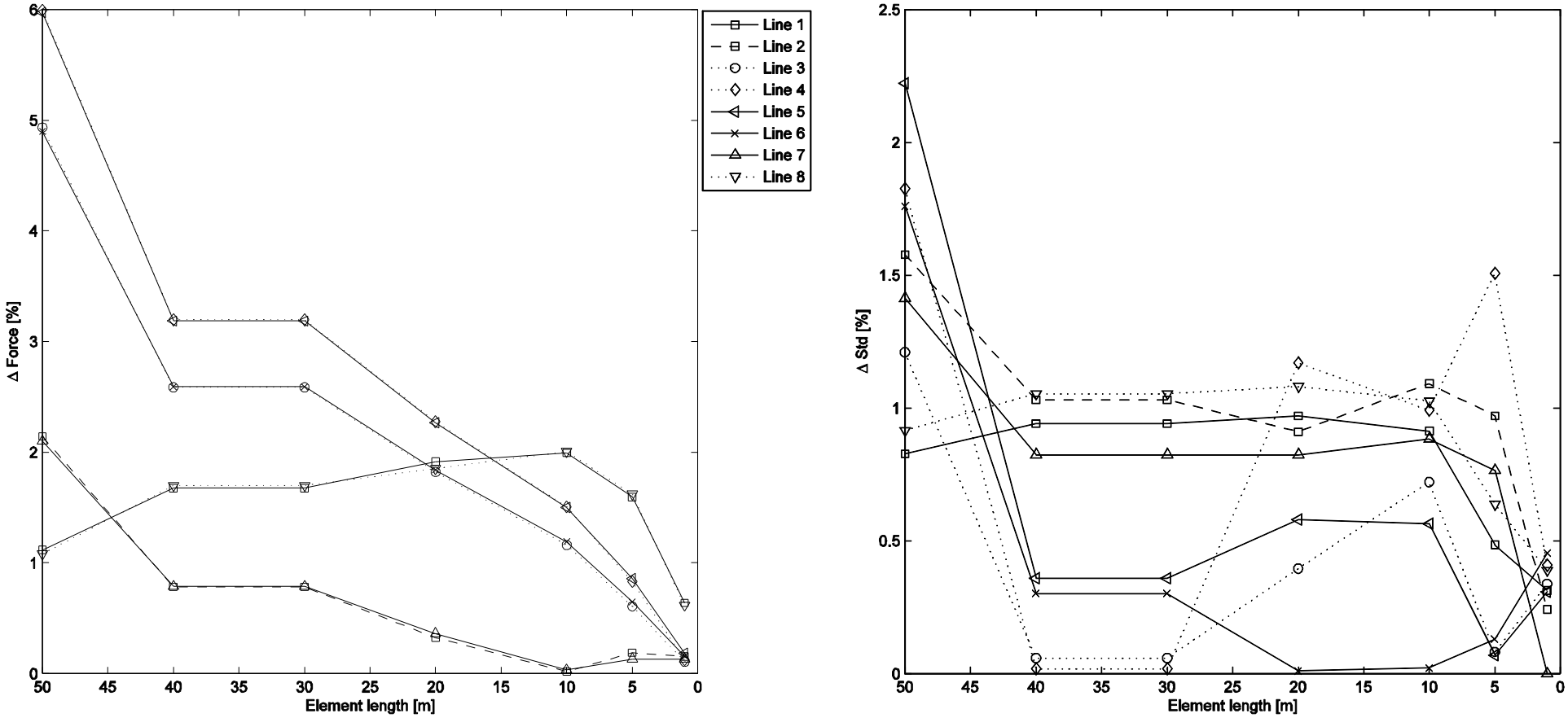

Figure E.2 Variation of a) force and b) standard deviation of the force in the fairlead line segment over element length

E.2. Middle segment

For the middle segment the element length will vary while the element length for the other segments are held fixed in order not to affect the results. The setup is seen in Table E.2. The convergence of the mean force and standard deviation is found in Figures E.4a and E.4b, respectively, and the difference between 50m and 5m elements is rather small. The result is normalized against the results with an element size of 1m.

Table E.2 Convergence test set-up for the middle segment

Segment	Length [m]	Element length [m]
Fairlead	50	10
Middle	300	X
Touch-down	950	10
Seabed	300	10

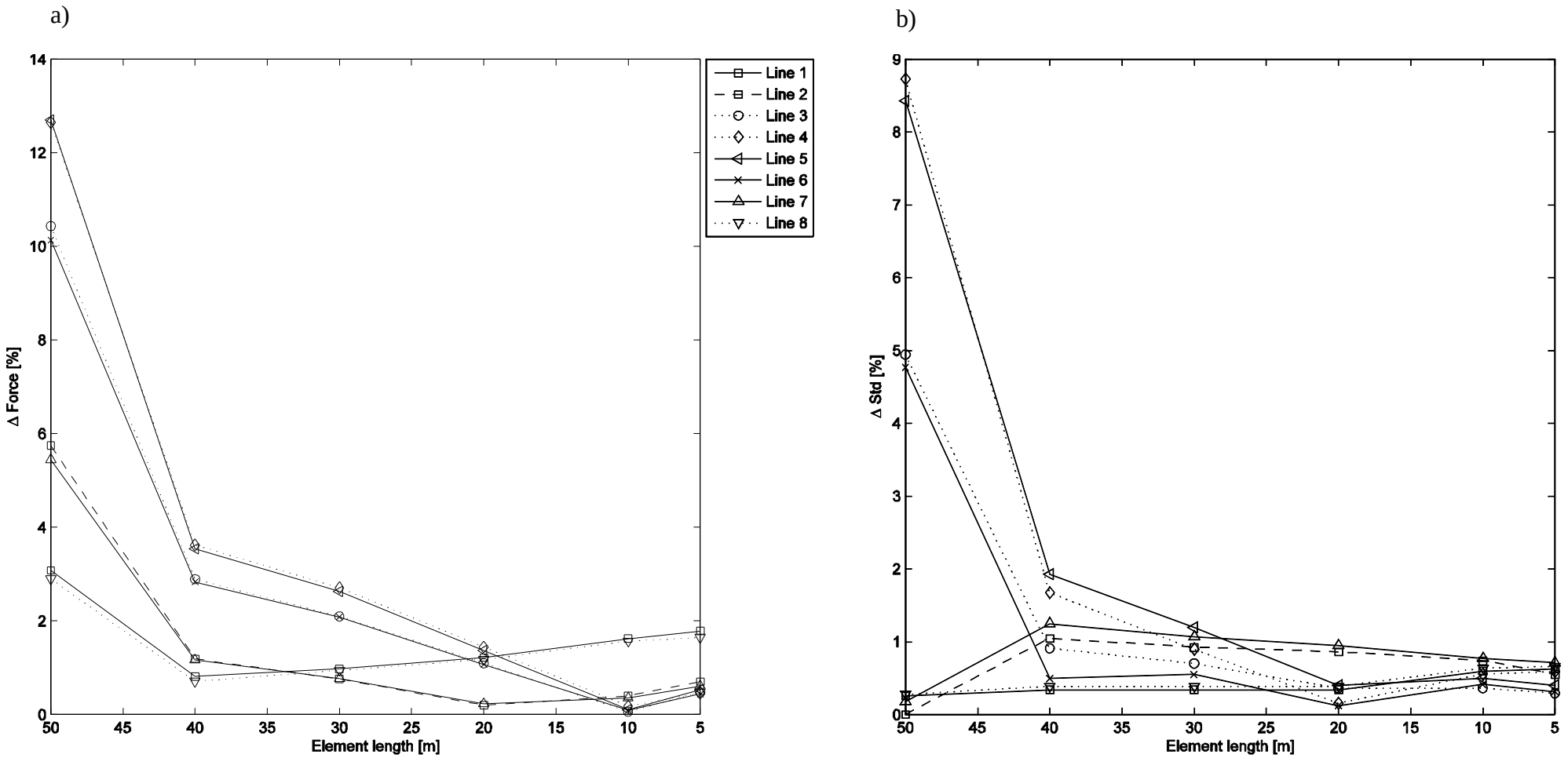

Figure E.4 Variation of a) force and b) standard deviation of the middle line segment over element length

E.3. Touchdown b segment

The touchdown segment describes the part of the mooring lines that will be both lying on the seabed and suspended in the water. It is the longest segment due to the effects from environmental forces which makes some lines go slack and have a large part of the length on the seabed, and some lines in tension which have a large suspended length. The element lengths for the tests can be found in Table E.3. Figure E.6 shows normalized results against the results for an element size of 10m.

The variation in the force and standard deviation is quite great, the trend being that the difference between results and element size decreases with a smaller element length. For further analysis a 10m element will be used in the Touchdown segment.

Table E.3 Convergence test setup for the touch-down segment

Segment	Length [m]	Element length [m]
Fairlead	50	10
Middle	300	10
Touch-Down	950	X
Seabed	300	10

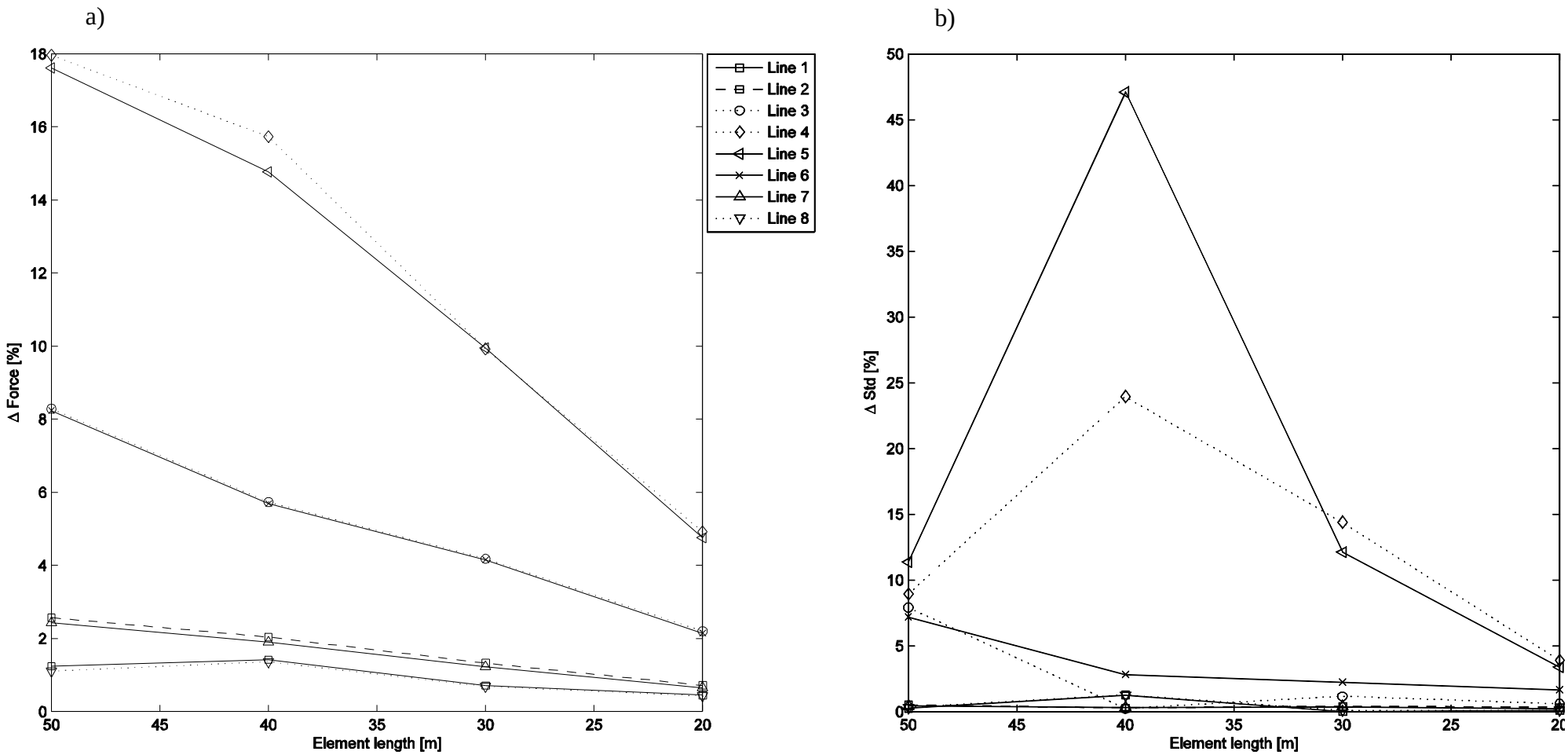

Figure E.6 Variation of a) force and b) standard deviation in the touchdown line segment over element length

E.4. Seabed segment

The last segment is the part of the line lying on the seabed . This part of the mooring line should lie on the seabed at all times. The element lengths for the different segments are found in Table E.4. The convergence is seen in Figures E.8a and E.8b. There are small differences in the results, 0.5 per cent for the force and 2 per cent for the standard deviation of the force, using 50m or 10m elements. The graphs in Figure E.7 are normalized against the 10m element values.

Table E.4 Set-up convergence test for the fairlead segment

Segment	Length [m]	Element length [m]
Fairlead	50	0.5
Middle	300	10
Touch-down	950	10
Seabed	300	X

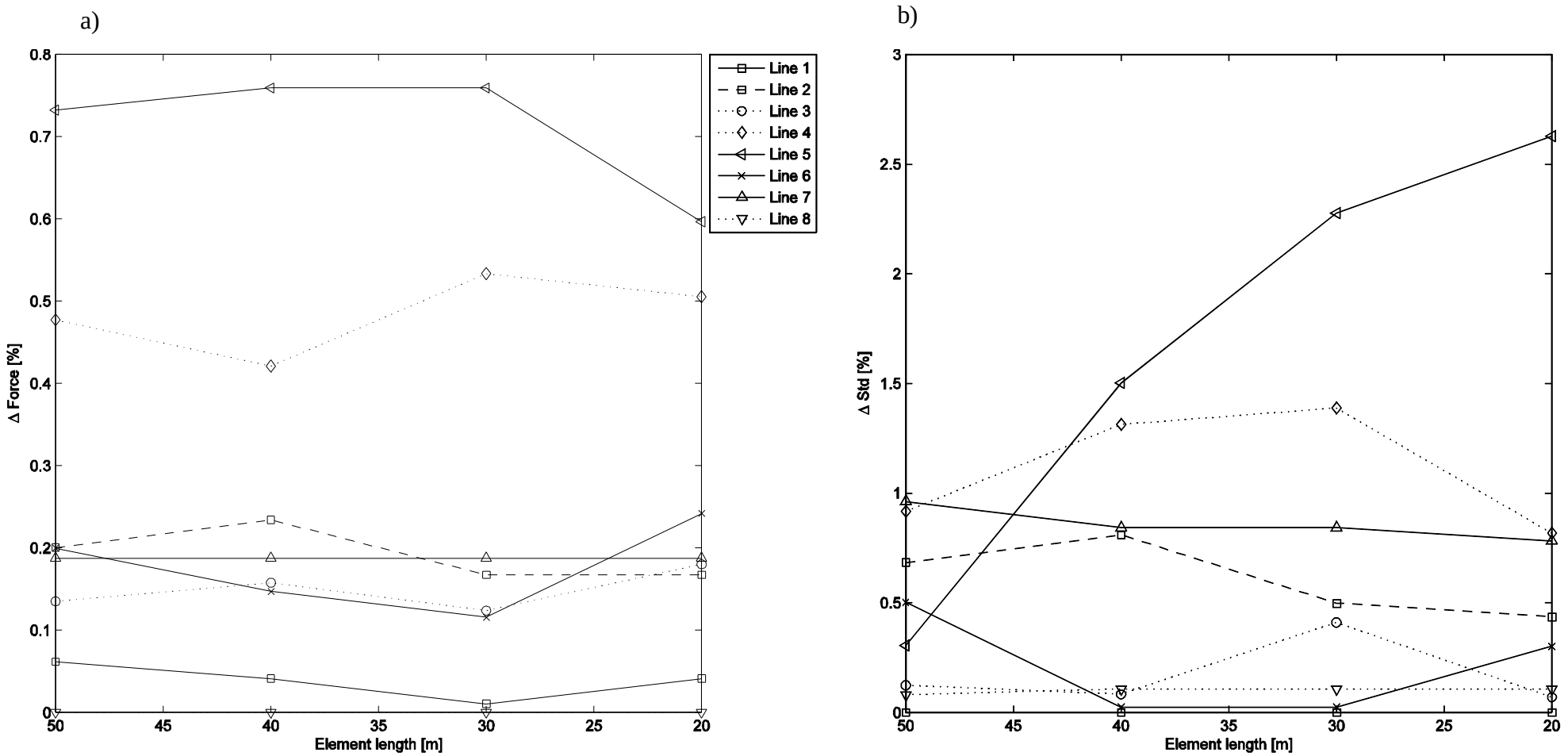

Figure E.8 Variation of a) force and b) standard deviation in the seabed line segment over element length